NOTICE

AVIS

The quality of this microform is heavily dependent upon the quality of the original thesis submitted for microfilming. Every effort has been made to ensure the highest quality of reproduction possible.

If pages are missing, contact the university which granted the degree.

Some pages may have indistinct print especially if the original pages were typed with a poor typewriter ribbon or if the university sent us an inferior photocopy.

Previously copyrighted materials (journal articles, published tests, etc.) are not filmed.

Reproduction in full or in part of this microform is governed by the Canadian Copyright Act, R.S.C. 1970, c. C-30.

La qualité de cette microforme dépend grandement de la qualité de la thèse soumise au microfilmage. Nous avons tout fait pour assurer une qualité supérieure de reproduction.

S'il manque des pages, veuillez communiquer avec l'université qui a conféré le grade.

La qualité d'impression de certaines pages peut laisser à désirer, surtout si les pages originales ont été dactylographiées à l'aide d'un ruban usé ou si l'université nous a fait parvenir une photocopie de qualité inférieure.

Les documents qui font déjà l'objet d'un droit d'auteur (articles de revue, tests publiés, etc.) ne sont pas microfilmés.

La reproduction, même partielle, de cette microforme est soumise à la Loi canadienne sur le droit d'auteur, SRC 1970, c. C-30.

THE UNIVERSITY OF ALBERTA

A Ring and Spring Model for Tunnel Liner Design

by

Susan Elizabeth Evison

A THESIS

SUBMITTED TO THE FACULTY OF GRADUATE STUDIES AND RESEARCH

IN PARTIAL FULFILMENT OF THE REQUIREMENTS FOR THE DEGREE

OF Master of Science

Department of Civil Engineering

EDMONTON, ALBERTA

FALL 1988

THE UNIVERSITY OF ALBERTA

RELEASE FORM

NAME OF AUTHOR   Susan Elizabeth Evison

TITLE OF THESIS   A Ring and Spring Model for Tunnel Liner Design

DEGREE FOR WHICH THESIS WAS PRESENTED Master of Science

YEAR THIS DEGREE GRANTED   FALL 1988

Permission is hereby granted to THE UNIVERSITY OF ALBERTA LIBRARY to reproduce single copies of this thesis and to lend or sell such copies for private, scholarly or scientific research purposes only.

The author reserves other publication rights, and neither the thesis nor extensive extracts from it may be printed or otherwise reproduced without the author's written permission.
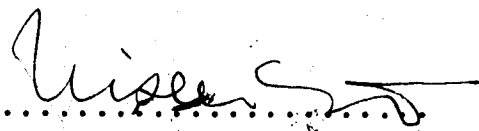
(SIGNED) ..Susan Evison..

PERMANENT ADDRESS:

.11. Berehaven Road......

.Seatoun Heights.........

Wellington, New Zealand

DATED ..October 14....1988
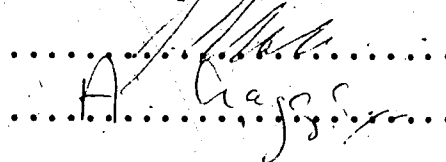
THE UNIVERSITY OF ALBERTA

FACULTY OF GRADUATE STUDIES AND RESEARCH

The undersigned certify that they have read, and
recommend to the Faculty of Graduate Studies and Research,
for acceptance, a thesis entitled *A Ring and Spring Model
for Tunnel Liner Design* submitted by Susan Elizabeth Evison
in partial fulfilment of the requirements for the degree of
Master of Science.

....

Supervisor

....

....

Date..October 11...1988........

DEDICATION

For my best friend John,

and our two girls,

Letitia and Rhiannon

ABSTRACT

Many methods are available for the analysis of the
ground-liner interaction process in soft ground tunnels. The
capacity to model complex configurations is available, but
the preference in practice is towards a simple discrete ring
and spring model. A fully embedded model of this type is
investigated for both deep and shallow soft ground
conditions and compares favourably with finite element and
analytical closed form solutions. The commonly used
partially embedded ring and spring model is shown to give
conservative results if good ground control conditions
exist.

ACKNOWLEDGEMENTS

Table of Contents

List of Tables

List of Figures

KEY NOTATION

A_s : cross-section area of liner (or support).

A_{sp} : cross-section area of spring in ring and spring model.

D : constrained soil modulus

E : modulus of elasticity for the soil.

E_s : modulus of elasticity for the support.

E_{sp} : modulus of elasticity for the springs in the ring and spring model.

I_s : moment of inertia of the support.

I_{sp} : moment of inertia of the springs.

K_o : in situ stress ratio of the soil.

k : spring constant = stress/displacement

k_r : radial spring constant

k_{ro} : radial spring constant describing convergence into a circular opening under uniform pressure.

k_{r2} : radial spring constant described by the distortional radial stress component.

k_t : tangential spring constant.

k_{t2} : tangential spring constant described by the shear stress component

ν : Poisson's ratio of the soil.

ν_s : Poisson's ratio of the support.

1. INTRODUCTION

1.1 Foreword

The design of a tunnel support involves issues such as the choice of the support system and the loads it will be required to resist during its service life. Many interacting factors strongly influence these decisions and, perhaps as a consequence of this, the design basis for soft ground tunnelling still contains an appreciable amount of empiricism.

In spite of the ability to simulate many complex aspects of the ground-liner interaction through numerical techniques, simple design oriented procedures are preferred in practice. Familiarity with known simple techniques and their limitations may be of more value in assessing the relative influence of the design parameters than the complex interpretation required in more sophisticated systems of analysis.

The current assumptions associated with ring and spring models in shallow tunnel conditions tend to accept that the soil in the crown region is unable to provide any arching self support against the adjacent soil. It was suggested (Negro, 1988) that a more logical approach would be to consider softened embedment regions which can be effected by assigning different spring constants to various locations around the lining contour. Variations of stiffness around the contour allowed virtually no improved convergence

1

towards the target solutions in the case history example investigated. The more important influence to be consider is the overall reduction in stiffness which occurs as a result of the excavation process.

The deficiences of the ring and spring solutions are the universal ones associated with two-dimensional models where no consideration of delayed lining installation is undertaken. These effects are manifested as stress and stiffness changes in the ground prior to lining activatic However, as explained in Chapter 5, it is possible to sensibly account for these effects in the design of the initial supports by following the guidelines proposed in design method by Negro (1988).

In the simplest situations involving continuous circular linings, the analytical solutions are perhaps mc appropriate to use. However, the appeal of the ring and spring numerical models increases as deviations from this simple configuration occur. This includes being able to assess non circular cross sections, mixed face condition: jointed liners as examples. These features enhance the practicality of the ring and spring model in terms of rapidly assessing the influence of various parameters for sensitivity and final design studies.

1.2 Aims

The intention of this thesis is to investigate the ability of a discrete ring and spring numerical model to simulate the ground-liner interaction phase of the tunnel liner design process. The model is to be compared with analytical ring and plate solutions and finite element solutions for both deep and shallow soft ground conditions.

Three different ground responses are to be analysed in order to establish the most appropriate representation to use in the spring model. Two spring arrrangements are considered, one with radial springs only, and the other including both radial and tangential springs.

The other aspect of the model which requires correct definition is the loading appropriate for given interface conditions and relative depth ratio.

The final objective is to establish the appropriate modifications to a design procedure (Negro, 1988) in order to define the parameters required for the spring model to be used as an alternate procedure for the liner-interaction phase.

1.3 Scope

In Chapter 2 the various aspects of the loading considerations are addressed and a broad classification of existing approaches to soil-lining interaction analyses is presented. Particular attention is given to the class of the ring and spring models and in Chapter 3, a description of

the components and the specific assumptions used in the discrete ring and spring model are presented.

In Chapter 4, the model is assessed in deep tunnel conditions by comparisons with available analytical solutions.

The results of the ring and spring model simulations of shallow tunnel situations are given in Chapter 5. An analytical ring and plate solution and a finite element analysis provide the basis for the comparison. The conservatism associated with the commonly used partially embedded spring model is established.

For temporary liners, an assessment is made of the ground stiffness reduction and stress release due to the tunnel excavation by following the design procedure proposed by Negro (1988). A slight modification of the procedure guidelines permits the evaluation of the spring constants directly, and a well documented case history is used to provide an example calculation to evaluate spring stiffnesses and loads required as input for the ring and spring approach.

A brief summary and conclusions can be found in Chapter 6.

2. AVAILABLE METHODS FOR PREDICTING LINING LOADS

2.1 Introduction

In this chapter, the general assumptions underlying the various liner (or support) design models for soft ground conditions are addressed. A classification of available methods for predicting the actions to be resisted by the liner is presented and provides the framework for a review of the specific design models which are brought into focus in this thesis.

Complementing empirical approaches are many analytical and numerical techniques that can be used to mathematically simulate the ground-liner interaction behaviour. Varying design requirements according to the proposed tunnel construction and use, and the different simplifying assumptions necessarily made to effect a solution have been instrumental in promoting proliferation of methods. Evidently, no one procedure is available which can adequately model all aspects of the tunnelling problem.

The empirical approaches provide a valuable reference basis against which the more mathematical approaches are evaluated. The analytical solutions are relatively uncomplicated to use, but the associated highly idealized assumptions limit their applicability. Expanding technology of computer capabilities has enabled numerical techniques to become very popular in recent years. Sophisticated simulation of problems is possible, but these analyses can

be quite costly, time consuming, complex and difficult to perform and interpret.

It would appear that any approach must be used with healthy discernment. It must be applicable to the problem at hand. The results must be interpreted properly. It is essential, therefore, to be familiar with the anticipated tunnelling conditions and to be sure that the proposed method of analysis can adequately simulate these.

2.2 Design Considerations

2.2.1 General

Within the context of this script, 'soft' ground is defined (Negro, 1988:1) as being any incompetent, soil-like material which would require continuous support in order to maintain the stability of an excavation. The design objective is to provide an economical, structurally sound and serviceable lining for the expected lifetime of the tunnel. By considering the interactive factors of the in situ environment, construction methodology and the lining system itself, the designer selects an appropriate model to analyse the problem at hand. Some of the fundamental aspects applicable to all models are briefly discussed in the remainder of this section.

2.2.1.1 Design Components

Usually the design considerations for tunnels in soft ground include the assessment of three major components (Negro, 1988:288): the stability of the excavation, the structural capacity and serviceability of the support system, and the integrity of existing structures and utilities in the vicinity.

Although these requirements are interactive, it is possible to highlight the more dominant influence in each. Stability is largely a function of the construction technology. The definition of the liner (or support) is principally determined by the magnitude and distribution of the applied loads acting on the tunnel liner. The damage potential to nearby buildings and services is associated with the deformation field induced by the excavation process.

Following the definition adopted by O'Rourke et.al. (1984:12), tunnel liners are differentiated as being for initial or final support. Initial support is installed to establish a stable opening for construction operations. Final support is used to ensure long term stability and serviceability requirements.

The geotechnical aspect of assessing the loads on the tunnel support is more strongly evident in the design of the initial support. It is generally assumed that the controlling influence in determining the operational loads for the initial support results from the interaction process

between the soil and the lining. The design of the final
support considers this interaction also, but more critical
situations may arise from changing physical conditions
occurring over the service life of the tunnel. Such effects
would include surcharge from future buildings, unloading
from adjacent excavations, readjustment of the ground water
regime, time dependent soil behaviour and liner decay.

The focus of the investigations in this thesis is
directed towards the liner response in the ground-liner
interaction process. The loads which are shared between the
liner and the ground according to their relative
stiffnesses, are generated by the excavation process. The
"excavation" loading condition describes the release of the
in situ stresses around the tunnel contour when an
excavation is performed in a medium which is initially
stressed.

2.2.1.2 Liner Behaviour

The structural failure of a circular lining which has
good contact with the surrounding ground generally results
from reaching some limiting combination of thrust and
bending. Shear and buckling failure modes are not normally
observed in shallow tunnels with liners of this type (Peck,
1969; Deere et al., 1969; after Negro, 1988:293) although
MacGregor (1988) has observed shear failures in precast
concrete storm sewers. Primarily then, the capacity of the
liner is dimensioned to resist critical combinations of the
thrust forces and moments generated in response to the

applied loading. Serviceability criteria are assessed with respect to acceptable deformations or diameter changes developing under these same loads.

The commonly adopted assumption of linear elastic behaviour to describe the lining response usually leads to a conservative design. However, the actual degree of conservatism is not excessive in view of the modern design approach promoting flexible linings which attract relatively small bending moments (Negro, 1988:294).

Throughout this work, the lining is assumed to behave in a linear elastic manner. The liner description is further constrained by its consideration as a continuous circular element.

2.2.2 'Shallow' and 'Deep' In Situ Stress Fields

The distinction between 'shallow' and 'deep' tunnelling conditions varies considerably according to the criteria used to identify this boundary. (Negro, 1988:163)

Described in relation to a horizontal ground surface, the three principal stresses in the soil prior to excavation are mutually perpendicular with orientations that are vertical and horizontal. The horizontal principal stresses are assumed to act parallel and perpendicular to the tunnel axis. The magnitude of the vertical stress is equal to the weight of the overburden, γz, where z is the depth of a point below the surface. The horizontal stress is the product of the vertical stress with the in situ stress

ratio, K_o. In Figure 2.1(a), the broken circular contour of radius, R, represents a section through the tunnel axis indicating the location of the future tunnel lining. The cover depth, H, is measured from the ground surface to the tunnel crown.

By assuming that zero longitudinal displacements occur parallel to the tunnel axis, a two-dimensional condition of plane strain is realized. This assumption is commonly found in ground-liner interaction analyses and facilitates the expressions for the in situ stress distribution acting on the future tunnel contour.

Ideally deep conditions are those in which the influence of the ground surface and the increase of the gravitational stress gradient across the tunnel profile from crown to invert are negligible. The in situ stresses for deep conditions are described in polar co-ordinates in Figure 2.1(b). The expressions for radial stress, σ_r, and shear stress, τ, acting on the imaginary contour of radius R are, for $\theta=0$ at the crown,

$$\sigma_r = \frac{1}{2}\gamma z\{(1+K_o)+(1-K_o)\cos2\theta\} \qquad [2.1]$$

$$\tau = \frac{1}{2}\gamma z(1-K_o)\sin2\theta \qquad [2.2]$$

In addressing the idealized behaviour of shallow tunnels, Negro (1988:163) draws the following conclusions:

"(a) when studying the tunnel lining response or the

(a) rectangular coordinates

$K_o = 0.5$
$Z/R = \infty$

normal stress

$$\sigma_r = \frac{1}{2}\gamma z\{(1+K_o)+(1-K_o)\cos2\theta\}$$

shear stress

$$\tau = \frac{1}{2}\gamma z(1-K_o)\sin2\theta$$

(b) polar coordinates

Figure 2.1 Insitu Stresses Around an Ideally Deep Circular Tunnel Prior to Excavation (after Negro, 1988: modified)
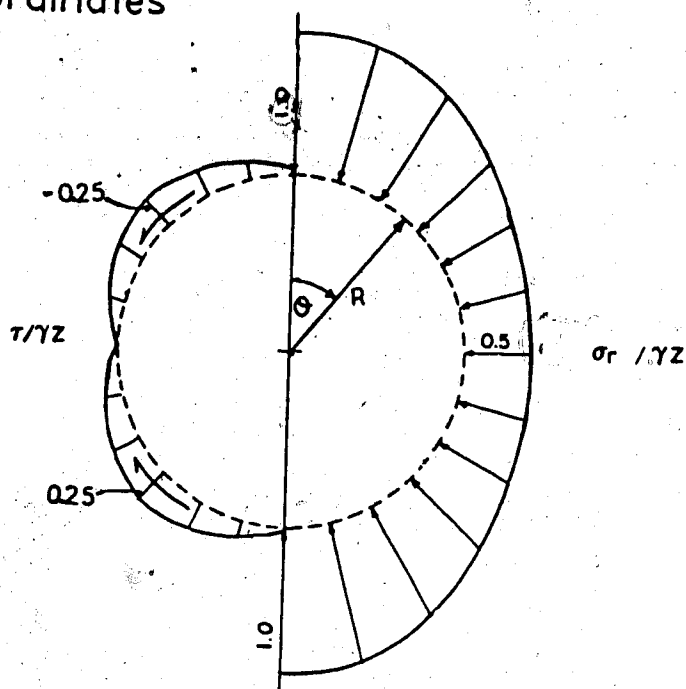
behaviour of the ground immediately around the opening; the presence of the stress free ground surface can be neglected for relative tunnel depths (H/D) of greater than 1.5 where D is the diameter. However, the influence of the gravitational stress gradient should always be taken into consideration.

(b)when studying the displacement field around a tunnel or the possible mode of collapse of the ground, the effect of the ground surface as well as the action of gravity should always be considered."

In a shallow tunnel, the gravity action dictates that the symmetry of the in situ stress field exists about the vertical axis only. This is illustrated in Figure 2.2. The expressions for the radial stress, σ_r, and shear stress, τ, differ from equations [2.1] and [2.2] respectively by the inclusion of the terms which account for gravity, where for $\theta=0$ at the crown,

$$\sigma_r = \tfrac{1}{2}\gamma z\{(1+K_o)+(1-K_o)\cos2\theta\}-\tfrac{1}{4}\gamma R\{(3+K_o)\cos\theta+(1-K_o)\cos3\theta\} \quad [2.3]$$

$$\tau = \tfrac{1}{2}\gamma z(1-K_o)\sin2\theta - \tfrac{1}{4}\gamma R(1-K_o)(\sin\theta+\sin3\theta) \quad [2.4]$$

2.2.3 Physical Ground Response Near the Tunnel Face

It has already been mentioned in Section 2.2.2 that a plane strain condition is commonly accepted in practice. For sections further away than about two tunnel diameters ahead

(a) rectangular coordinates

(b) polar coordinates

normal stress

$$\sigma_r = \frac{1}{2}\gamma z\{(1+K_o)+(1-K_o)\cos2\theta\}-\frac{1}{4}\gamma R\{(3+K_o)\cos\theta+(1-K_o)\cos3\theta\}$$

shear stress

$$\tau = \frac{1}{2}\gamma z(1-K_o)\sin2\theta - \frac{1}{4}\gamma R(1-K_o)(\sin\theta+\sin3\theta)$$

Figure 2.2 In Situ Stresses Around a Shallow Circular Tunnel Prior to Excavation (after Negro, 1988:modified)

of or behind the face, this assumption provides an adequate description of the prototype.

The 2-D analytical models generally assume instantaneous excavation and liner activation, and that the full in situ stress distribution provides the load input for the soil-liner interaction process. These boundary conditions assume that no radial displacement occurs prior to the interaction phase.

In actual tunnels, the assumption of zero longitudinal displacement is violated in the active excavation zone close to the face. Radial displacements and stress reduction have already occurred even if the liner could be activated right at the face. Further displacements occur in practice because of the delay associated with installing the lining. The input parameters of the two-dimensional models enable the user to take account of the processes but typically the various methods of doing this differ in source and applicability.

Negro (1988) proposes a logical process to account for the 3D effects in two dimensional models, and this is described and used in Chapter 5 of this thesis.

2.2.3.1 Longitudinal Component Displacement

Typically the stress and st   responses for a tunnel excavation can be zoned accordi   r the behaviour is predominantly two or three di   Plane strain conditions would exist when the lon   dinal displacements parallel to the tunnel axis were zero. This enables analyses

to be performed by considering only the displacements occurring in a plane section perpendicular to the tunnel axis.

However, in the vicinity of the advancing face, the longitudinal component of the induced displacements is non zero. This leads, for example, to concerns regarding the face and heading stability (Negro, 1988:127). Here, a region of three dimensional stress-strain behaviour exists which is apparent both ahead of and behind the advancing face. The extent of this zone will vary depending on several parameters, but available evidence reported by Negro (op. cit.:2,175) permits the regions to be approximately defined. With tunnel liner activation specified to occur at one diameter (2R) behind the face, most tunnels exhibit predominantly three-dimensional behaviour within the region bounded by one to two diameters ahead of the face to one diameter behind the location of liner activation as shown in Figure 2.3. The longitudinal movement of the ground ahead of the advancing face is towards the face. As the face passes the point in question, the soil starts moving back to its original position (Ranken and Ghaboussi, 1975; Branco, 1981; Heinz, 1984; after Negro 1988:124). Field measurements indicate that the final differential longitudinal movement tends to be small (Eisenstein and Branco, 1985:58), but it is obvious that if the soil is strain path dependent, its behaviour is not completely described in a two dimensional representation (Branco, op.cit.).

direction of advance

approximate transition zone of 3-D behaviour

2-D behaviour

2-D behaviour

~2R to 4R

~2R

~2R

radius

liner

specified location of liner activation

future tunnel contour
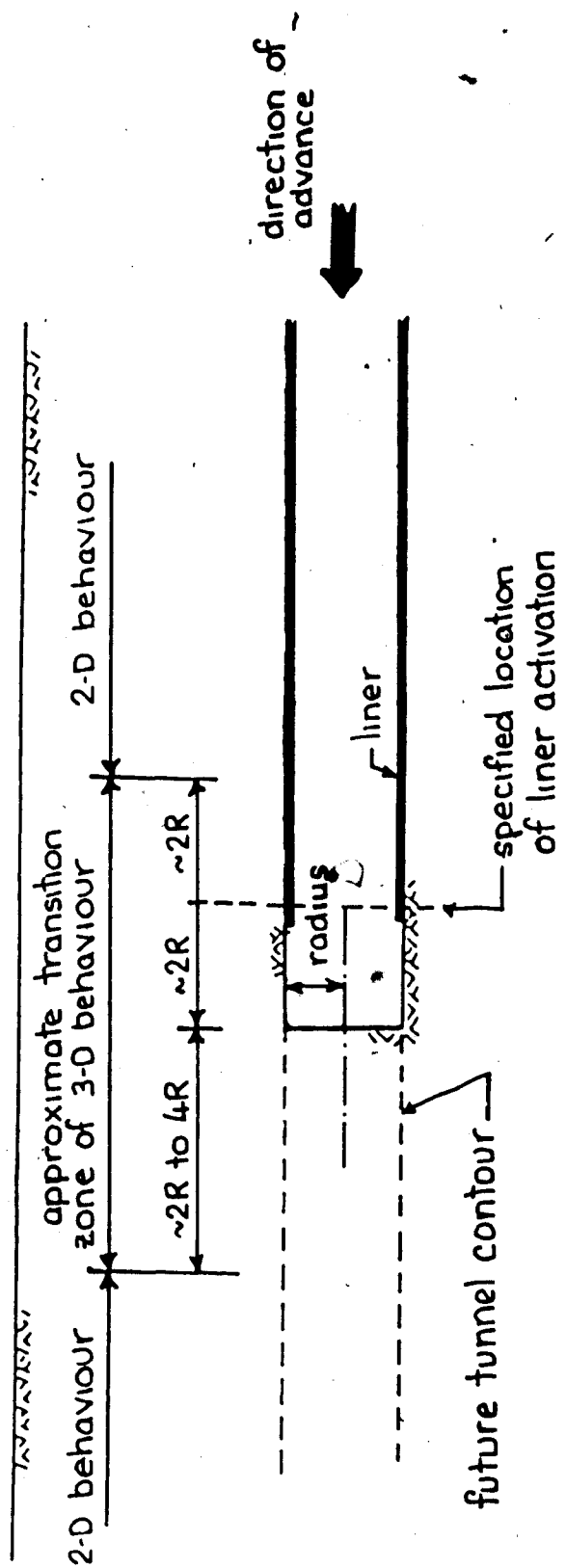
Figure 2.3 Longitudinal Profile of Excavation with

Approximate Zoning of Two and Three Dimensional Behaviour
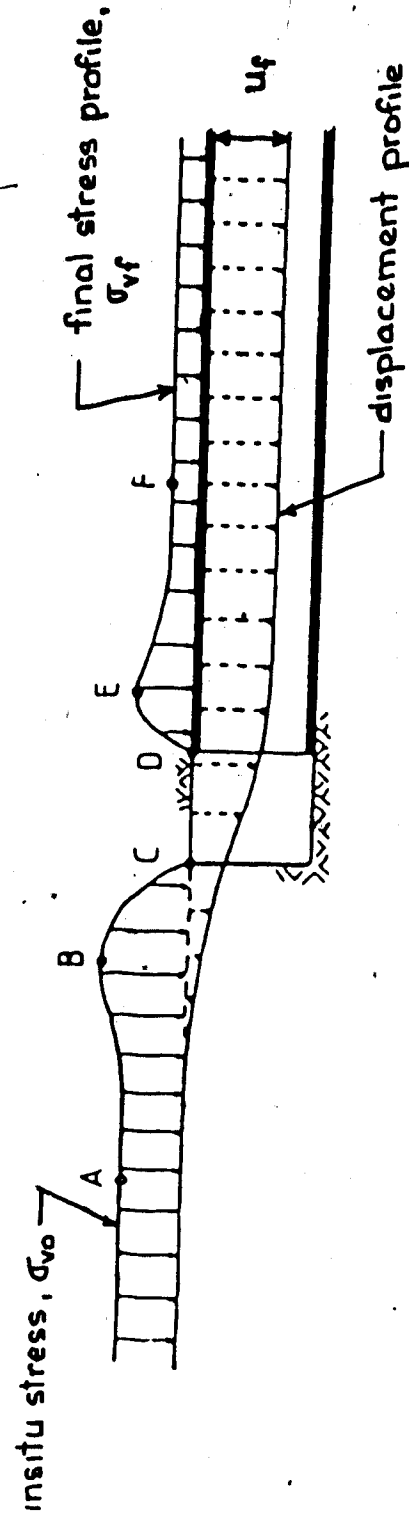
Figure 2.4 Vertical Stress and Displacement Distributions along the Crown (Eisenstein et. al. 1984, after Negro 1988; modified)

2.2.3.2 Longitudinal Profile of Radial Displacement Distribution

The assumption of zero initial radial displacement is often implicitly imposed in model formulations. The validity if this assumption is affected by the radial crown displacement profile parallel to the tunnel axis. The excavation process provokes a movement of surrounding ground into the tunnel opening. The three-dimensional nature of the displacements close to the advancing face allow the radial displacements to be initiated ahead of the face. The radial crown displacements in a longitudinal profile are illustrated in Figure 2.4. Liner activation and consequent interaction allow the induced ground displacements to stabilize in equilibrium with the liner. This equilibrium displacement is indicated as u_f in the same figure.

2.2.3.3 Longitudinal Profile of Radial Stress Distribution

The picture becomes a little more complete by exploring the radial stress changes occurring along the tunnel crown. Apart from possible stress concentrations at points B and E in Figure 2.4 due to arching over the unsupported length, CD, the vertical in situ stress, σ_{vo}, existing at A, falls to zero at C. It remains at this value along the unsupported heading, C-D. Subsequent ground-lining interaction promotes an increase in vertical stress to attain equilibrium conditions at F with an associated magnitude, σ_{vf}.

2.2.3.4 Summary

In spite of the marked three dimensional behaviour close to the face, the assumption of plane strain is reasonable for sections at a distance of greater than two diameters from the face (Ranken and Ghaboussi, 1975; after Negro, 1988:126). The remaining discussion is concerned with the two dimensional plane strain representation.

2.2.4 Soil-Liner Interaction

2.2.4.1 Stiffness Ratios

Soil-liner interaction is a consequence of the resistance that the liner mobilizes against the movement of the surrounding ground mass into the excavated opening. When the liner is installed, the stiffness of the global system changes. Interaction between the soil and the lining allows displacements leading to distributions of external stresses acting on the liner which are different from the original in situ conditions. An equilibrium condition will eventually be achieved which, in part, is dependent on the relative stiffness of the soil and the lining. This stiffness is normally defined in terms of compressibility (C) and flexibility (F) ratios. Several formulations for C and F exist.

The formulation presented by Einstein and Schwartz (1979:501) for these ratios shall mostly be used here. It considers the stiffness of a perforated ground mass which

These expressions are:

$$C' = \frac{ER(1-\nu_s^2)}{E_s A_s(1-\nu^2)} \qquad [2.5]$$

$$F' = \frac{ER^3(1-\nu_s^2)}{E_s I_s(1-\nu^2)} \qquad [2.6]$$

where E, ν and E_s, ν_s are elastic constants for the ground and support respectively, A_s, I_s are the cross sectional area and moment of inertia of the support per unit length of tunnel and R is the radius. Note that a rigid liner corresponds to C=F=0.

The expressions in equations 2.5 and 2.6 reflect that the lining can interact with the soil in two ways. The compressibility ratio describes the soil-liner system stiffness under a symmetric loading condition, so that a circular lining deforms in axial compression with no bending. The flexibility ratio reflects the flexural stiffness of the system in response to a purely asymetric loading condition.

When comparing with other approaches which assume a different formulation of the stiffness ratios, the differences must be taken into account.

2.2.4.2 Ground-Liner Interface Conditions

At the instant of liner installation, the physical radial and tangential contact between the lining and the surrounding ground mass will also influence how the in situ stresses alter to provide the loading conditions that are

resisted by the liner. By defining the extreme contact conditions for a given set of liner properties and K_o, a range of loadings can be bounded which contains the expected response.

A full radial contact condition providing a complete embedment of the liner is to be preferred in practice since this would prevent load concentrations which cause additional bending in the liner.

Two extreme circumstances can be recognized with respect to the shear strength available at the interface between the soil and lining. The situation where no relative tangential displacement occurs between the soil and lining is referred to as the "no-slip" condition and is approximately realized when the maximum mobilized shear stress does not exceed the available interface shear strength. Assuming that this interface shear strength is zero defines the condition of "full slip" and physically implies that the relative tangential movement between the two components can occur freely.

Negro (1988:101) argues that in prototypes, the interface condition more likely approaches the no slip case. This is based on considerations of the outer surface roughness associated with liners which permit full ground contact and the fact that the mobilized shear stresses tend to be relatively small particularly in view of the stress release and displacements that occur as a consequence of the delay in liner installation.

In this thesis, full radial contact will be assumed to exist and the problem will be bounded by considering no slip and full slip cases.

2.2.5 External Loads Acting on the Lining

In the analyses, the assumptions of plane strain conditions, a continuous circular lining profile and linear elastic behaviour for the lining and soil mass are made. In describing the loadings that the liner recognizes, it is further assumed that the excavation and liner installation occur instantaneously and simultaneously so no ground displacement takes place prior to ground-liner interaction. This is shown in Figure 2.5 in a manner that allows comparison with Figure 2.4. The distributions of in situ stresses acting on a cylinder of soil representing the future tunnel contour have been illustrated in Figures 2.1(a) and 2.2(b) for deep and shallow conditions respectively. When assessing the loads to be supported by the liner, it is convenient to refer to these in situ stress states. Except in special instances, the induced stress distributions to be supported by the liner are different from the preconstruction ground conditions.

2.2.5.1 Ideally Deep Tunnel Conditions

In general terms, a very rigid liner does not deform significantly and so the original stresses applied to the liner will not alter much. The lining is therefore required to resist moments created by the difference between the
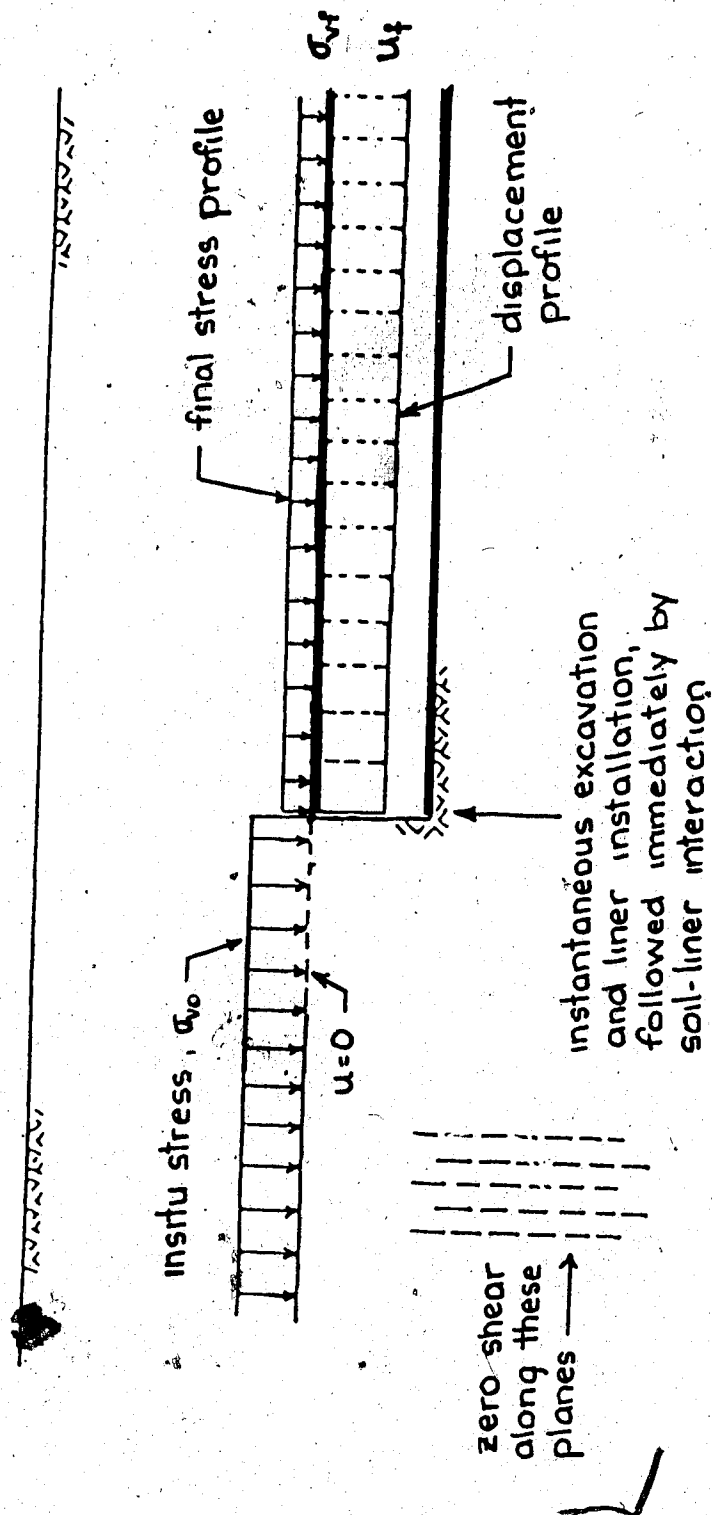
Figure 2.5 Assumed Longitudinal Stress and Displacement
Distributions for Establishing Liner Loads in 2D Model

horizontal and vertical stresses. In contrast, a relatively
flexible liner deforms and allows stress redistributions
which result in negligible bending moments in the lining.

For a rigid and incompressible liner (F=C=0) installed
in a soil mass having an insitu stress ratio of unity, the
stresses acting on this support will equal the in situ
stresses regardless of the interface condition.

If K_o is different from unity, then the two cases of
interface conditions must be taken into consideration. Under
a no-slip situation, the same rigid liner will be required
to support a stress distribution as described by the in situ
state shown in Figure 2.1. Under the above assumptions, the
ground mass is effectively 'unaware' of its altered
circumstances.

If the interface shear is now reduced to zero for the
rigid liner, thus allowing full slip, the stress
distribution imposed on the rigid lining will be different
from the in situ stress state. The associated redistribution
of normal and shear stresses is described by Ranken
(1978:60) and Negro (1988:90) and is discussed here as it is
fundamental to understanding the loading distributions.

For clarity, consider K_o to be less than unity. In the
no slip condition, the interface strength is such that the
soil adheres to the lining and no relative movement occurs.
If the interface strength is nulled, then the soil must move
in order to regain overall system equilibrium. The laws of
nature dictate that the movement will be from regions of

higher pressure to lower so the tangential 'flow' of the soil will be from the crown and floor towards the springline (see Figure 2.6). This will have the effect of enhancing the normal pressures in the crown and floor regions, and the action of the soil migrating away from the springline will decrease the normal pressures acting there. The opposite movements will occur when K_o is greater than 1.

Note that no displacements of the rigid liner have occurred (F=C=0), so that for K_o different from unity, the altered stress distribution shown in Figure 2.7(b) is due to the full slip interface condition alone.

Most linings do not conform to this unique recipe. Deformations and stress changes generally occur in response to the applied loading with the resulting equilibrium condition depending on the relative stiffness of both interacting components. Recall from Section 2.2.4 that these are expressed by means of the flexibility and compressibility coefficients. Allowing the soil to displace with the liner permits mobilization of shear resistance within the soil mass. Such encouragement of the soil to provide some self support alters the so-called arching process which will reduce the magnitude of the stresses applied to the liner. The dynamics of the load exchange occurring between the soil and liner indicate that the interaction process is complex and interdependent.
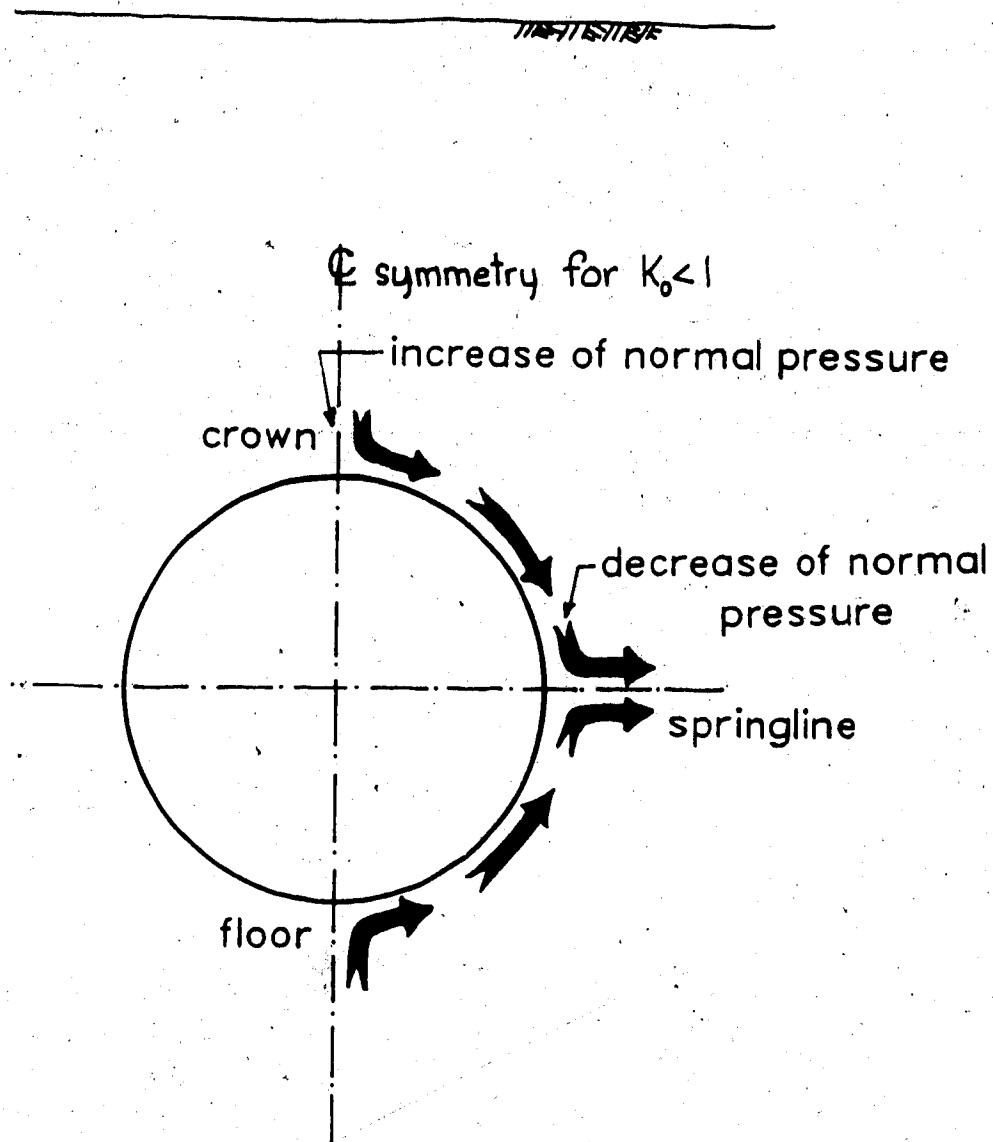
Figure 2.6 Soil "Flow" Around Rigid Liner for Full Slip
Condition

2.2.5.2 Shallow Tunnel Conditions

In this discussion, the effect of the stress free surface boundary is ignored, so that the distinguishing features of shallow tunnel analysis are a consequence of the gravitational stress gradient only.

The introduction of a lining demonstrates one such special feature. The lining recognizes a resultant upward force equal to the weight, $\gamma \pi R^2$ per unit length, of the excavated material. Because of this, a rigid liner (F=C=0) installed prior to any displacement will be required to sustain normal and shear stress distributions which are different from the in situ stress state shown in Figure 2.2, even for the no-slip condition. The normal stresses acting on the crown will increase while those applied at the floor decrease. The shear stress distribution also alters, increasing in the shoulder regions and decreasing in the haunches. The resulting distribution on the rigid liner is shown in Figure 2.8.

The buoyancy response is most pronounced for a rigid liner. For more common liner configurations, the response is tempered in accordance with the relative stiffness parameters.

The overall tunnel heave is an artefact of elastic analyses where the creation of the opening and liner installation occur simultaneously. The effect tends to be suppressed in real tunnels since the liner installation is delayed and non homogeneous ground conditions occur.

$\sigma_r = \frac{\gamma z}{2} \{(1+K_o)+(1-K_o)\cos2\theta\}$

$\tau = \frac{\gamma z}{2}(1-K_o)\sin2\theta$

(a) no slip

$\sigma_r = \frac{\gamma z}{2} \{(1+K_o)+\lambda(1-K_o)\cos2\theta\}$

$\tau = 0$

(b) full slip

$K_o < 1$
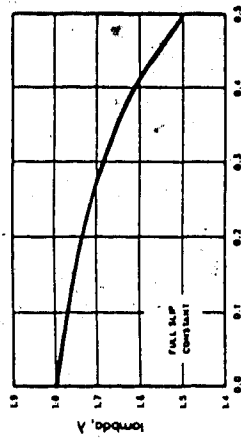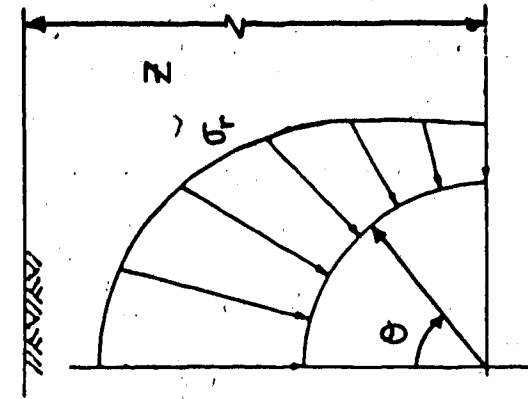
Figure 2.7 Stress Distribution Around a Rigid Liner of an
Ideally Deep Tunnel

normal stress

$$\sigma_r = \frac{1}{2}\gamma z\{(1+K_o)+(1-K_o)\cos2\theta\}-\frac{1}{4}\gamma R\{(1+K_o)\cos\theta+(1-K_o)\cos3\theta\}$$
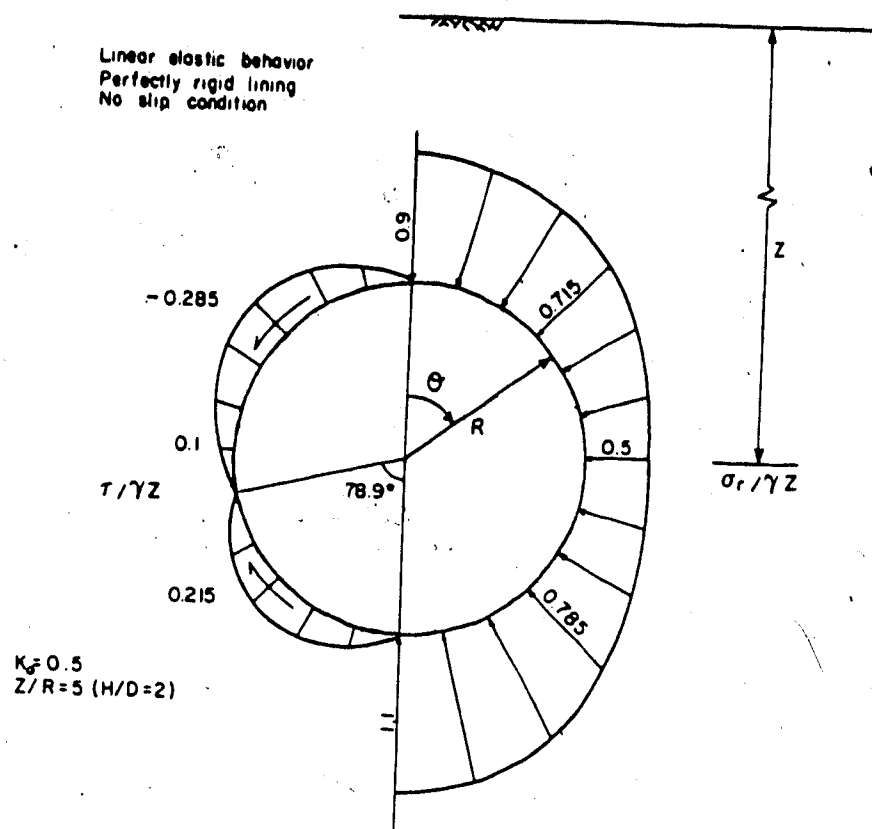
shear stress

$$\tau = \frac{1}{2}\gamma z(1-K_o)\sin2\theta + \frac{1}{4}\gamma R\{(1+K_o)\sin\theta-(1-K_o)\sin3\theta)\}$$

Figure 2.8 Stress Distribution Around a Rigid Liner of a Shallow Tunnel (after Negro, 1988:modified)

2.3 Classification of Methods

2.3.1 General

Because of the many approaches available for lining load prediction, it is convenient to present a classification of some typical examples which enables the ring and spring model to be seen in perspective.

Figure 2.9 is a reproduction from Negro (1988:332) and distinguishes five main groups according to the calculation procedure on which a particular method is developed.

2.3.2 Empirical and Semi-Empirical Methods

These approaches include the earth pressure theories and the methods in which the lining performance is specified beforehand.

2.3.2.1 Earth Pressure Theories

In this approach, it is usual for the ground loads to be considered as independent of the ground displacements and for the lining-ground interaction to be ignored. The applied loading corresponds to poor ground control conditions in which large displacements lead to substantial shear strength mobilization in the ground mass. The use of these theories in practice seems to be waning in favour of methods which include the ground-lining interaction and acknowledge that the loads are dependent on the occurring displacements. They might provide useful guidelines once calibrated with field data for specific conditions existing at a particular site
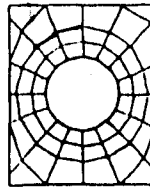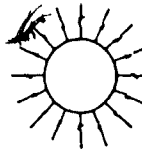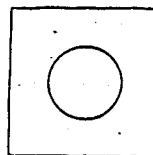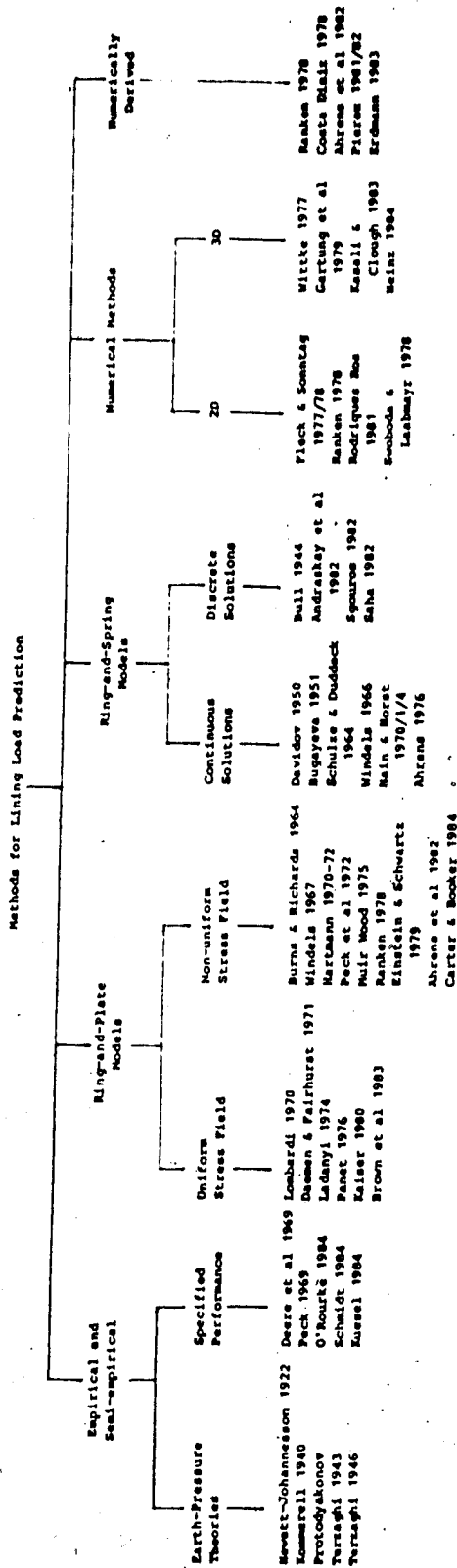
Figure 2.9 Classification of Some Typical Examples of

Methods for Lining Load Prediction (after Negro,

1988:modified)

and may be utilized to extrapolate experience within the
vicinity. Such results may be inappropriate outside the
boundaries for which they were established.

2.3.2.2 Methods which Specify Tunnel Performance

These methods recognize the ground-liner interaction
and are applicable under conditions of good construction
quality and flexible liner design. In this approach, a
circular tunnel lining is to be designed for a uniform ring
compression corresponding to the overburden pressure at the
springline, plus an imposed distortion measured as a
percentage change in the lining radius. The focus of the
method is on the distortions being acceptable in terms of
the lining serviceability requirements. It is possible to
assume this attitude because appreciable passive resistance
is mobilized within the soil mass at displacement magnitudes
which are much smaller than those associated with causing
lining distress. Two anomalies are evident in the underlying
assumptions (Negro, 1988:343). Firstly, the consideration of
full overburden is arguable under conditions of good lining
contact and good ground control. Secondly, the assumption of
uniform ring compression is in conflict with the need to
account for moments generated by the imposed distortion. In
spite of these drawbacks, this type of approach is felt to
provide a useful tool in the preliminary dimensioning of a
lining.

2.3.3 Ring and Plate Models

2.3.3.1 General

In these models, the ground is represented by a plate and the support in a circular opening is represented by a continuous ring. These solutions are subdivided into two categories according to whether the in situ stress field is uniform or non-uniform. In both cases, they are analytically developed as closed form solutions which are considered easy to handle. They assume a state of plane strain which simulates a section of the tunnel far from the advancing face and is therefore unaffected by the three dimensional stress transfer mechanisms associated with the active excavation zone. All the available solutions assume the plate to be of infinite extent, but the presence of a stress free ground surface has little effect on lining loads for cover to diameter ratios of greater than 1.5. Most of the approaches neglect the gravitational stress gradient, so that they can be applied only to ideally deep tunnels in which the increase of in situ stress with depth from crown to invert is negligible.

2.3.3.2 Uniform Stress Field Solutions

By assuming the in situ stress ratio, K_o, to be unity and ideally deep conditions, the ground reaction and the support reaction can be evaluated independently. Both responses are assessed with respect to the radial stresses and displacements at the tunnel contour with the equilibrium

of the interaction process being described by the
intersection of the two curves representing the ground
reaction and the support reaction. This class of solutions
form the "convergence-confinement" models and the simplicity
generated by excluding the lining distortion makes room for
more elaborate representations of the ground response. The
liner response is typically treated as linear elastic. The
major limitation of this approach for shallow tunnel
conditions lies in the adoption of a uniform stress field.
ch a stress field prevents the approach from providing an
essment of the moments which develop in the lining.

2.3.3.3 Non-Uniform Stress Field Solutions

Most of these solutions have been surveyed by a number
of authors and a useful summary of these is presented by
Negro (op. cit.:Table 4.6). This subgroup includes solutions
in which the in situ stress ratio, K_o, differs from unity or
the stress non-uniformity is due to gravity. The inclusion
of these distortional aspects provides these solutions with
enhanced generality, but requires that simple linear elastic
material behaviours be used for the lining and ground. All
solutions are derived assuming a plane strain condition. The
liner is assumed to be installed in close contact with the
surrounding ground prior to any displacement development. In
recognition of this unlikely situation in reality, some
approaches have evolved to account for the displacements
which occur prior to lining installation.

Most solutions consider an "excavation loading" condition where the opening is excavated and supported after the stress field is applied to the plate. This is an appropriate representation for the tunnelling prototype. Other solutions consider an "overpressure loading" scheme whereby the opening and support are in existence prior to the application of the stress field. This would simulate culvert construction with backfilling, or delayed surcharge conditions applied to an existing tunnel. The majority of the solutions consider both interface shear conditions of full-slip and no-slip. Most also assume the lining to be a thin membrane whose behaviour is approximated by thin shell theory, which although easier to manipulate, is not as rigorously correct as the thick liner developments. However, both approaches give essentially identical results provided the ratio of the lining thickness to mean lining radius is smaller than 0.1 (Ranken 1978:312). Some approaches use second order theories, but generally the resulting second order terms can be neglected for common lining thicknesses.

The most complete set of solutions for the deep tunnel situation is provided by Ranken (1978), which include overpressure and excavation loading options, both ground-lining interface conditions, and thick and thin liner assumptions. The correct excavation loading solutions from various sources for deep tunnels virtually coincide for values of thrust and moment. This is expanded further in Chapter 4.

While all solutions account for K_0 different from unity
in some form or other, the full account of gravity is seen
only in one approach. This is the solution by Hartmann
(1970, 1972:after Negro, 1988:356) which includes the heave
caused by unbalanced vertical stresses.

2.3.4 Ring and Spring Models

Similar to the ring and plate models, a condition of
plane strain prevails, non-uniform stress fields can be
applied and the support is represented by a ring, but in
this class of models the ground is portrayed by springs.
Conceptually, the soil stiffness is related to the stiffness
of the spring members which, when subjected to loads,
provide reactions which depend on the displacements.

Two approaches to the analysis of ring and spring
models are identified according to whether the ring
embedment provided by the springs is discrete or continous.
In the discrete approach, a finite number of springs is used
and the liner is described by a piecewise linear frame.
Figure 2.10 is a sketch of such a ground-lining interaction
system in which the ring is embedded at 16 discrete points.
The solution to this is procured numerically and is greatly
facilitated by the use of computer programs for frame
analysis.

If the number of springs is infinite, then a continuous
embedment conditions is realized with a fully circular
lining profile. As well as using numerical approaches, the

radial spring
member

liner (or support)
member
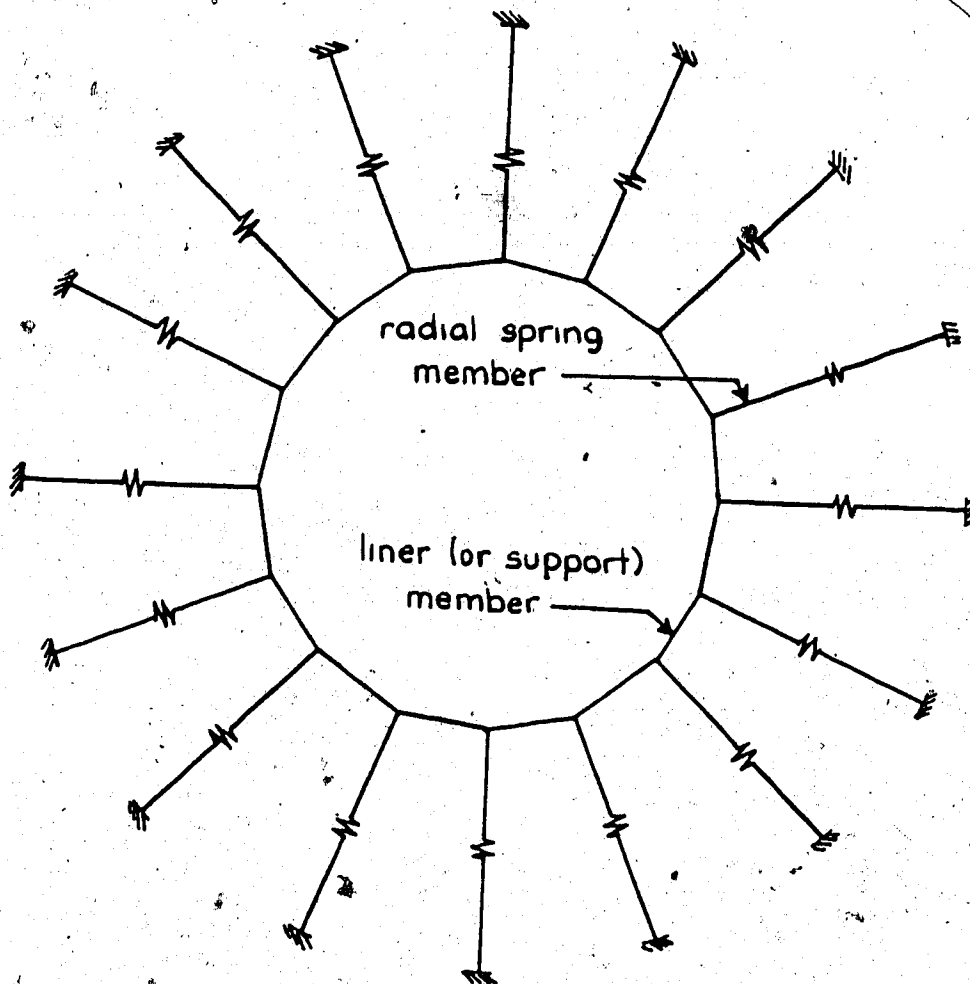
Figure 2.10 Fully Embedded Discrete Ring and Spring showing
Support Confinement at Sixteen Locations

solution can be derived analytically by treating the liner as an elastically embedded shell.

Many of the ring and spring models have been extensively reviewed, particularly by authors hailing from West Germany where the models have seen most of their development. Much attention has been paid to the comparison of the spring models and the plate and it is seen that an equivalence between the two is possible provided the ground reaction is continous and tangential springs are included in the spring model analysis (Duddeck and Erdmann, 1985:252).

All things being equal, if tangential springs are included in the model, it is anticipated that a stiffer ground response will be realized so that the loads carried by the liner are reduced. Most models use only radial springs to provide the ring embedment and this assumption is expected to lead to a safer estimate of the lining moments and thrusts.

It is possible to include the influence of the interface conditions of full-slip or no-slip by applying the appropriate stress distribution as active loads onto the system. The altered stress distribution due to the full-slip interface condition is discussed in Section 2.2.5 and the concepts are applied in Chapter 4.

The loading conditions assumed fall broadly into two categories. One assumes a localized concentration of material resting over the crown region, such as that associated with loosened ground loads and neglects other in

situ stresses. The second category adopts an all round stress distribution, mostly as the full in situ value. Negro (1988:364) records that some authors assume a proportionally reduced distribution (Andraskay et.al., 1972), some include a full account of gravity (Hain and Horst, 1970, 1971, 1974), and others partly account for gravity in order to eliminate the buoyant effect of the tunnel in shallow conditions (Schulze and Duddeck, 1964; Windels, 1966 after Erdmann, 1983:35).

Most models of both categories assume a partially embedded system in which no springs act to support the ring over the crown 90° region. Because active springs respond to share the applied loading with the ring, a region devoid of embedment requires that the ring carries the full load associated with this region.

The ring and spring models present the opportunity for a variety of facets of particular lining configurations to be addressed. Several authors have capitalized on this and the following are cited by Negro (op.cit.) Non-linear behaviour of the liner (Ahrens, 1976; Sgouros, 1982), second-order effects due to bending deformations and liner contraction as a result of tangential compression (Ahrens, 1976; Windels, 1966) and consideration of non-circular profiles (Hain and Horst, 1970; Andraskay et.al., 1972) represent features that might reasonably predominate in specific tunnelling systems.

One general limitation associated with this group is an inability to account for the stiffness and stress reductions occurring prior to lining activation as is the case with other two-dimensional approaches. A specific drawback lies in the selection of a relationship linking the ground stiffness to the representative spring stiffness. Further attention is given to this aspect in Chapter 3.

2.3.5 Numerical Methods

These are methods which make use of procedures such as finite element analyses for the prediction of lining loads. They differ from the numerical solutions adopted in the discrete ring and spring models in that the lining and the ground are both treated as a continuum. Along with other features this constitutes a major asset of this group of solutions since the lining loads and the ground displacement field are able to be obtained simultaneously. Both two and three dimensional analyses are possible, but the complexity associated with the latter detracts from its potential for practical use. Also, at times, it may be more appropriate to use the solutions provided by the simpler ring-and-plate or ring-and-spring procedures.

However, in modelling shallow tunnelling conditions, the numerical methods are very much favoured. The use of finite element techniques in shallow tunnel design is covered extensively by Negro (1988:Chapter 5).

Once again, accounting for the three dimensional
effects in the more practical two dimensional methods is the
predominant concern of this group.

2.3.6 Numerically Derived Methods

In the development of these methods, sensitivity
studies covering ranges of values of influencing variables
are performed using numerical procedures. The results are
generalized for the given spectrum of conditions by using
dimensional analysis. The subsequent normalized coefficients
provided by such parametric analyses allows bending moments
and thrusts, for example, to be evaluated for other
configurations which comp within the original conditions.
Negro (1988:939) uses such an approach in the development of
his design method.

3. THE RING AND SPRING MODEL

3.1 Introduction

As an introduction to ring and spring models, a description of the traditionally accepted configuration for such models used in designing shallow soft ground tunnel supports is presented in Section 3.2. The most striking feature of the traditional ring and spring models is the assumption that the soil over the crown region is unable to mobilize any arching resistance when the support deflects inwards at the crown. In other words, a condition of soil failure is accepted in the soil over the crown. This is represented in the model by having no springs in the corresponding region as shown in Figure 2.1(b(i)).

The justification for studying a discrete ring and spring model results from the synopsis of the International Tunnelling Association's survey of existing practice (Duddeck, 1981). The soft ground sections of this survey, also reinterpreted by Negro (1988), indicate that the discrete ring and spring model is the most popular method for assessing lining loads in shallow tunnels.

The versatility of the model allows assessments of many varied aspects arising from such sources as irregular liner geometry or properties, segmental linings and soil stratification.

If "good ground control conditions" (Negro, 1988:166) are realized in the tunnelling operation, the soil in the

42

crown region normally will provide some self support by arching. The soil consequently carries a portion of the loads rather than transmitting all of the soil self weight to the liner in the vicinity of the crown. In many tunnelling operations, these boundary conditions are perhaps more appropriate than accepting the recommended partially embedded approach. The geometric representation for this analysis uses a fully embedded ring and spring model with active springs in the crown region. These springs carry part of the applied loads in response to inward deflection of the liner. Such a model is described in Sections 3.4 and 3.5.

The behaviour of the soil is assumed to be linear elastic. In these analyses it is convenient to relate the deformation, u, occurring as a result of an imposed stress, σ, as a ratio, σ/u. This is defined as the "spring constant", k, of the soil. It is worth stressing that the spring constant is describing the soil behaviour only.

The spring constant can be used to determine the modulus of elasticity of the springs for the ring and spring model. This is done by calculating the stiffness of the springs required to produce the same amount of displacement, u, caused by the same stress, σ. This relationship is established in Figure 3.4.

A brief parametric study presented in Section 3.6 indicates that the inclusion of tangential springs in the model serve to reduce the maximum moments and thrusts to be resisted by the liner.

A description of the computer program, Plane Frame
Truss (PFT), used to process the numerical analyses is given
in Section 3.7. This completes the description of the fully
embedded model which will be compared with analytical deep
and shallow solutions in Chapters 4 and 5.

3.2 Existing Practice in Selection of a Design Model

As seen in the preceding chapter, many design methods
are available for the design of linings in soft ground
tunnels. Apart from the empirical approaches, the methods
are based on a soil representation as a continuum or as
springs.

An assessment of lining design practice was performed
by a task group of the International Tunnelling Association.
The results of questionnaires sent in 1978 to participating
members is reported in a synopsis by Duddeck (1981).
Subsequent investigations (Duddeck and Erdmann, 1982, 1985)
into the most commonly used design models, report a
convergence of opinion towards the basic assumptions
underlying soft ground tunnel design and also towards the
selection of a design model which is appropriate for the
prevailing conditions.

Duddeck and Erdmann's (op.cit.) recommendations are
summarized below, but it can be appreciated that several of
these are open to debate.

The assumptions which are generally considered
appropriate to design models for tunnels in soft ground,

are:

1. It is sufficient to consider plane strain conditions for the lining and the ground.

2. The soil pressures acting on the lining are equal to the full in situ stresses in the undisturbed ground for long term loading. Consideration of factors such as cohesion, stiffness, excavation procedure, relative depth and time to ring closure may justify load reductions.

3. Equilibrium and compatibility conditions are both met by consideration of the interface bond between the soil and the lining.

4. The ground-lining interaction process produces lining deformations which result in reaction stresses in the ground. This effect is accounted for in the spring models by assigning appropriate stiffnesses to the spring members. If the consequent load sharing is assumed not to occur, then the bedding provided by springs is neglected where inward deflection occurs.

5. The material behaviour of the ground and lining are generally assumed to be linear elastic.

Duddeck and Erdmann (1982, 1985) propose the following guidelines for the selection of an appropriate design model. These are shown in Figures 3.1(a) and (b).

<u>(i) For Shallow Tunnels:</u> $H < 2.5D$

A model without reduction of the ground pressure at the crown or an equivalent continuum (finite element) model may be appropriate.

(ii) For Moderately Deep Tunnels: $1.5D \leqslant H \leqslant 4.5D$

The use of a deep continuum model may be proposed with the full in situ stresses applied to the structural model.

(iii) For Deep Tunnels: $H \geqslant 2.5D$

A deep continuum model with a certain amount of reduction of the in situ stresses may be appropriate.

The depth boundaries overlap in all three cases so reductions can be made to the applied loads on the liner according to the various influencing parameters already described. It is seen in Section 5.3 that these recommendations provide a very conservative and discontinuous design envelope when compared with approaches which are perhaps more appropriate.

For the shallow tunnel conditions described in (1) above, the partially embedded ring and spring model is seen to be used in several different ways. A selection of approaches is illustrated in Figure 3.2 where it is seen that the differences arise mostly in the assumed loads (or stress distributions) applied to the frame representing the liner.

The approaches favoured by Bull (1944), Bugayeva (1951) and Rosza (1963) apply the dead load of the soil in the crown region only which effectively ignores the existence of

the stress gradient across the opening. Schulze and Duddeck
(1964), and Windels (1966) approximate the stresses created
by excavating a core of soil and apply this stress
distribution around the entire tunnel contour. Their
approximations both assume the stress distribution is
symmetric about the horizontal axis. This allows the gravity
effects to be partly accounted for and yet eliminates the
effect of the overall tunnel heave which was discussed in
Section 2.2.5.1. As a consequence, the analytical solutions
are simpler and more compact.

3.3 Constituent Components of Stress Distributions

3.3.1 Deep Conditions

The assumption of linear elastic behaviour enables a
non-uniform in situ stress distribution around the future
tunnel contour to be resolved into constituent parts. For
deep conditions, the decomposition is as shown in Figure 3.3
where the normal stress is the sum of a symmetric component
and a distortional ($\cos 2\theta$) component, and the shear stress
is described by the shear ($\sin 2\theta$) component.

3.3.2 Shallow Conditions

For shallow conditions, the expressions include the
effect of the gravitational stress gradient which alters
both the normal and shear stress distributions. These are
given as equations 2.3 and 2.4 in Chapter 2 and are

obviously more complicated. Various approximations have been
used to simplify these and yet still endeavour to represent
these shallow conditions. Table 3.1 gives the in situ
stresses for deep and shallow conditions. Also shown are the
approximations used by Schulze and Duddeck (1964) and
Windels (1966) to simplify their analytical solutions.

3.4 Selection of Discrete Ring and Spring Model

In searching for a ground-lining interaction model to
incorporate into his shallow tunnel design method, Negro
(1988) reinterpreted the soft ground tunnelling sections of
the ITA survey synopsis (Duddeck, 1982). Among other
conclusions, Negro (1988) identified the popularity of the
discrete ring and spring models for the prediction of
thrusts and moments in the final support for shallow
tunnels.

The discrete ring and spring model cannot reasonably
compete with the ease afforded by the analytical ring and
plate solutions in simple geologic, geometric and loading
conditions. The versatility of the spring model comes into
account when conditions become more complex when it can
provide assessments of the relative influence of various
parameters.

The ability to define member end fixity enables
segmental liners with low moment capacity joints to be
modelled. The individual description of member properties
permits irregularities in cross section to be assessed. The

Table 3.1 Radial And Tangential Stress Components on Future Tunnel Contour

	σ_{ro}	σ_{r2}	
DEEP	$\frac{\gamma z}{2}(1+K_o)$	$\frac{\gamma z}{2}(1-K_o)\cos 2\theta$	$\frac{\gamma z}{2}(1-K_o)\sin 2\theta$
SCHULZE & DUDDECK (1964)	$\frac{\gamma}{2}(1+K_o)\left[z - 0.3R \cdot \frac{(3+K_o)}{(1+K_o)}\right]$	$\frac{\gamma}{2}[z(1-K_o) - 0.3R(3+K_o)]\cos 2\theta$	$\frac{\gamma z}{2}(1-K_o)\sin 2\theta$
WINDELS (1966)	$\frac{\gamma}{2}(1+K_o)\left[z - \frac{R}{1+K_o}\right]$	$\frac{\gamma}{2}(1-K_o)\left[z - \frac{R}{(1-K_o)}\right]\cos 2\theta$	$\frac{\gamma}{2}(1-K_o)(z - 0.707R)\sin 2\theta$
SHALLOW	$\frac{\gamma z}{2}[(1+K_o) + (1-K_o)\cos 2\theta] - \frac{\gamma R}{4}[(3+K_o)\cos\theta + (1-K_o)\cos 3\theta]$		$\frac{\gamma z}{2}(1-K_o)\sin 2\theta - \frac{\gamma R}{4}(1-K_o)(\sin\theta + \sin 3\theta)$

Note: Expressions are given for $\theta = 0$ at the Crown.

Table 3.1 Radial And Tangential Stress Components on Future Tunnel Contour

(i) shallow   (ii) moderately deep   (iii) deep

(a) geometry

(i) without reduction   (ii) continuum model   (iii) continuum model
of ground pressures   with full insitu   with reduced
at crown   stresses   insitu stresses
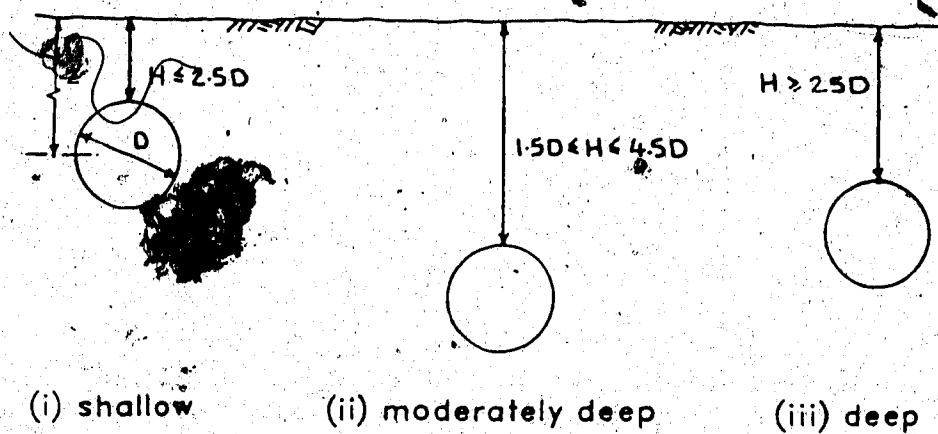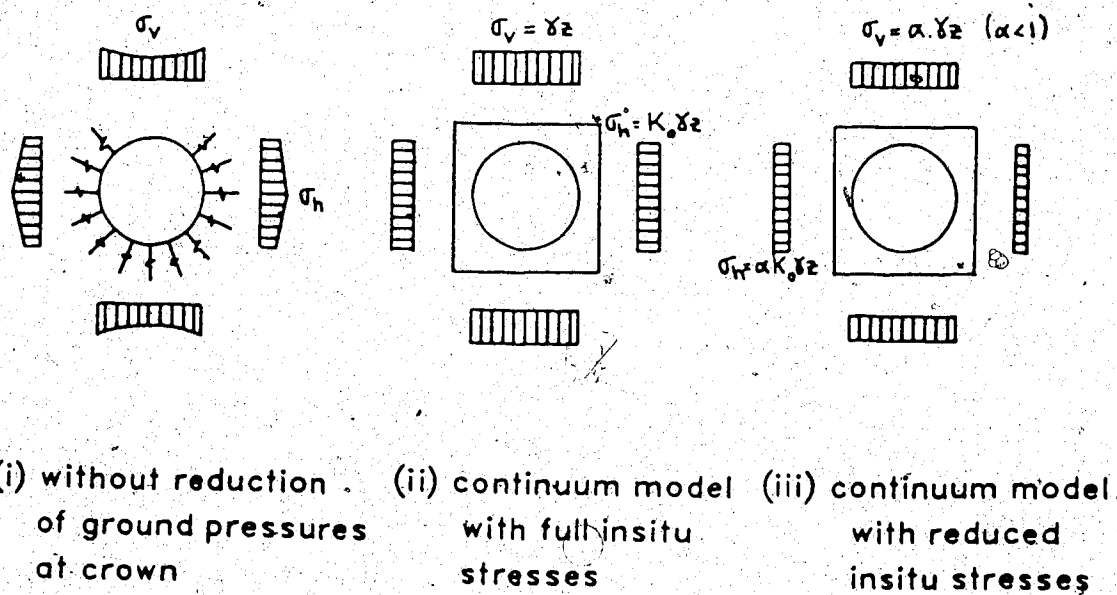
(b) recommended plane strain structural model

Figure 3.1 Commonly Accepted Recommendations for Soft Ground
Tunnel Liner Design
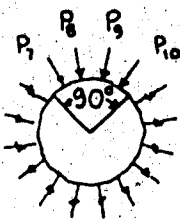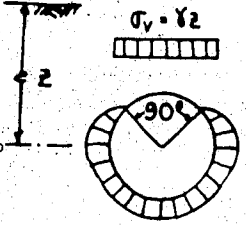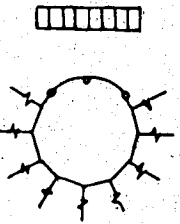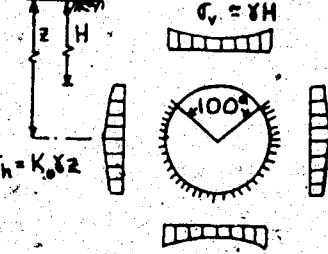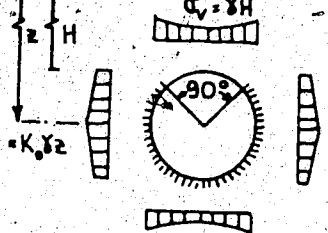
Bull (1944)		Discrete ground reaction provided by radial springs. Partial embedment with no springs in crown 90°. Soil loads $(P_1, \ldots P_n)$ applied all around contour as discrete radial and/or tangential forces at midpoint of linear segments. (Note, only P_7 to P_{10} are shown for clarity)
Bugayeva (1951) (after Szechy 1967)	$\sigma_v = \gamma z$	Continuous ground reaction which is compatible at floor and springline only. Partial embedment - crown 90° Active load at crown only No springs in crown 90°.
Rosza (1963) (after Duddeck 1972)		Discrete ground reaction Partial embedment Active load at crown
Schulze & Duddeck (1964)	$\sigma_v = \gamma H$ $\sigma_h = K_o \gamma z$	Continuous ground reaction Partial embedment - crown 100° Active applied loads assume equal radial stresses at floor and crown which are approximately equal to overburden, γH. Partial account of gravity eliminates heave. May or may not include shear stress.
Windels (1966) (after Erdmann, 1983)	$\sigma_v = \gamma H$ $\sigma_h = K_o \gamma z$	Continuous ground reaction. Partial embedment - crown 90° Crown and floor radial stress equal to overburden, γH. Radial insitu stress at SL. Partial account of gravity. Optional shear stress.

Figure 3.2 Selection of Ring and Spring Models and their Loading Approximations for Shallow Conditions

$$\sigma_{r\theta} = \frac{\gamma z}{2}(1+K_o)$$

(i) symmetric

$$\sigma_{rz} = \frac{\gamma z}{2}(1-K_o)\cos 2\theta$$

(ii) distortional

$$\tau = \frac{\gamma z}{2}(1-K_o)\sin 2\theta$$

(iii) shear
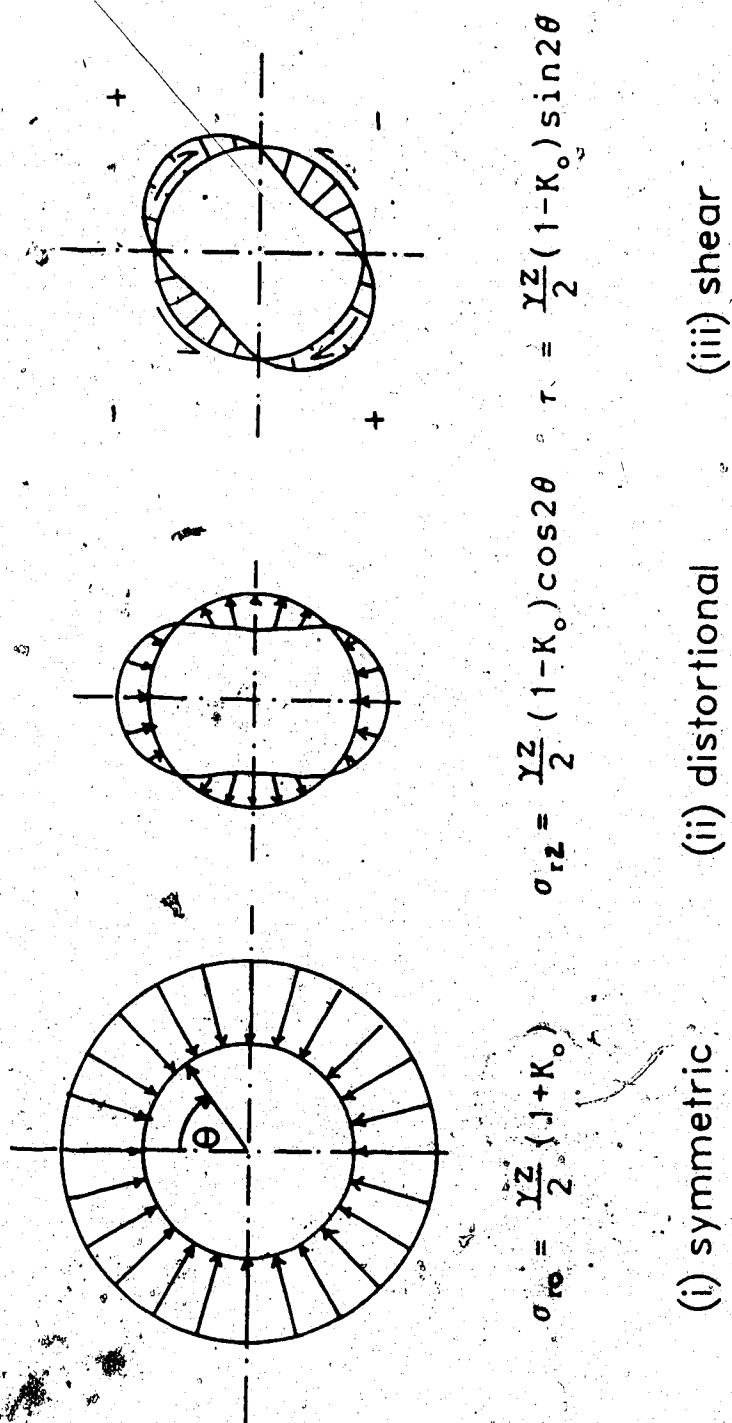
Figure 3.3 Components of a Deep Non-Uniform In Situ Stress Distribution (after Erdmann, 1983:modified)

options available from varying the spring stiffness include modelling different soil strata, assessing softened or weakened regions selectively around the tunnel contour and permits the popular embedment separation assumption to be effected in the upper crown quarter.

The flexibility in defining the geometry of the profile enables non-circular openings to be considered and by using a spring member which links two liners, it can potentially describe twin tunnel lining systems.

The predominant drawback of the discrete ring and spring model lies in defining the springs to represent the soil response. The ground is not a linear elastic material and the assumption that it is introduces error. However, in view of the lack of accuracy with which the soil properties and behaviour are typically known, this simple approach is justified.

3.4.1 The Spring Constant of the Soil

By assuming the soil behaviour is described by linear elasticity, the applied stress, σ, is uniquely related to the induced displacement, u, as a constant ratio, $k = \sigma/u$. This property of the soil is called the "spring constant" within this script, although different terminologies will be found elsewhere. A stress distribution existing around the tunnel opening will induce a corresponding soil displacement.

Examples of stress distributions around a tunnel
opening are the components given in Figure 3.3. The induced
displacements may be different for each case, so that ratio,
σ/u, defining the spring constant, k, will vary. The stress
distributions given in Figure 3.3 and their associated
displacements, are appropriate to describe the soil response
in a deep "unlined" tunnel opening, or describe the response
of an opening with an infinitely flexible liner.

With the liner installed, the stress distribution
components will alter according to the liner stiffness and
will depend on the interface slip conditions. These
conditions define the spring constants associated with a
deep "lined" tunnel.

In summary, the spring constant is defining the soil
response according to the ratio of stress to the induced
displacement. This varies according to whether the tunnel
opening is unlined or lined, and if lined, whether the
soil-liner interface provides full slip or no slip
conditions.

3.4.2 Representation of the Soil Response in the Ring and Spring Model

In the ring and spring model, the springs are used to
represent the soil response. The properties of the springs,
in particular the stiffness, E_{sp}, must therefore be
compatible with the soil response.

The spring constant, $k = \sigma/u$, describing the soil response can be used to determine an appropriate stiffness, E_{sp}, for the spring member of the ring and spring model. This is implemented by estimating the stiffness, E_{sp}, required in the spring to produce the same displacement, u, under the load equivalent to the stress, σ, defining k. The relationship and its assumptions are developed as shown in Figure 3.4 to produce the following equality:

$$k = \frac{E_{sp}}{R} \qquad\qquad [3.1]$$

where R is the length of springs and is taken equal to the tunnel radius.

In the usage of the ring and spring model prior to the early 1980s, the value chosen for the spring constant took serveral different forms. Most commonly, it was arbitrarily related to the constrained modulus, D, of the soil which was the recommendation through German literature of the time. This gives the spring constant as:

$$k = \frac{D}{R} = \frac{(1-\nu)}{(1+\nu)(1-2\nu)} \cdot \frac{E}{R} \qquad\qquad [3.2]$$

where E, ν are the tangent modulus and Poisson's ratio of the soil respectively.

In some analytical ring and plate approaches (eg. Muir Wood, 1975; Morgan, 1961), the liner is to deform

For a linear elastic material, define the soil spring constant

$$k = \sigma/u$$

i.e. stress, σ, causes displacement, u.

A spring member of the ring and spring model has an elastic modulus, E_{sp}. The displacement of the spring member caused by force, P is

$$u = \frac{P \cdot L_{sp}}{E_{sp} \, A_{sp}}$$

where A_{sp}: area of the spring member
L_{sp}: length of the spring member

For the soil displacement to be compatible with the spring displacement:

$$\frac{\sigma}{k} = \frac{P \cdot L_{sp}}{A_{sp} \, E_{sp}}$$

For equivalent load, $\sigma = \dfrac{P}{A_{sp}}$

Therefore

$$k = \frac{E_{sp}}{L_{sp}}$$

It is customary to arbitrarily set the spring length, L_{sp}, equal to the radius of the tunnel, R.

When this is done:

$$k = \frac{E_{sp}}{R}$$

Figure 3.4 Relationship Between the Soil Spring Constant and the Spring Stiffness of the Ring and Spring Model

into an ellipse. The radial stress, σ, associated with this deformed shape produces corresponding displacements

$$u = \frac{(1+\nu)}{3} \cdot \frac{R}{E} \cdot \sigma$$

In this case, it would be possible to describe the soil response as the spring constant

$$k = \frac{\sigma}{u} = \frac{3}{(1+\nu)} \cdot \frac{E}{R}$$

Other authors (for example Ebaid and Hammad, 1978; Sungur, 1984 after Negro; 1988:371) elect the spring constant to be:

$$k = \frac{1}{1+\nu} \cdot \frac{E}{R}$$

This originates from the convergence of a deep tunnel in elastic ground under a uniform stress field and corresponds to the symmetric component given in Figure 3.3.

The above expressions for k are either arbitrary or model only a portion of the load system.

Duddeck and Erdmann (1982, 1985) report that a full correspondence exists between the analytical ring and plate solutions and the continuously embedded ring and spring models. Ahrens et.al. (1982 after Erdmann 1983:27) establish spring constants for the soil response around an incompressible (C'=0) liner for both full slip and no slip

interface conditions. To obtain the matching solutions for the incompressible liner conditions, the model needed to have both radial and tangential springs.

To obtain a full correspondence for flexible liners, it is necessary to include the soil-lining interaction response with its dependence on the relative stiffness parameters and the interface conditions of full and no slip.

Erdmann (1983:90) generalizes the no slip conditions to include the influence of liner compressibility. The equations given in Section 3.4.3.3 indicate that the spring constants are essentially independent of the flexibility of the lining.

3.4.3 The Spring Constants for Constituent Stress Modes - Deep Tunnels

A non-uniform in situ stress state can be separated into constituent components. The decomposition for deep conditions is shown in Figure 3.3. The response of the ground and lining to each of these constituent modes is different so the resulting spring constant defining the behaviour is distinct for each stress pattern.

When the tunnel is excavated, in situ radial and shear stresses are both released at the tunnel walls. In the symmetric component the distortional effects are not considered, but they must be taken into account when deriving the spring constants associated with the radial distortional component and the shear (tangential

distortional) component.

3.4.3.1 Spring Constant for Symmetric Stress Component

In an unlined tunnel, the hydrostatic part of the in situ stress, σ_{ro}, causes an inward radial displacement, u_{ro}, of the tunnel contour, where

$$u_{ro} = \frac{(1+\nu)}{E} \cdot R \cdot \sigma_{ro}$$

When the support interacts with the ground, these radial stresses are partially restored according to the interaction parameters, so that an outward pressure, σ_{ro}', is exerted on the ground with corresponding displacements

$$u_{ro}' = \frac{(1+\nu)}{E} \cdot R \cdot \sigma_{ro}'$$

In both the lined and unlined tunnel responses, the form of the equations identifies the spring constant as

$$k_{ro} = \frac{1}{(1+\nu)} \cdot \frac{E}{R} \qquad\qquad [3.3]$$

3.4.3.2 Spring Constants for Distortional Stress Components - Unlined Tunnel

The expression describing the radial distortional stress component is $\sigma_{r2} = \bar{\sigma}_{r2}\cos2\theta$. The corresponding inward radial displacement which occurs in an unlined tunnel is

$$u_{r2} = \frac{(1+\nu)(3-4\nu)}{E} \cdot R \cdot \sigma_{r2}$$

allowing the associated spring constant to be defined as

$$k_{r2u} = \frac{1}{(1+\nu)(3-4\nu)} \cdot \frac{E}{R} \qquad [3.4]$$

Similarly, the shear stress component $\tau = \bar{\tau}\sin2\theta$ produces tangential displacements

$$u_t = - \frac{(1+\nu)(3-4\nu)}{E} \cdot R \cdot \tau$$

The negative sign enters the expression since the direction of the resulting displacements is opposite to the sense of the applied stress. Thus,

$$k_{t2u} = - \frac{1}{(1+\nu)(3-4\nu)} \cdot \frac{E}{R} \qquad [3.5]$$

Note that these expressions apply equally to a tunnel which has an infinitely flexible liner. Such a liner would not provide any resistance to the soil deformations.

3.4.3.3 Spring Constants for Distortional Stress
Components - Lined Tunnel

Ahrens et.al. (1982) developed expressions for the spring constants for the soil response around an incompressible liner (C'=0) liner, and recognizes the interface conditions of full slip and no slip.

In the full slip situation, only the radial stresses are partially restored and the tangential stresses are zero. The spring constants describing the soil response are

$$k_{r21\text{-}FS} = \frac{3}{(1+\nu)(5-6\nu)} \cdot \frac{E}{R} \tag{3.6}$$

and

$$k_{t21\text{-}FS} = 0 \tag{3.7}$$

For no slip conditions, partial restoration of both distortional and shear stresses occur and the resulting spring constants for the soil response around an incompressible liner are identified as

$$k_{r21\text{-}NS} = \frac{3(1-\nu)}{(1+\nu)(3-4\nu)} \cdot \frac{E}{R} \tag{3.8}$$

and

$$k_{t21\text{-}FS} = \frac{-3(1-2\nu)}{(1+\nu)(3-4\nu)} \cdot \frac{E}{R} \tag{3.9}$$

The tangential spring constant is negative for the reasons discussed earlier. For easy referencing, these equations are tabulated in Table 3.2, and the constants kR/E are presented in graphical form in Figures 3.5 and 3.6 for the radial and tangential expressions, respectively.

	Symmetric	Distortional	Shear
UNLINED	$k_{ro} = \dfrac{1}{(1+\nu)} \cdot \dfrac{E}{R}$	$k_{r2u} = \dfrac{1}{(1+\nu)(3-4\nu)} \cdot \dfrac{E}{R}$	$k_{t2u} = \dfrac{-1}{(1+\nu)(3-4\nu)} \cdot \dfrac{E}{R}$
LINED - NO SLIP	$k_{ro} = \dfrac{1}{(1+\nu)} \cdot \dfrac{E}{R}$	$k_{r2\ell-NS} = \dfrac{3(1-\nu)}{(1+\nu)(3-4\nu)} \cdot \dfrac{E}{R}$	$k_{t2\ell-NS} = \dfrac{-3(1-2\nu)}{(1+\nu)(3-4\nu)} \cdot \dfrac{E}{R}$
LINED - FULL SLIP	$k_{ro} = \dfrac{1}{(1+\nu)} \cdot \dfrac{E}{R}$	$k_{r2\ell-FS} = \dfrac{3}{(1+\nu)(5-6\nu)} \cdot \dfrac{E}{R}$	$k_{t2\ell-FS} = 0$

Ahrens et al. (1982)
for C' = 0)

Table 3.2 Radial and Tangential Spring Constants for Lined
and Unlined Tunnel Openings - Deep Conditions

The curve associated with the constrained modulus, D, is also included in Figure 3.5. The trend to be observed in both Figures 3.5 and 3.6 is that an increasing magnitude in the value of KR/E indicates a stiffer soil response. It is seen in Figure 3.5 for instance, that the curve for the constrained modulus represents a very stiff soil, especially as ν approaches 0.5.

Erdmann (1983:90) presents generalised expressions for the radial, k_{r2}, and tangential, k_{t2}, spring constants resulting from the distortional radial and shear stress components. These are formulated in the no-slip conditions to include the liner compressibility effects.

$$k_{r2} = \frac{6(1-\nu)+3(-4+6\nu)(I_s/A_sR^2) + (1/(1+\nu))(ER/E_sA_s)}{2(3-4\nu)(1+\nu)+(3-4\nu)(ER/E_sA_s)} \cdot \frac{E}{R}$$

[3.10]

$$k_{t2} = \frac{-3(1-2\nu)+(5-6\nu)(I_s/A_sR^2) + (1/(1+\nu))(ER/E_sA_s)}{(3-4\nu)(1+\nu)+3(3-4\nu)(1+\nu)(I_s/A_sR^2)+(3-4\nu)(ER/E_sA_s)} \cdot \frac{E}{R}$$

[3.11]

For an incompressible (C'=0) liner, equations [3.10] and [3.11] reduce to the expressions given by [3.8] and [3.9] respectively.

For an infinitely compressible liner (C=∞), equations [3.10] and [3.11] reduce to the expressions for an unlined opening given by [3.4] and [3.5], respectively.

Legend
- kro
- *kr2:LINED−NS
- *kr2:LINED−FS
- kr2:UNLINED
- CONSTRAINED MODULUS

C' = 0

*AHRENS ET AL.(1982)

kr*R/E

poisson's ratio, v
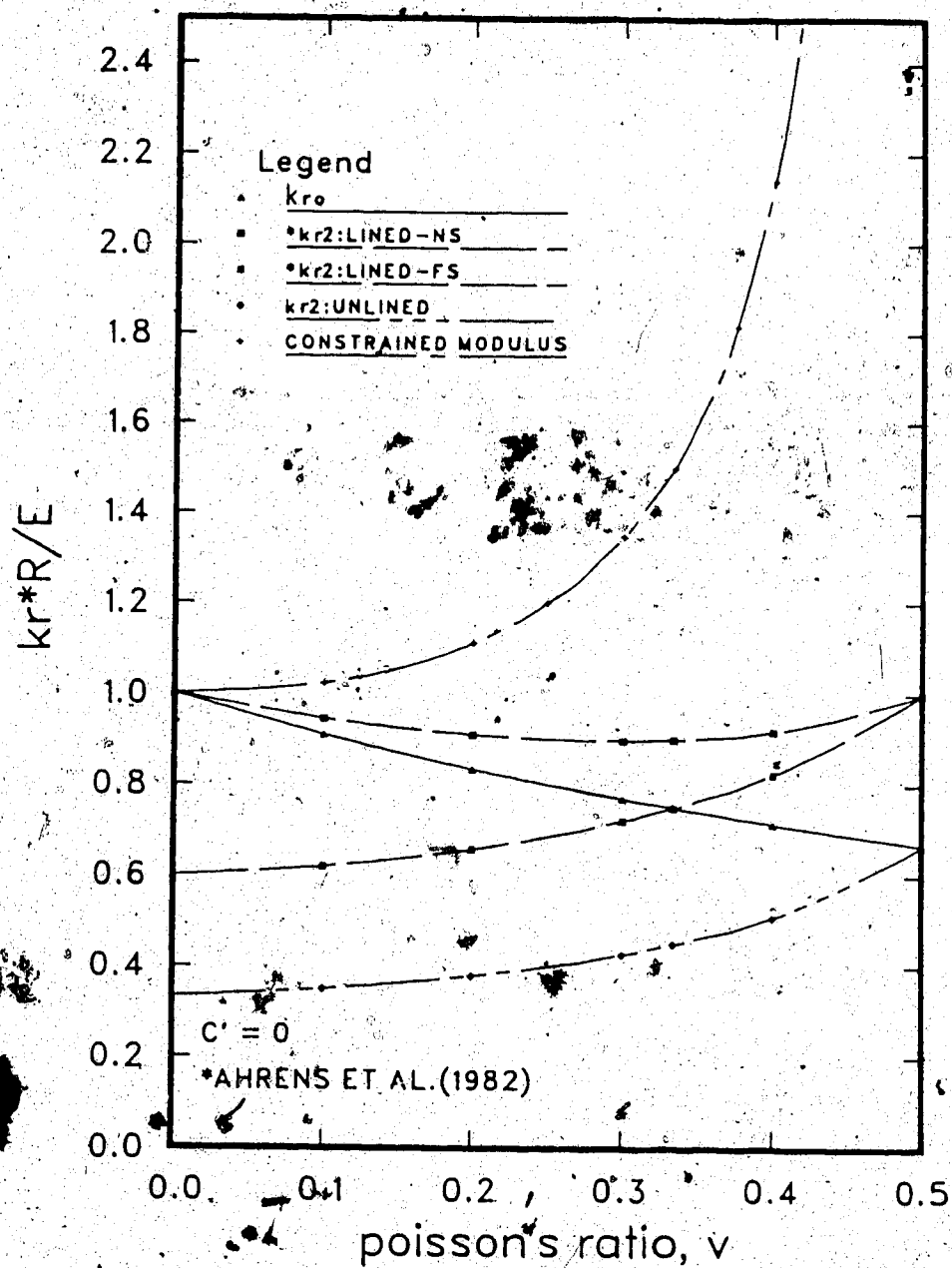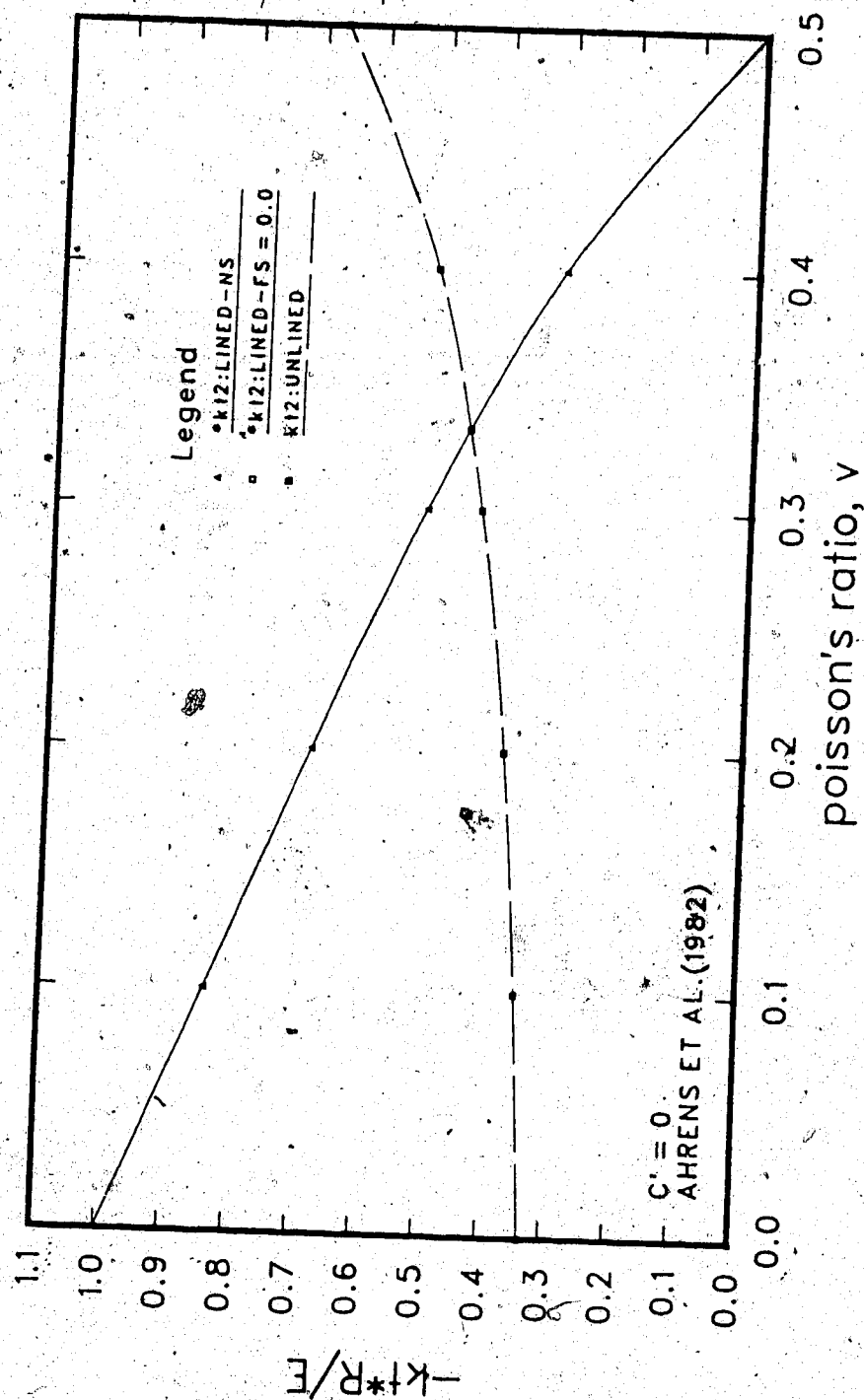
Figure 3.6 Spring Constants for Tangential Stress Components

3.4.3.4 Spring Constants for Combined Radial Stress
Component - Unlined Opening

Depending on the parameters being investigated, it may
be more convenient to describe a spring constant, k, which
is a function of θ, but which is applied to the combined
radial stress component. The displacements take the
arithmetic form, $u_r = u_{ro} + u_{r2}$, so that

$$\frac{\sigma_r}{k_r} = \frac{\sigma_{ro}}{k_{ro}} + \frac{\sigma_{r2}}{k_{r2}} \qquad [3.12]$$

For an unlined opening and substituting equation [3.3] into
equation [3.4] to give $k_{r2} = k_{ro}/(3-4\nu)$, equation [3.12]
becomes

$$k_r = k_{ro} \cdot \frac{\sigma_r}{\sigma_{ro} + (3-4\nu)\sigma_{r2}}$$

Cancelling $\gamma z/2$ in the expressions for σ_r, σ_{ro} and σ_{r2} gives

$$k_r = k_{ro} \cdot \frac{(1+K_o) + (1-K_o)\cos2\theta}{(1+K_o) + (3-4\nu)(1-K_o)\cos2\theta} \qquad [3.13]$$

The tangential spring constant can be expressed as

$$k_t = -\frac{k_{ro}}{(3-4\nu)} \qquad [3.14]$$

3.4.3.5 Summary - Deep Tunnels

Duddeck and Erdmann (1982, 1985) report that in order to obtain a complete correspondence between the continuous ring and spring models and the ring and plate analytical approaches, the interaction process with relative stiffness considerations and interface shear conditions must be accounted for. This cannot be achieved by considering only the deformation responses in an unlined opening.

The full correspondence necessitates using a fully embedded continuous ring and spring model and requires the corresponding stiffness matrix to include the tangential bedding for no slip conditions.

3.4.4 Spring Constants for Shallow Tunnel Model

In principle, it is possible to perform a similar process to that described in Section 3.5.1 to establish the spring constants for shallow tunnels. The ring and plate solution by Hartmann (1970,72 after Negro 1988:1117) includes the effect of gravity in its formulation and provides the analytical tool to establish these spring constants.

Negro (1988:372) derives expressions for the radial and tangential spring constants for unlined shallow conditions by differentiating the appropriate Hartmann equations. The resulting expressions for the combined radial spring constant, k_r, and for the tangential spring constant, k_t are given in Figure 3.7. By substituting $n=\infty$, the expressions
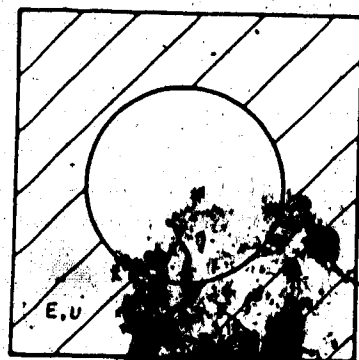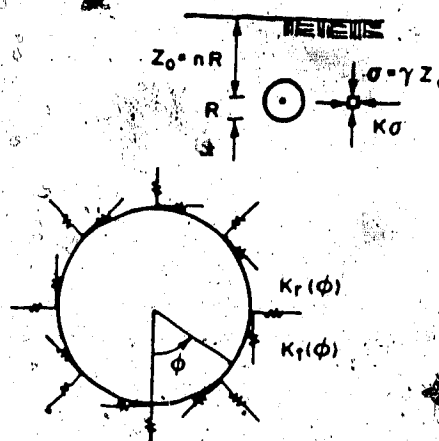
CONTINUUM MODEL   SPRING MODEL

$$K_r = K_{r0} \frac{\left[(1+K)(1+\frac{1}{2n}\cos\phi) + (1-K)(\cos2\phi + \frac{1}{2n}\cos3\phi) \right]}{\left[(1+K)(1+\frac{1}{4n}\cos\phi) + (3-4\nu)(1-K)(\cos2\phi + \frac{1}{4n}\cos3\phi) \right]}$$

$$K_t = K_{r0} \frac{\left[(1+K)\frac{1}{2n}\sin\phi - (1-K)(\sin2\phi + \frac{1}{2n}\sin3\phi) \right]}{\left\{ -(1+K)\frac{1}{4n}\sin\phi + (1-K)\left[(3-4\nu)\sin2\phi + \frac{1}{4n}\sin3\phi \right] \right\}}$$

with

$$K_{r0} = \frac{1}{1+\nu}\,\frac{E}{R} \qquad n = \frac{Z_0}{R} \qquad K = \frac{\sigma_H}{\sigma_V}$$

Figure 3.7 Spring Constants for Equivalence Between Ring and Spring Model and Analytical (Ring and Plate) Solution for Shallow Unlined Tunnel (after Negro, 1988:modified)

reduce to those for deep conditions given by equations
[3.13] and [3.14]. It is explained in Chapter 5 that the
lined response version of the spring constants is expected
to give values which provide unconservative estimates of the
liner actions. However, this may be confirmed by future
research work.

3.5 Geometry for the Discrete Ring and Spring Model.

If "good ground control conditions" (Negro, 1988:166)
prevail, then it is reasonable to assume that the soil above
the crown actively shares the loads distributed in the
ground-liner interaction process.

The ring and spring model which appropriately
represents these conditions is a fully embedded model with
active springs all round the lining contour. This is
preferred to the usual embedment separation assumption which
is equivalent to a fully collapsed and usually unacceptable
event in an urban area.

The fully embedded discrete ring and spring model
treats both the soil and the lining as linear elastic,
homogeneous materials. In the present work, the circular
lining is represented by a weightless, thin piecewise linear
polygonal frame of constant thickness. The ground mass
represented by 24 discrete radial springs at regular 15°
intervals, as shown in Figure 3.8.

The spring interval of 15° was selected after
comparative studies revealed that virtually no improved

accuracy was available with a smaller 5° spring spacing. Also, the 15° interval assumption has two nodes between the sections of maximum and zero moments which allow the moment gradients to be observed.

The lining is assumed to be installed in the opening prior to any displacements occurring in the ground. Full radial contact between the soil and the liner is assumed which allows the analyses to be bounded by the tangential contact conditions of full slip and no slip.

The frame system is activated by an "excavation" loading condition and the solution is formulated for plane strain which is appropriate for the tunnel problem away from the advancing face. The "excavation" loading condition describes the stresses which are produced by removing a core of soil from ground conditions which are initially defined by an in situ stress state.

The relative stiffnesses are automatically accounted for since each member in the frame system is described in terms of its cross-section area, moment of inertia and stiffness.

Tangential springs can also be included in the model. In this study, they are oriented at 90° to the radial springs and connect also at each 15°. They are assumed to have the same length and cross sectional area as the radial springs. The stiffness of these members must be input as a positive value, even though calculated from the tangential spring constant which is negative as a result of the sign

convention. The tangential springs can be oriented in either direction and the assumption of linear elastic behaviour permits the interchange in signs.

The joints of the liner itself are continuous, but the spring connection to these node points is pinned. The outer end of each spring is fixed in space and against rotation. This is shown as the enlarged detail in Figure 3.8!

3.6 The Response of the Discrete Ring and Spring Model

It is worth emphasizing that the springs are representing the soil response to imposed stress distributions which are applied as forces at the node points of the liner.

The model responds in such a way that the radial pressures activate the radial springs and the shear stress distributions activate tangential springs if they are included in the model.

.For the deep no slip condition, the stress distribution given in Figure 2.7(a) is input to the analysis. Similarly, the deep full slip input loads are obtained from the stress distribution given in Figure 2.7(b).

The procedure of simply assigning the shear stress distribution as zero without altering the radial pressures (Duddeck and Erdmann, 1985) does not give the correct full slip liner actions.

This is because the radial springs are representing individual columns of soil which are free to slide with
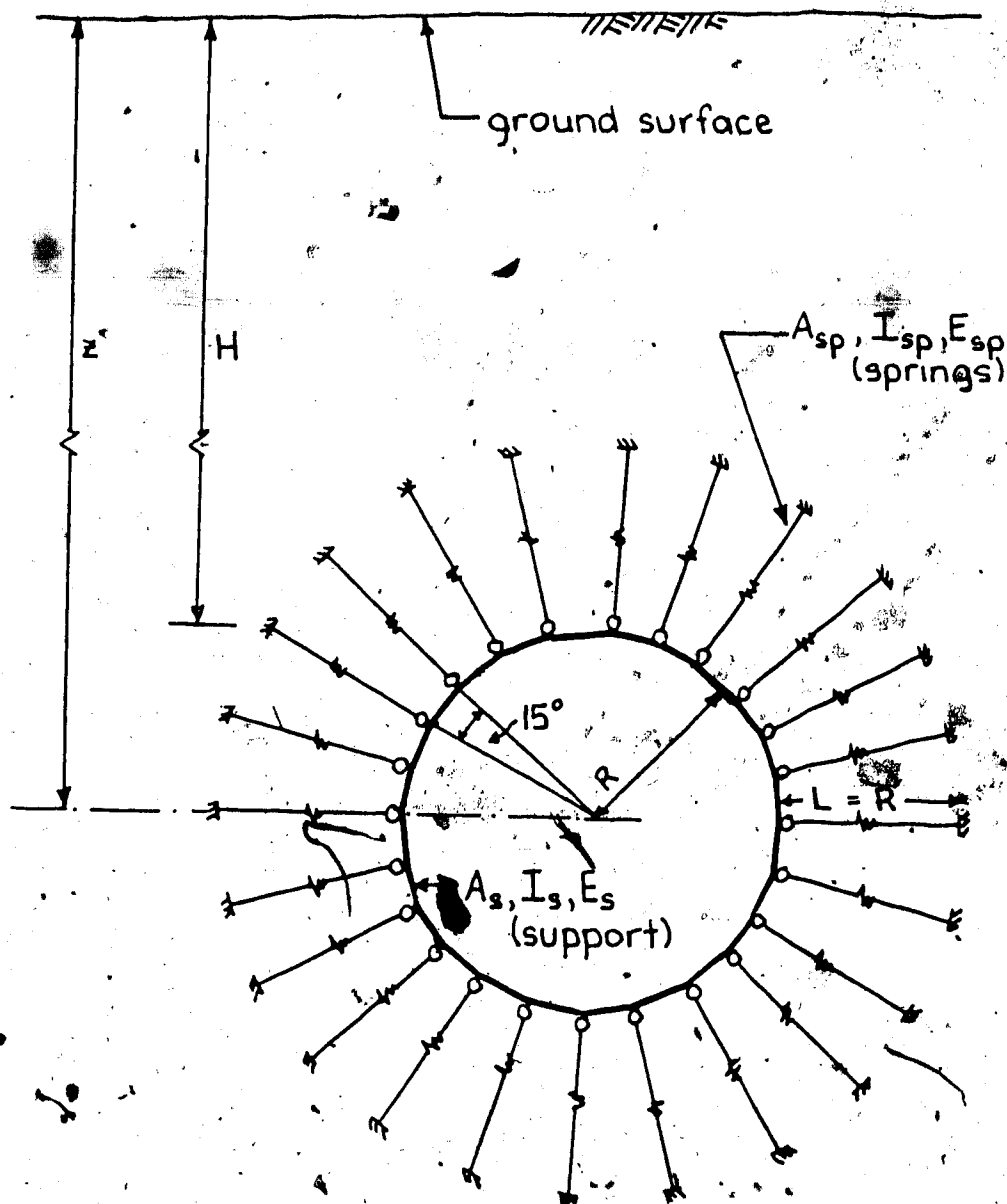
Figure 3.8 Geometry for Fully Embedded Discrete Ring and Spring Model

respect to each other. They are not interconnected and so cannot transmit shear stress from column to column. In other words, the spring representation cannot model the continuum properties of shear stress transfer and so cannot simulate the alteration in radial stress for the full slip condition by simply ignoring the shear stress.

The no-slip system is responding to a non-zero shear stress and requires tangential springs to be included.

The full slip response system is represented by considering only the radial springs.

The comment (O'Rourke et.al., 1984:20) that the stiffness of the tangential springs can be varied to simulate conditions ███ n no slip and full slip is valid provided a simultaneous account is made of the contributing distortional and shear stresses. An appropriate partial release of the shear stress would be chosen from between τ_{NS} = $\frac{YZ}{2}(1-K_o)\sin2\theta$ and τ_{FS} = 0. This also requires altering the distortional radial stress to a value conversant with the shear stress reduction. This will lie between the no slip component, σ_{r2-NS} = $\frac{YZ}{2}(1-K_o)\cos2\theta$ and the full slip component, σ_{r2-FS} = λ . $\frac{YZ}{2}(1-K_o)\cos2\theta$. Note that λ is constant for a given value of Poisson's ratio, ν. The graph showing the variation in λ with ν is seen in Figure 2.7.

A restatement of the above identifies that the interface shear conditions of full slip and no slip are included in the applied loading distributions and are not generated by the response of the system alone. The

disadvantage suggested by O'Rourke et.al. (1984) that the model ignores the variation of shear stress in response to normal loads on radial planes is, in part, overcome by describing the input loads in the appropriate full slip or no slip configuration.

Negro (1988:374) comments that in the discrete ring and spring model, some tangential shear develops even for a deep uniform loading condition. This is possible in a model that includes both tangential and radial springs. A uniform load causes a node point to displace inwards which may result in an extension force in the tangential spring member. This imposes a shear and an upward displacement component on the node.

An analysis which iterates the displacements and forces may produce such an extension force in the tangential member. This describes a more complex model than the program used in this thesis where equilibrium is satisfied in the undeformed geometry. This assumes that a radial force produces a corresponding displacement and a zero tangential force produces no additional displacements.

3.7 Influence of Tangential Springs - Deep Conditions

Intuitively, it is necessary to represent the soil with tangential springs to model the shear component non-uniform distribution. This situation occurs in an unlined opening as a result of excavation, and in a lined opening when the system is responding under a no slip

boundary condition.

The influence of the tangential springs can be assessed by performing a parametric investigation of the no slip stress distribution. Because the tangential springs are not activated under uniform stress, the study can be performed on the deep distortional and shear stress components which produce the moments and variations of thrust.

A discrete ring and spring model with 24 radial and 24 tangential springs is used for the analyses. By inspecting Figures 3.5 and 3.6, a range of values for the ratio of the tangential to radial spring constant is used such that

$$0 < \frac{k_{t21-NS}}{k_{r21-NS}} < 1.0$$

The influence of the flexibility ratio is also included by considering values of $F'=1$ and $F'=100$. An in situ stress ratio of $K_o = 0.5$ is used throughout. The results are graphed in Figures 3.9 to 3.12 and are discussed individually.

3.7.1 Tangential Springs - Influence on Moments

The variation in the moment coefficient for the half tunnel contour is shown in Figure 3.9. The moments decrease only slightly in response to a relative increase in the tangential spring stiffness. The decrease in the moments carried by the liner as the flexibility of the liner increases is seen in the figure and this relationship is

discussed extensively in Chapters 4 and 5. The influence of the tangential springs is virtually negligible.

3.7.2 Tangential Springs - Influence on Thrust

The thrusts shown in Figure 3.10 are composed of two components, $\bar{T}$ and ΔT, which are analysed separately and then superimposed.

The average thrust, $\bar{T}$, is the thrust resulting from the uniform load component, σ_{ro}, (see Figure 3.3). The radial spring stiffness required for these analyses is the k_{ro} value associated with $k_t/k_r=0$ and 1.0.

The differential thrust component, ΔT, results from the non-uniform stress distributions applied to the model. The increasing stiffness provided by the tangential springs serves to decrease the maximum differential thrust occurring in the lining section. The effect of this is more pronounced as the liner flexibility increases. In terms of maximum thrust, the omission of tangential springs provides a more conservative estimate by providing a higher maximum value.

3.7.3 Tangential Springs - Influence of Flexibility Ratio

Figure 3.11 illustrates maximum moments, M, and thrusts, T, with the effect of the tangential springs normalized to the values of the moments, M_o, and thrusts, T_o, produced from a model which has radial springs only.

It is seen that the effect of increasing tangential spring stiffness serves to reduce the maximum values of

moment and thrust to be carried by the liner.

It is also observed that the effect which the tangential spring stiffness has is enhanced as the flexibility of the liner increases.

3.7.4 Tangential Springs - Interaction Diagram Aspects

Figure 3.12 is an example of a typical moment-thrust envelope established for the critical design section assuming it is a reinforced concrete section with a specified rebar content ($p = A_s/bd$) on each face. The diagram is the locus of points corresponding to failure of the cross-section. Points inside the line represent "safe" combinations of moment and thrust. In deep tunnel conditions, the maximum moments occur at both the springline and the crown, so the maximum thrust occurring at the springline ($K_o < 1$) produces the critical design combination for $k_t/k_r = 0$. When the tangential stiffness is increased it is observed that combination of thrust and moment at the springline becomes less critical for combinations above the balanced failure point. Although the crown thrust increases, and more rapidly for increasing lining flexibility, it is unlikely to reach the value of the original springline maximum. In addition, the associated moment decreases at k_t/k_r increases, so that the crown section also becomes less critical.

In deep tunnels, the critical section will generally be above the balanced failure point, and this permits the

assumption that disregarding the tangential springs will result in a more conservative estimate of the structural capacity. A typical deep tunnel response could well be described by "D" in Figure 3.12 for $K_o < 1$.

For very shallow tunnels in which thrust forces tend to be smaller, individual studies may be required, particularly in cases where a flexible lining is used. This is portrayed in Figure 3.12 by "S" where the thrust level is below balanced failure point.

3.8 Plane Frame Truss (PFT) Computer Program

The analysis of the discrete ring and spring model must be performed numerically and this is facilitated by the Plane Frame Truss (PFT) computer program prepared by S. H. Simmonds of the University of Alberta. This program is available through the Civil Engineering computing library at the University of Alberta. Given the geometry, member properties and loading for a two-dimensional structure, the linear elastic computations are performed using the direct stiffness method.

3.8.1 Input for PFT

The users manual for the PFT program is available through the Civil Engineering Department at the University of Alberta. Only those aspects addressed which apply specifically to the frame model portraying the soil-structure interaction will be discussed here.
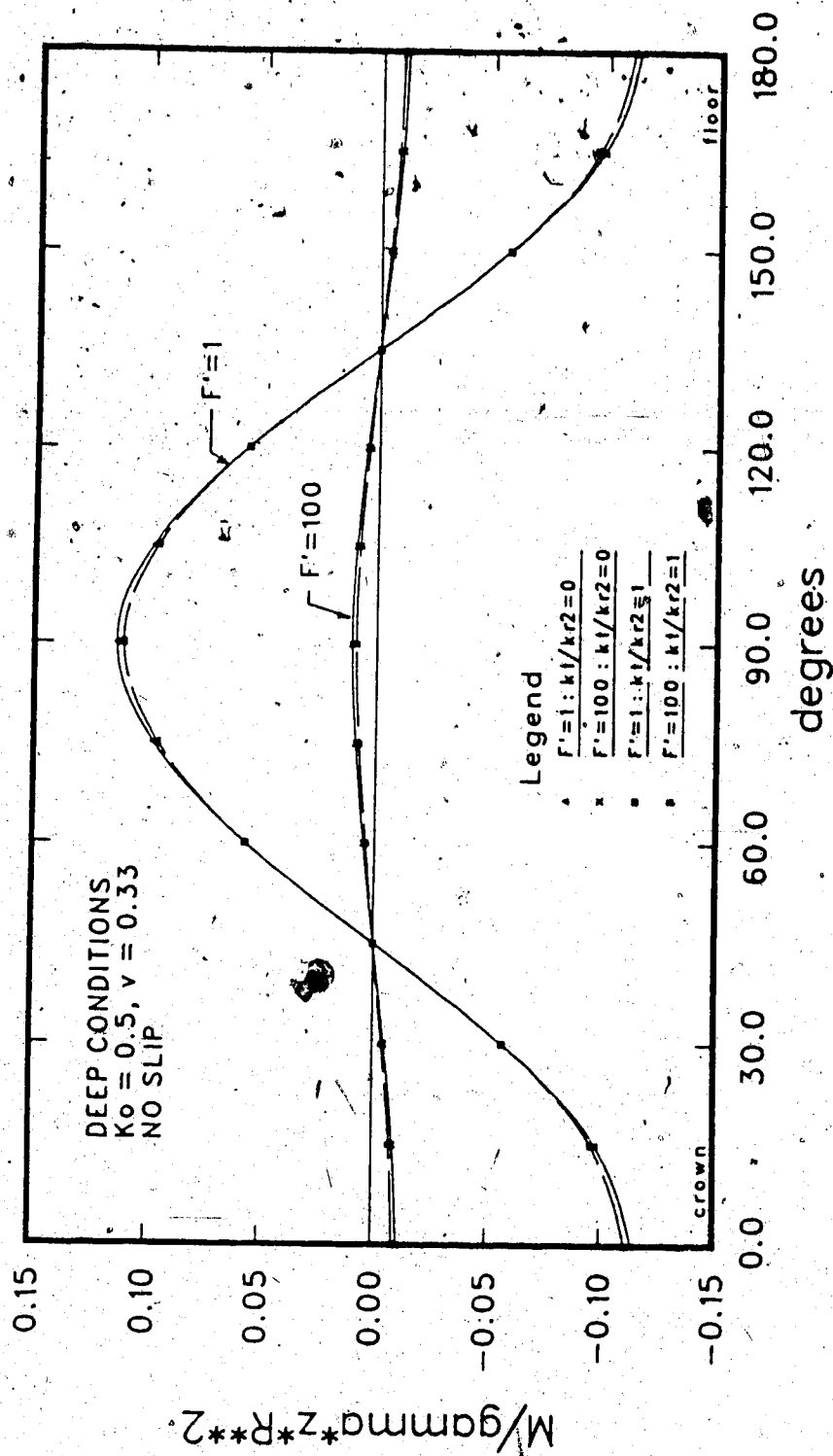
Figure 3.9 Influence of Tangential Springs on Moments.
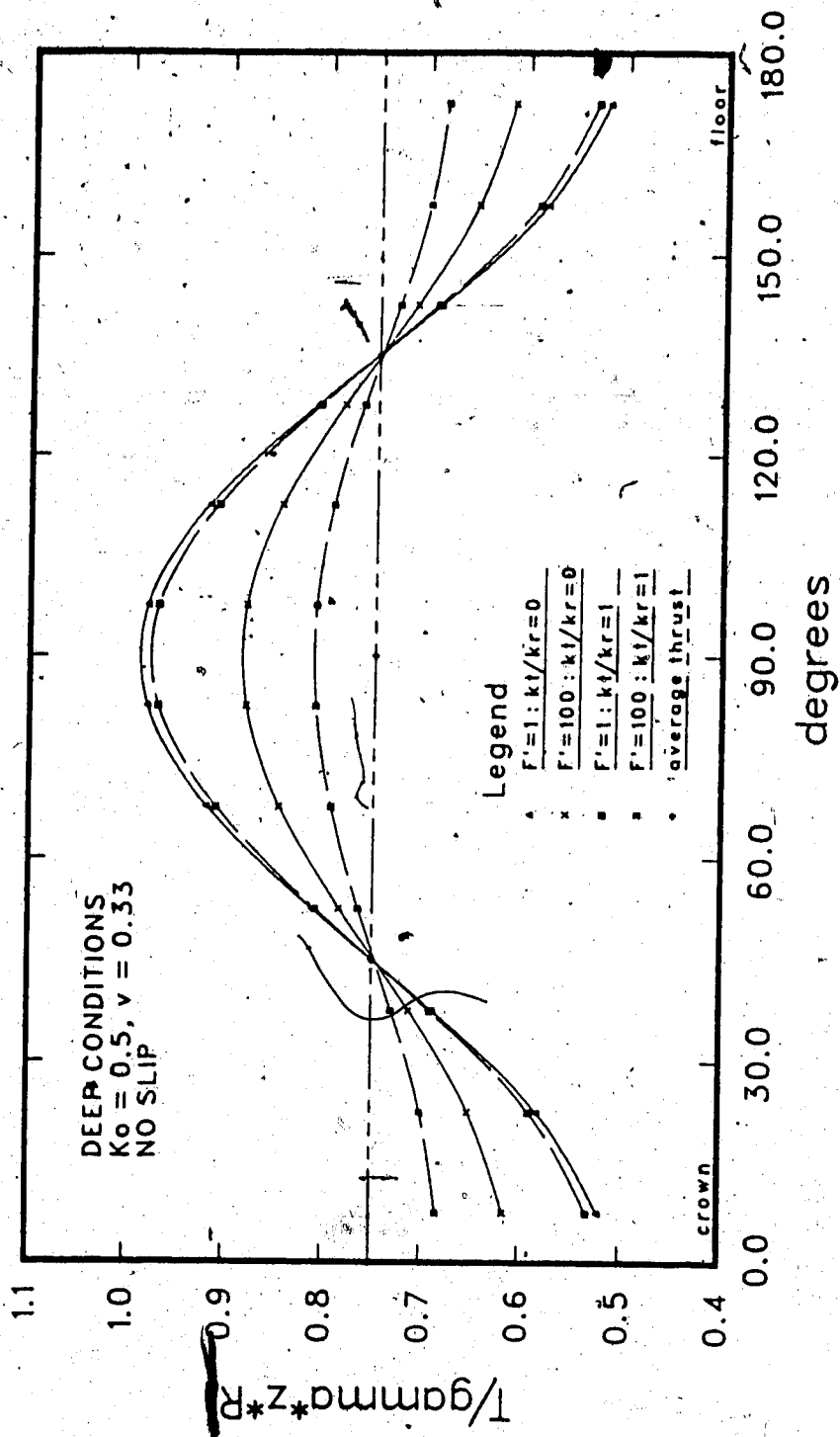
Figure 3.10 Influence of Tangential Springs on Thrust
Distribution

DEEP CONDITIONS
Ko = 0.5, v = 0.33
NO SLIP

Legend

▲	F'=1: kt/kr=0
✕	F'=100: kt/kr=0
■	F'=1: kt/kr=1
■	F'=100: kt/kr=1
●	average thrust

T/(gamma*z*R)

degrees

crown

floor
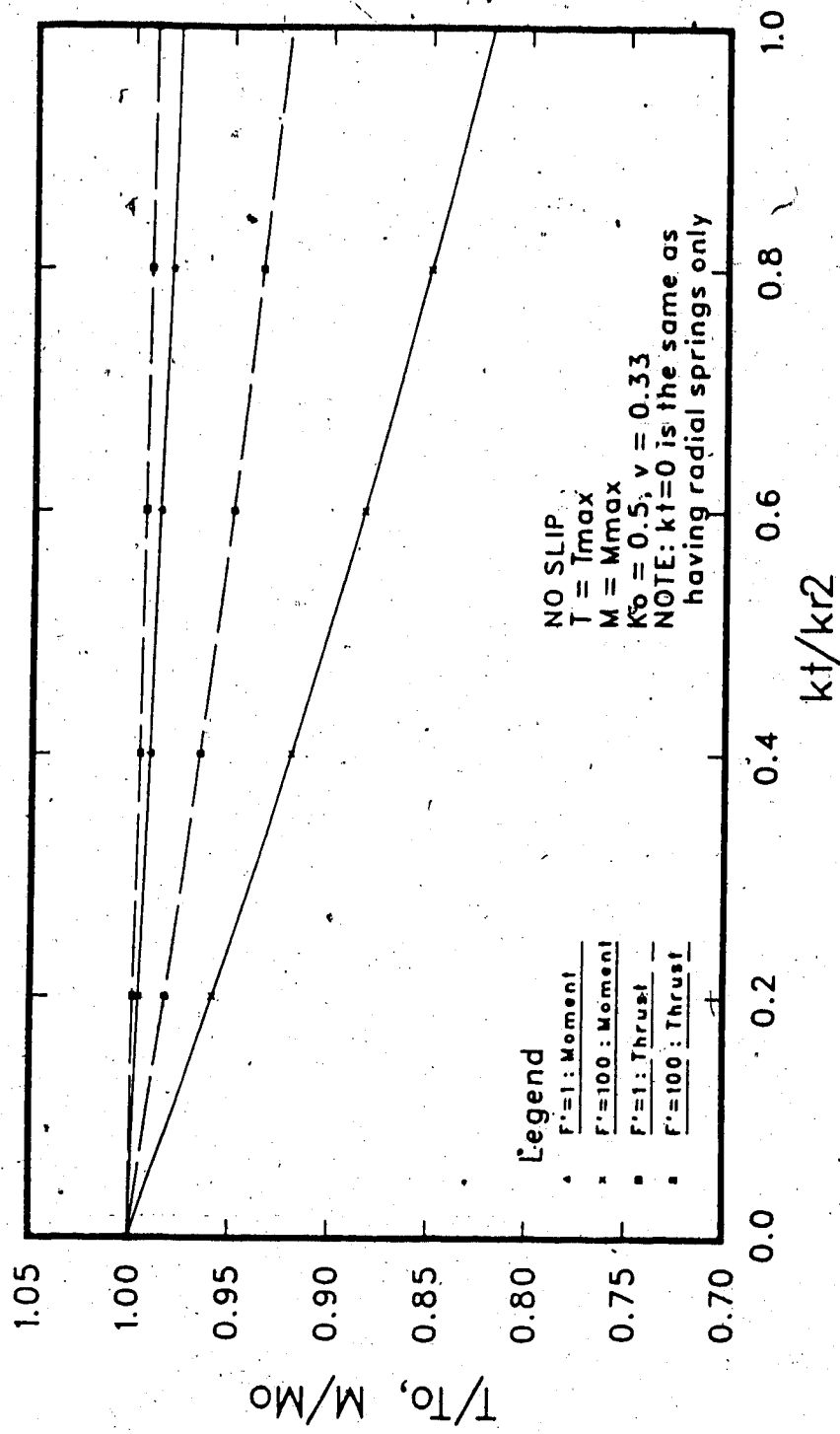
Figure 3.11 Influence of Tangential Stiffness on Maximum

Moments and Thrusts
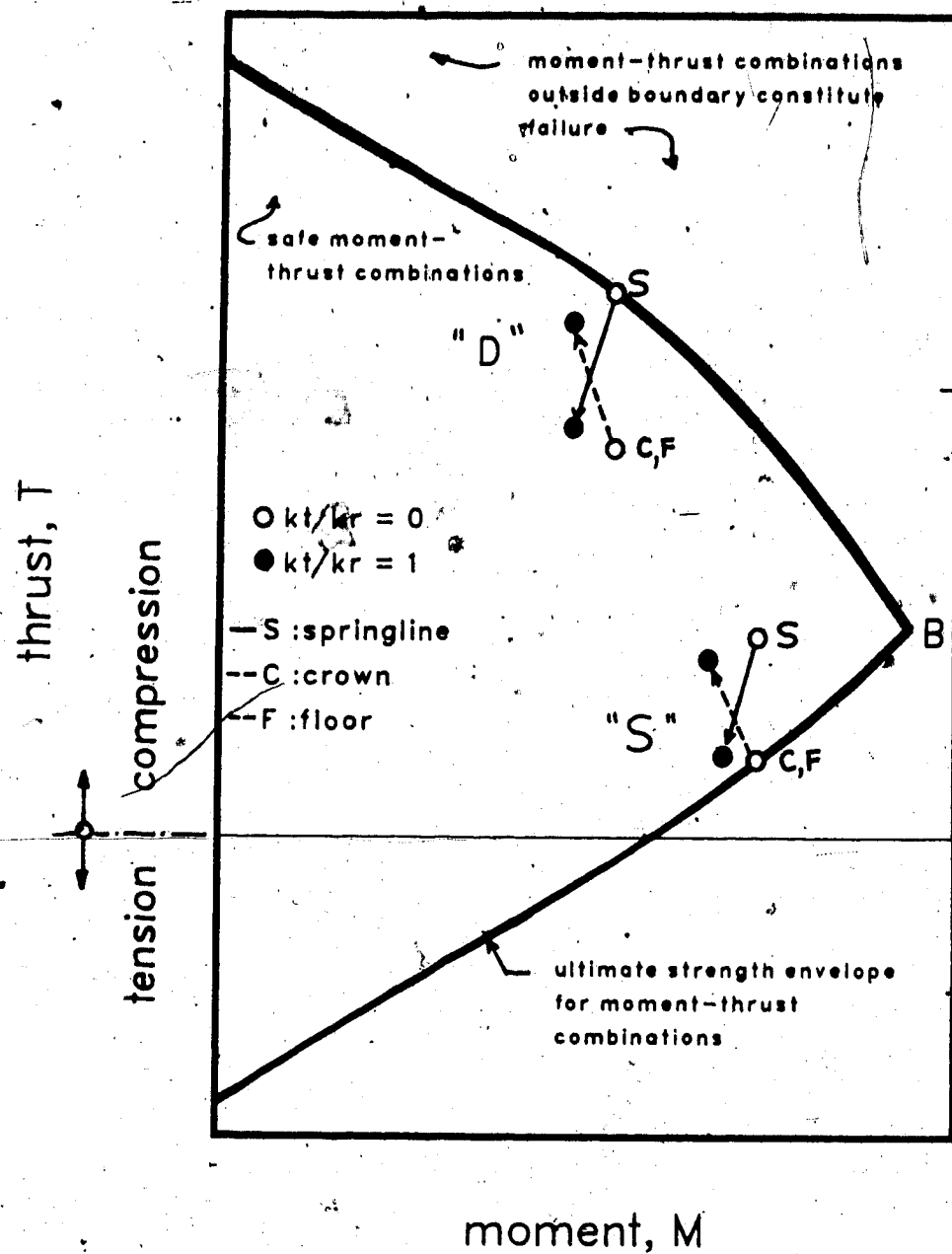
Figure 3.12 Tangential Spring Influence - Interaction
Diagram Aspects

The proposed geometry of the frame shown in Figure 6.8 is set into the program as numbered members with associated joints identified by horizontal and vertical coordinates. Each member is assigned its cross-sectional area, moment of inertia and Young's modulus.

The spring members each have a cross-sectional area equivalent to the tributary area described by the distance between the discrete springs at the point where they meet the centreline of the liner times the unit width of the longitudinal tunnel section. Since the liner is modelled as a series of line elements along the axis of the liner, the springs are assumed to be connected to the midplane of the liner. The length of the spring members is set equal to the tunnel-radius, R. The Young's modulus for the springs is linked to the stiffness modulus of the soil according to the relationship, $k = E_{sp}/R$. As already discussed in Section 3.5, the value of the spring stiffness, E_{sp}, will vary according to the displacement defining k.

The end fixity of each member is specified. The outer nodes of the spring members are fixed in space, but the springs themselves are assumed to be hinged at the inner ends only. The moment of inertia, I_{sp}, for the springs is arbitrary, but the program dimensions will restrict the use of an absurd value. A 'reasonable' range of values was considered to lie within a few orders of magnitude less than the moment of inertia of the liner, I_s, such that $10^3 < I_s/I_{sp} < 10^7$. This relatively small value of the moment of

inertia of the springs means that the members resist only axial loads.

Each end of the liner segments is considered to be continuous with full moment capacity. In the parametric study, the thickness, t, of the liner was assumed to be 0.1R from which the moment of inertia and the cross sectional area can be calculated. In an analysis of a given problem the actual thickness would be used to calculate the liner properties.

The piecewise continuous liner is activated by an excavation loading. This is input as equivalent vertical and horizontal forces applied at the liner node points. The relatively small moments generated by the resolution of the stress distribution into point loads are not included in the loading system. The resolution of the loading stress distribution in this manner is preferred to applying uniformly distributed loads along the liner members. The latter approach generates fixed-end beam moments along the discrete liner members which is inappropriate for representing the prototype response.

3.8.2 Output

The output from the PFT program provides an echo check of the input data, displacements, rotations and bending moments at the joints, and member thrust and shear forces.

The available information permits the lining to be structurally proportioned for capacity and serviceability

requirements.

Sample input and output files are included in Appendix

A

4. ANALYSIS OF DISCRETE RING AND SPRING MODEL FOR DEEP TUNNELS

4.1 Introduction

The analytical solution (Ranken, 1978) which is most appropriate to compare the discrete ring and spring model with, is presented for both no slip and full slip interface shear conditions. The solution is applicable for deep tunnels and for an "excavation" loading condition. For soil conditions which are initially defined by an in situ stress state, the excavation loading describes the stresses produced by removing a core of material from the soil.

A description of the influence that the compressibility and flexibility ratios have on the structural actions of moments, thrusts and displacements is given for the analytical solution.

A series of parametric studies using the discrete ring and spring model are described. Two sets of input data are used, one of which provides a soil-liner configuration in which the liner is virtually incompressible and is responding only to changes in the flexibility ratio. The second set uses data in which the compressibility of the liner dominates so that the ability of the spring model to simulate the effects of the compressibility ratio is assessed.

Three different ground response situations are investigated. Firstly, the analyses use the spring constants

86

obtained by considering the soil response around a lined opening. These spring constants in turn, define the stiffnesses of the springs in the ring and spring model. This set of analyses is called the "Lined Spring Constant Combination" in this script. Similarly, the spring constants describing the soil behaviour around an unlined opening provide the spring stiffnesses for the "Unlined Combination". The finals series of analyses are performed by simply using the spring constant, k_{ro}, which describes the convergence of the soil under uniform pressure. This is called the "k_{ro} Only" series.

It is important to not that the spring constants are simply describing different soil responses. These are subsequently converted to spring stiffnesses which represent the ground behaviour in the ring and spring model analyses.

It is seen that although no particular set stands out as unquestionably superior for all aspects, the "k_{ro} only" approach which uses a soil stiffness defined by uniform convergence most consistently provides results which encompass the analytical solution.

4.2 Analytical Solution for Deep Tunnels - Ranken

4.2.1 General

The analytical solutions for excavation loading assume a lined tunnel is to be constructed in a ground mass subjected to a system of in situ stresses as shown in Figure

2.1. The solutions assume that the excavation and liner installation occur instantaneously and simultaneously so no ground displacement or relaxation occurs prior to ground-liner contact and interaction. Both the soil and liner are treated as linear elastic, isotropic and homogeneous materials. The opening is circular, the ground mass is represented by an infinite plate and the lining by a weightless cylindrical shell of constant thickness.

Solutions obtained by combining the theory of elasticity and thin shell theory are termed "thin liner" solutions. Those based entirely on the theory of elasticity are called "thick liner" solutions.

Although thick liner solutions are theoretically more correct, the simpler equations provided by assuming a thin liner are used where possible. The two approaches provide essentially identical results for liner thicknesses which are smaller than 10% of the radius of the opening (Ranken, 1978:318). The "thin liner" derivations provide two-dimensional, plane strain solutions which are given in polar co-ordinates and these are used for comparing with the discrete ring and spring model.

4.2.2 Summary of the Ranken Solutions

The notations and positive sign conventions used by Ranken (1978) are illustrated in Figure 4.1. A summary of the no slip and full slip "thin liner" solutions are given in Figures 4.2 and 4.3 respectively.

The final forms of the thin liner equations are simplified by using stiffness ratios, C and F. Ranken (1978:339) adopts the definitions of Peck et al. (1972) where the compressibility ratio is

$$C = \frac{E \; R}{E_s \; A} \cdot \frac{(1-\nu_s{}^2)}{(1+\nu)(1-2\nu)}$$

[4.1]

and the flexibility ratio is

$$F = \frac{E \; R^3}{6 E_s I_s} \cdot \frac{(1-\nu_s{}^2)}{(1+\nu)} ,$$

[4.2]

Values of C and F equal to zero correspond to an incompressible and a flexurally rigid liner, respectively.

The individual terms in the expressions are as defined in Section 2.2.4.1. Equations 4.1 and 4.2 are related to equations 2.1 and 2.2 defining the stiffness ratios, C' and F', as

$$C = \frac{1-\nu}{1-2\nu} \cdot C'$$

[4.3]

$$F = \frac{1-\nu}{6} \cdot F'$$

[4.4]

For the graphical presentation of the results for the comparison between the discrete ring and spring model and the analytical solutions, usually the ratios C' and F' are generally used. A common range of values for F' found in practice is between 5 and 250 (Negro, 1988:377) and the
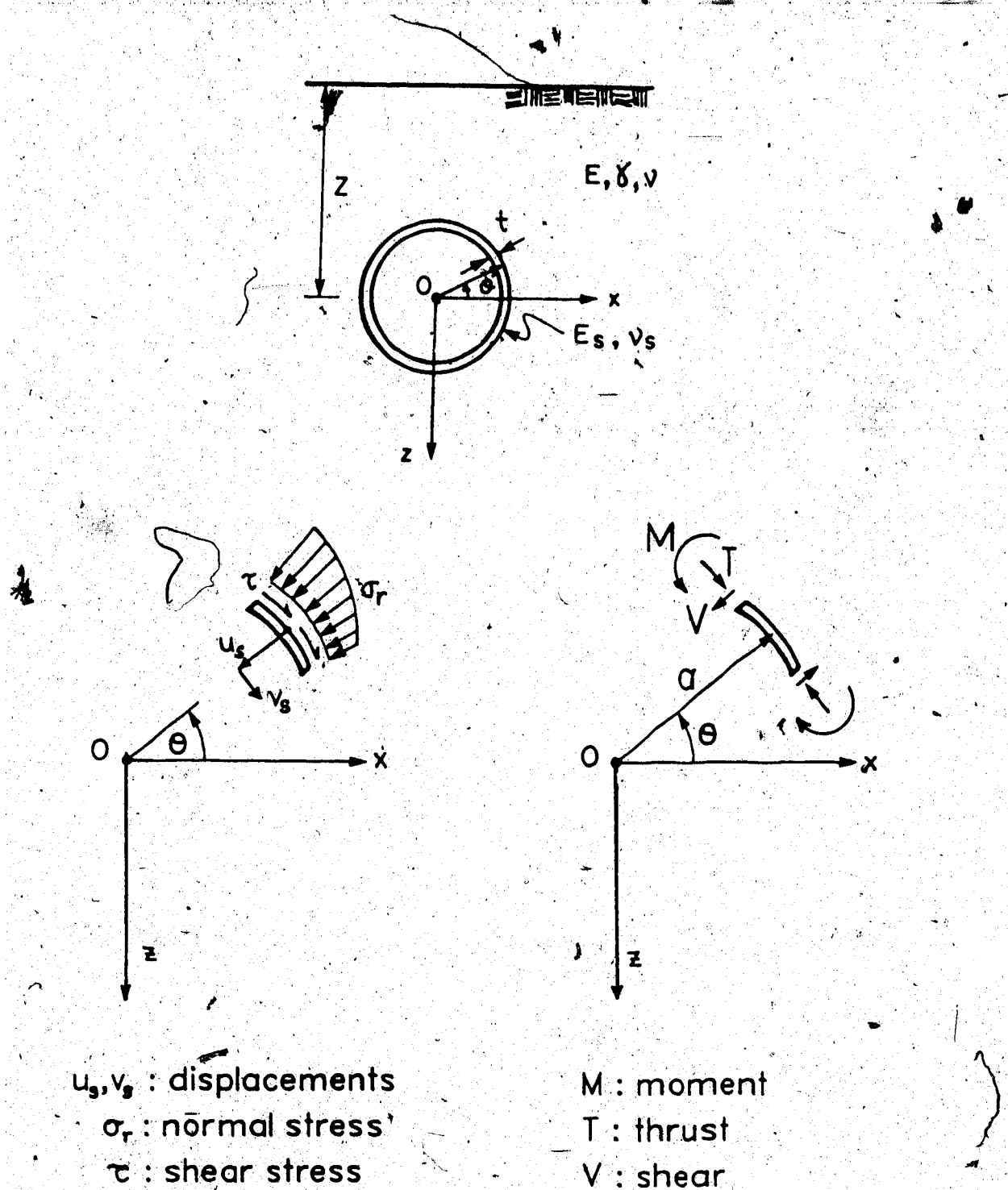
Figure 4.1 Notations and Positive Sign Conventions used in
Ranken's 'Thin Liner' Solutions

External Pressures Acting on Liner

$$\sigma_r = \left(\frac{\gamma z}{2}\right)\left\{(1 + K_o)\left[1 - L_n^*\right] - (1 - K_o)\left[1 + 3J_n^* - 2N_n^*\right]\cos 2\theta\right\}$$

$$\tau = \left(\frac{\gamma z}{2}\right)\left\{(1 - K_o)\left[1 - 3J_n^* + N_n^*\right]\sin 2\theta\right\}$$

Liner Displacements

$$u_s = \left(\frac{\gamma z a}{2}\right)\left(\frac{1 + v}{E}\right)\left\{(1 + K_o)\left[L_n^*\right] - (1 - K_o)(F)\left[1 + J_n^* - N_n^*\right]\cos 2\theta\right\}$$

$$v_s = \left(\frac{\gamma z a}{2}\right)\left(\frac{1 + v}{E}\right)\left\{(1 - K_o)\left[J_n^* + (1 - 2v)N_n^*\right]\sin 2\theta\right\}$$

Liner Thrust, Shear, and Moments

$$T = \left(\frac{\gamma z a}{2}\right)\left\{(1 + K_o)\left[1 - L_n^*\right] + (1 - K_o)\left[1 - J_n^*\right]\cos 2\theta\right\}$$

$$V = -\left(\frac{\gamma z a}{2}\right)\left\{(1 - K_o)\left[1 + J_n^* - N_n^*\right]\sin 2\theta\right\}$$

$$M = \left(\frac{\gamma z a^2}{2}\right)\left\{(1 + K_o)\left[\frac{L_n^*}{6F}\right] + \frac{1}{2}(1 - K_o)\left[1 + J_n^* - N_n^*\right]\cos 2\theta\right\}$$

Constants

$$L_n^* = \frac{(1 - 2v)\,C}{1 + (1 - 2v)\,C}$$

$$J_n^* = \frac{[2v + (1 - 2v)\,C]F + (1 - v)(1 - 2v)\,C}{[(3 - 2v) + (1 - 2v)C]F + \frac{1}{2}(5 - 6v)(1 - 2v)C + (6 - 8v)}$$

$$N_n^* = \frac{[3 + 2(1 - 2v)\,C]F + \frac{1}{2}(1 - 2v)C}{[(3 - 2v) + (1 - 2v)C]F + \frac{1}{2}(5 - 6v)(1 - 2v)C + (6 - 8v)}$$

Expressions for C and F are given as Equations 4.1 and 4.2. Positive sign conventions are illustrated in Figure 4.1.

Figure 4.2 Ranken's Solution for Excavation Loading - No Slip

External Pressures Acting on Liner

$$\sigma_r = \left(\frac{\gamma z}{2}\right)\left\{(1 + K_o)\left[1 - L_F^*\right] - 3(1 - K_o)\left[1 - 2J_f^*\right]\cos 2\theta\right\}$$

$$\tau = 0$$

Liner Displacements

$$u_s = \left(\frac{\gamma z a}{2}\right)\left(\frac{1 + \nu}{E}\right)\left\{(1 + K_o)(L_f^*) - (1 - K_o)(2F)\left[1 - 2J_f^*\right]\cos 2\theta\right\}$$

$$v_s = \left(\frac{\gamma z a}{2}\right)\left(\frac{1 + \nu}{E}\right)\left\{(1 - K_o)(F)\left[1 - 2J_f^*\right]\sin 2\theta\right\}$$

Liner Thrust, Shear, and Moments

$$T = \left(\frac{\gamma z a}{2}\right)\left\{(1 + K_o)\left[1 - L_f^*\right] + (1 - K_o)\left[1 - 2J_f^*\right]\cos 2\theta\right\}$$

$$V = -\left(\frac{\gamma z a}{2}\right)\left\{(1 - K_o)\left[1 - 2J_f^*\right]\sin 2\theta\right\}$$

$$M = \left(\frac{\gamma z a^2}{2}\right)\left\{(1 + K_o)\left[\frac{L_f^*}{6F}\right] + (1 - K_o)\left[1 - 2J_f^*\right]\cos 2\theta\right\}$$

Constants

$$L_f^* = \frac{(1 - 2\nu)\, C}{1 + (1 - 2\nu)\, C}$$

$$J_f^* = \frac{F + (1 - \nu)}{2F + (5 - 6\nu)}$$

$$N_f^* = \frac{4F + 1}{2F + (5 - 6\nu)}$$

Expressions for C and F are given as Equations 4.1 and 4.2. Positive sign conventions are illustrated in Figure 4.1

Figure 4.3 Ranken's Solution for Excavation Loading - Full Slip

variation which occurs with different parameters is more clearly seen when a logarithmic scale is selected for F'. The use of a linear scale (Ranken, 1978:72) compresses this range into a narrow zone which tends to obscure some aspects of the behaviour.

Most tunnels in soil have a compressibility ratio, C', between zero and 2 (Negro, 1988:95), although for common lining and soil configurations, this range is more likely bounded by zero and 0.5 (Negro, op.cit.:1122).

4.2.3 Typical Moment and Thrust Distributions Around the Liner

The external stress distributions acting on the liner are balanced by the thrust and moments within the liner. Figure 4.4 illustrates typical distributions for these structural actions showing, for K_o different from unity, the influence of no slip and full slip interface conditions. The thrusts are compressive, and the moments are plotted on the compression face of the liner.

The thrusts, as shown in Figure 4.4(a), can be noticeably altered by the interface conditions. The difference in magnitude between the springline and the crown values (or floor) is greater for the no slip condition. On the other hand, the maximum moments which occur at the crown, springline and floor are slightly enhanced in the full slip condition as seen in Figure 4.4(b).

Because of the direct relationship existing between moments and displacements, the displacement response pattern imitates that for the moments.

By inspecting the equations in Figures 4.2 and 4.3, it is seen that the expressions for moment and thrust each consist of two terms. The first term is independent of θ (circumferential location) and describes the response to the uniform component of the applied stress. For the thrust, this term represents the average value, $\bar{T}$, while for the moments it represents the second order moments generated by increased curvature of the lining under uniform compression. The second term in each equation is a function of θ and produces the variation in magnitude around the liner contour in response to the distortional and shear components. It is convenient to separate them in this way because the influence of the compressibility and flexibility ratios on the distribution of moments and thrusts affects each term differently.

4.2.4 The Compressibility Ratio

4.2.4.1 Influence of the Compressibility Ratio on Moments

The first term of the moment equation describes the magnitude of the second order moments which are produced as a result of the relative compressibility of the liner. For common linings, this contribution to the overall moments is very small and is often neglected.

(a) thrusts

—— no slip
---- full slip
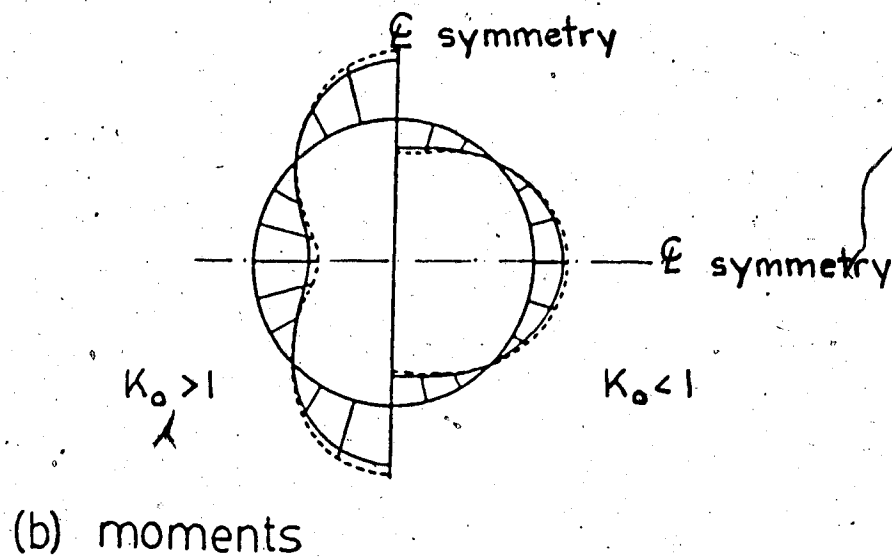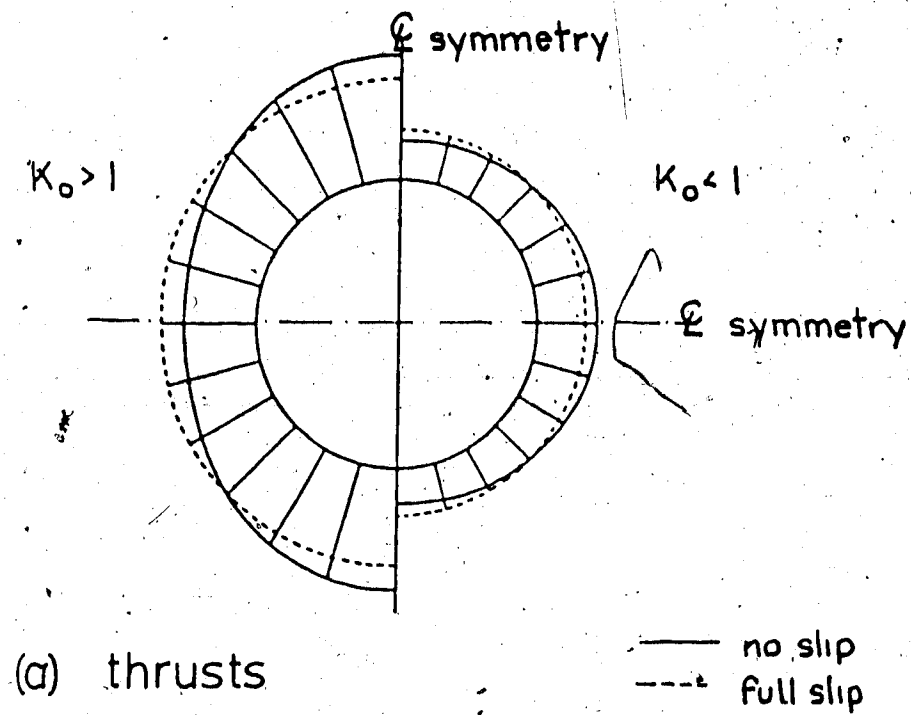
(b) moments

Figure 4.4 Typical Distributions of Liner Thrusts and
Moments (after Ranken, 1978:modified)

The second term in the moment equation for full slip is independent of C and while the corresponding term in the no slip equation is a function of² both C and F, it is influenced only slightly by C (Ranken 1978:76)

4.2.4.2 Influence of the Compressibility Ratio on Thrusts

Similar to the moments, the second term of the thrust equations is either independent of C or very slightly influenced by C (Ranken op.cit.) The strongest influence that C exerts is on the average thrust term. The variation of the compressibility ratio with the average thrust coefficient, $T/\gamma zR$, is illustrated in Figure 4.5 for $K_o=2.0$ and 0.5. For all values of K_o, increasing the compressibility ratio reduces the magnitude of the average thrust. When the effects of both thrust terms are combined, it is reasonable to assume that the most conservative estimate for the maximum total thrust is obtained when C=0.

Note that the average thrust term response is the same for both full slip and no slip. Also shown in the same figure is the significant variation in the average thrust with differing Poisson's ratio, ν.

4.2.4.3 Influence of the Compressibility Ratio on Radial Displacements

The radial displacements of the liner imitate the moment distribution and their corresponding sensitivity to the compressibility ratio, C.

With respect to the compressibility ratio, the radial displacement coefficient, $uE/\gamma zR$, is slightly more affected than the moments are. This is because the displacements are more strongly affected by changes in the Poisson's ratio which influence the constants containing C (see Figures 4.2 and 4.3). For virtually incompressible liner configurations, the constant inward displacement generated in response to the uniform load component is small compared with the displacements produced by the distortional component.

4.2.5 The Flexibility Ratio

It is seen from the equations for moments and thrusts in Figures 4.2 and 4.3 that the first term in each is independent of the flexibility ratio, F.

The distortional components of the loading which generate the variation in magnitude of moment and thrust around the lining contour are strongly influenced by the flexibility ratio. The effect of increasing flexibility is to reduce the extreme values of the variation which occur.

4.2.5.1 Influence of the Flexibility Ratio on Thrust

Figures 4.6(a) and (b) illustrate the influence of the flexibility ratio on the total thrust coefficient, $T/\gamma zR$, for no slip and full slip, $K_o=0.5$ and $\nu=0.33$. The horizontal axis is the half circle circumference starting from $\theta=0°$ at the crown to the floor where $\theta=180°$. The maximum thrusts occur at the springlines for $K_o<1$ and as just discussed, the response to F seen in these diagrams is attributed to the
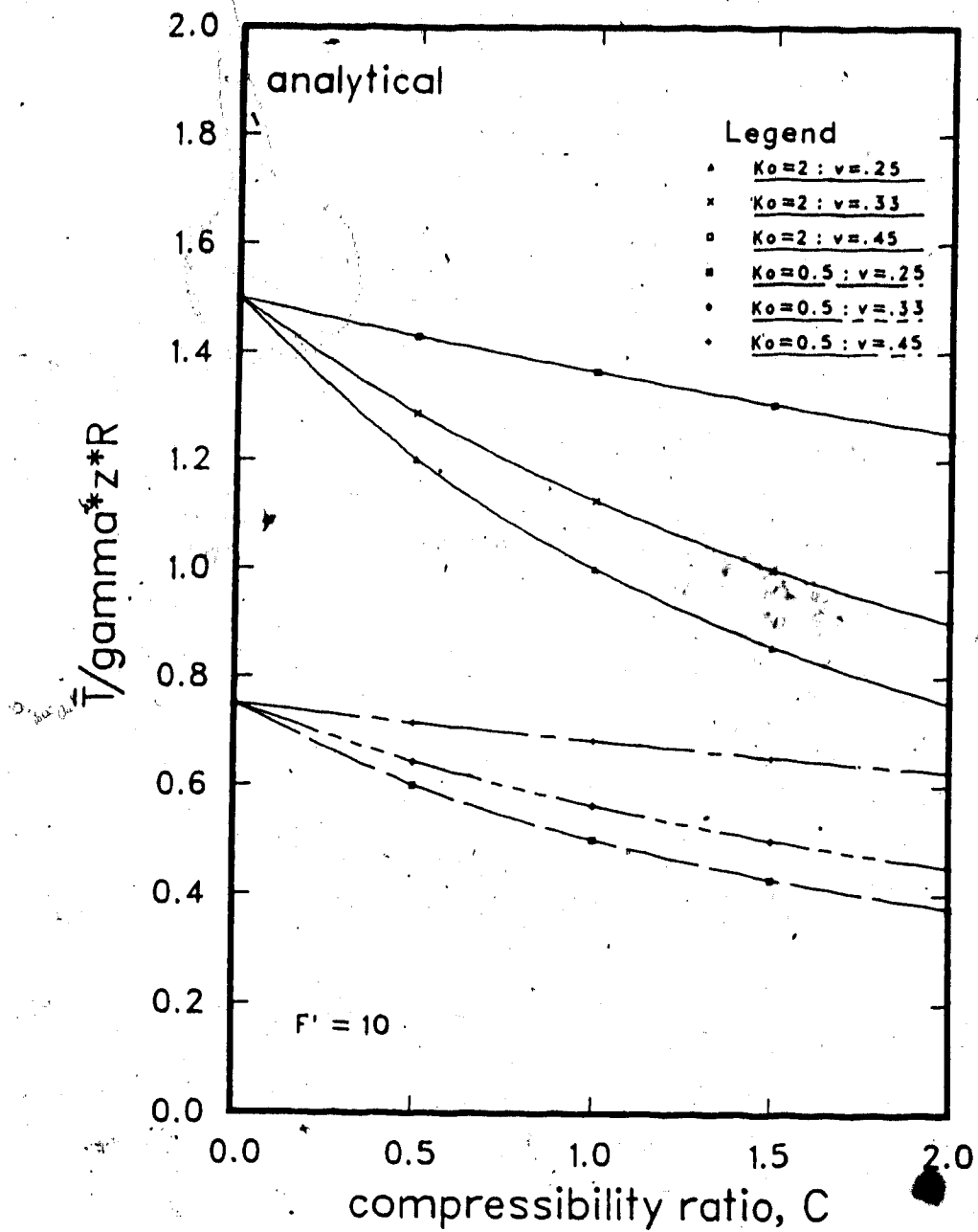
Figure 4.5 Variation of Average Thrust Coefficient with Compressibility Ratio

distortional load components. The difference between the
peak values for the same F' in Figures 4.6(a) and (b)
reiterates the tempering influence that the full slip
interface condition has on the distribution around the
liner.

Figure 4.7 illustrates the variation of the maximum
thrust differential coefficient, n, with the flexibility
ratio. The term, ΔT_{max}, is the maximum deviation of the
thrust from the average thrust, $\bar{T}$. Separating the actively
responsive term of the thrust in this manner permits a more
generalized presentation and highlights the influence of
Poisson's ratio, ν. Once again, the difference in the degree
of distortion caused in the thrust distribution is seen for
the interface conditions. The full slip response is
essentially independent of ν, and n rapidly approaches zero
for larger values of F' so the overall thrust distribution
approaches the uniform distribution given by the average
thrust term. The no slip response is more affected by ν and
as F' increases, the coefficient n approaches a constant non
zero value of $1-(2\nu/3-2\nu)$, indicating that the total thrust
variation is decreased, but still exists.

4.2.5.2 Influence of the Flexibility Ratio on Moments

Figure 4.8 illustrates the effect of F' on the moment
coefficient for no slip and full slip, $K_o=0.5$ and $\nu=0.33$.
The maximum moments occur at the crown, floor and
springline, and it can be seen that while the influence of
the interface condition is not very strong, the full slip
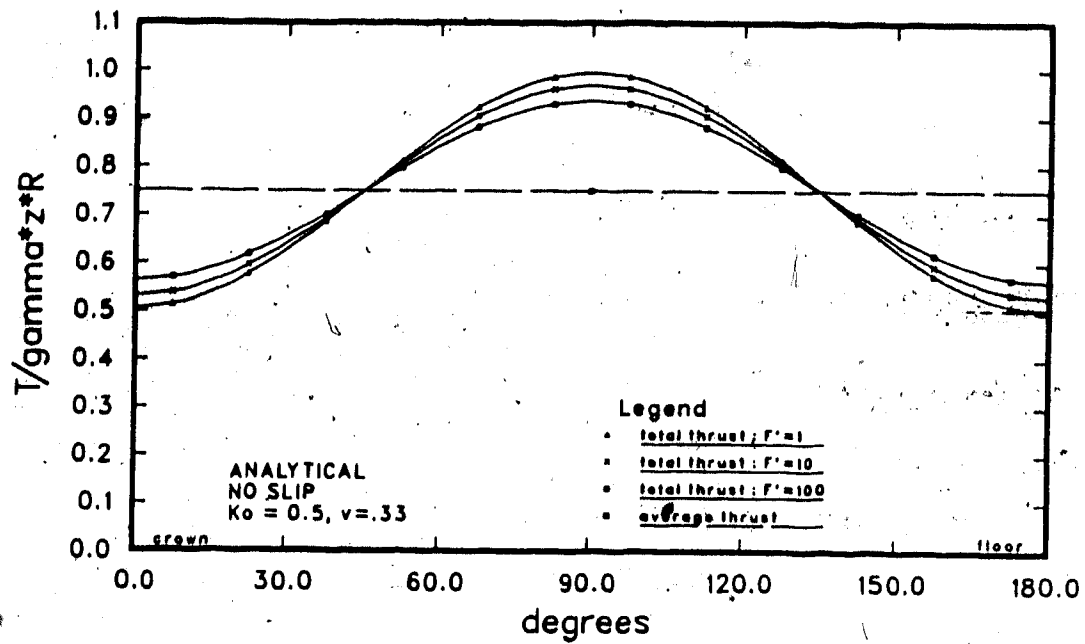
(a) no slip
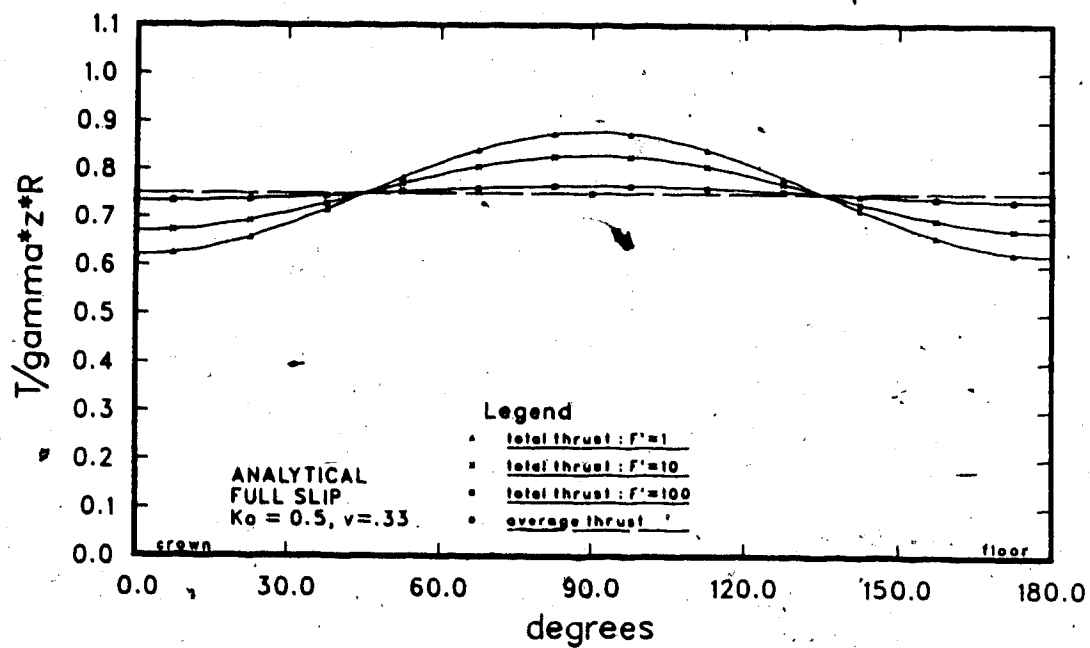
(b) full slip

Figure 4.6 Variation of Total Thrust Coefficient with Flexibility Ratio

$$\Delta T_{max} = n \left\{ \frac{1-K_o}{2} \cdot \gamma z \cdot R \right\}$$

Legend.
- no slip: v=.25
- no slip: v=.33
- no slip: v=.45
- full slip: v=.25
- full slip: v=.33
- full slip: v=.45

analytical
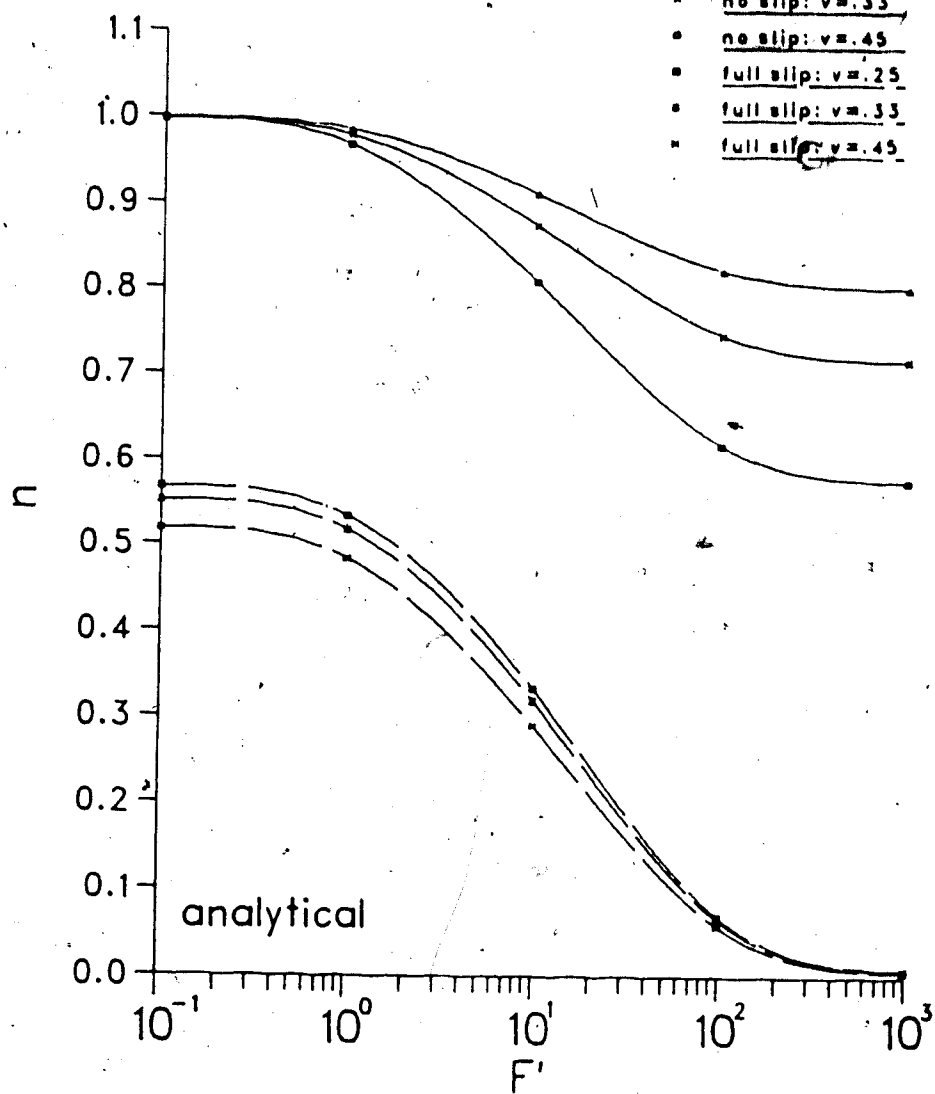
Figure 4.7 Variation of Maximum Thrust Differential
Coefficient with Flexibility Ratio

moments for a given K_o and ν are always slightly greater in magnitude than for its no slip counterpart. This difference decreases as F' increases.

The more generalized presentation for the moment behaviour in response to F' is given in Figure 4.9 where the maximum moment coefficient, m, is plotted against F'.

The influence of Poisson's ratio, ν, on the full slip moments is less than 10% in the common range of values for F'. The no slip moments are independent of ν.

4.2.5.3 Influence of the Flexibility Ratio on Radial Displacements

As for the moments and thrusts, the first term in the expressions for the radial displacements is independent of F. The distortional load component is responsible for the variation from the uniform inward component resulting from the response to liner compressibility. For an incompressible liner and $K_o<1$, the maximum inward displacement occurs at the crown and floor and is equal in magnitude to the outward displacement at the springline.

Figures 4.10(a) and (b) show the influence of the flexibility ratio on the maximum radial displacement coefficient, $uE/\gamma zR$. It is seen that both the full slip and no slip curves rapidly approach constant non-zero values with increasing flexibility.

The influence of Poisson's ratio is quite marked, with the full slip condition accentuating the effect.
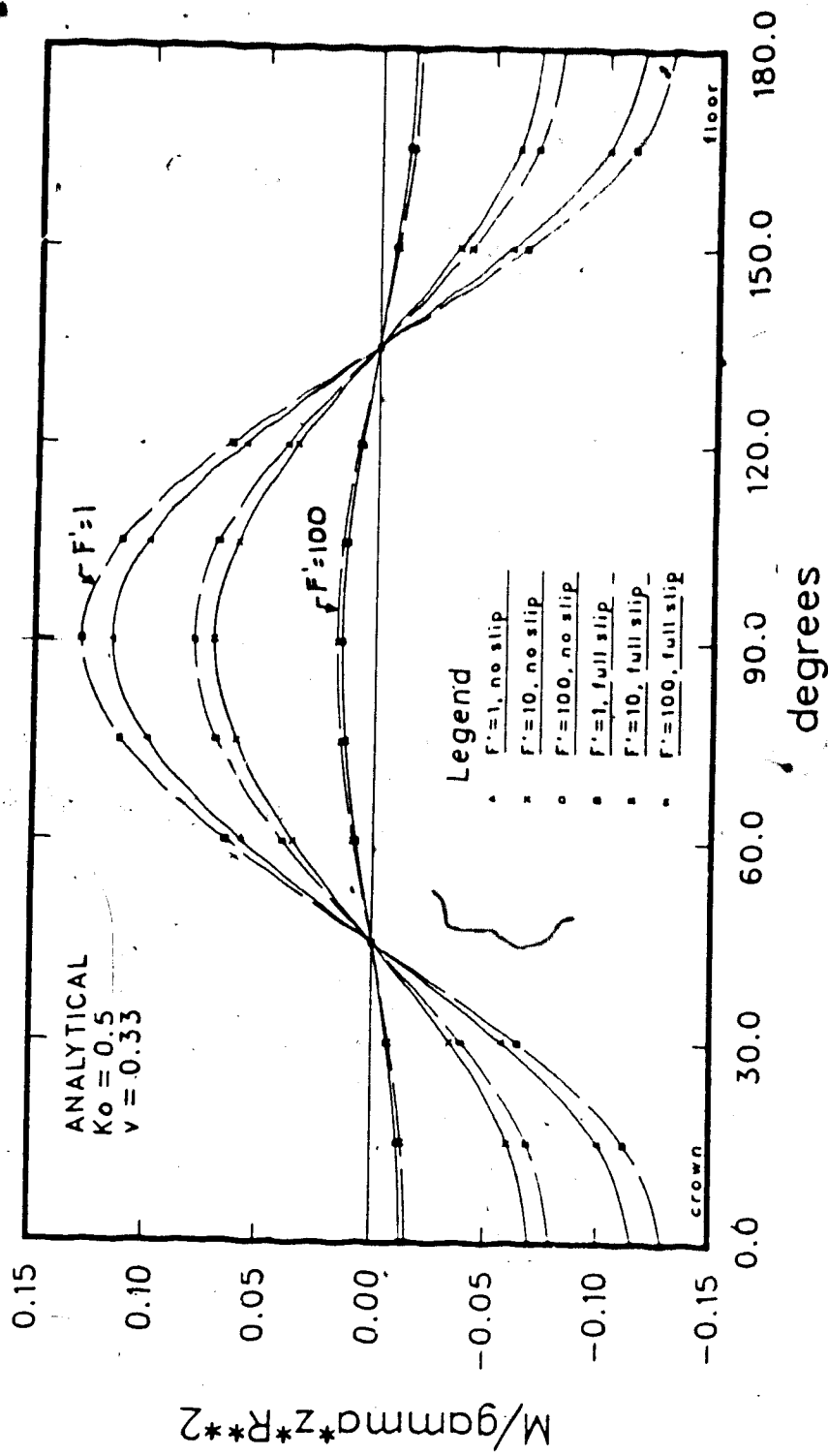
Figure 4.8 Variation of Moment Coefficient with Flexibility Ratio

$$M_{max} = m \left(\frac{1-K_o}{2} \cdot \gamma_z \cdot R^2 \right)$$
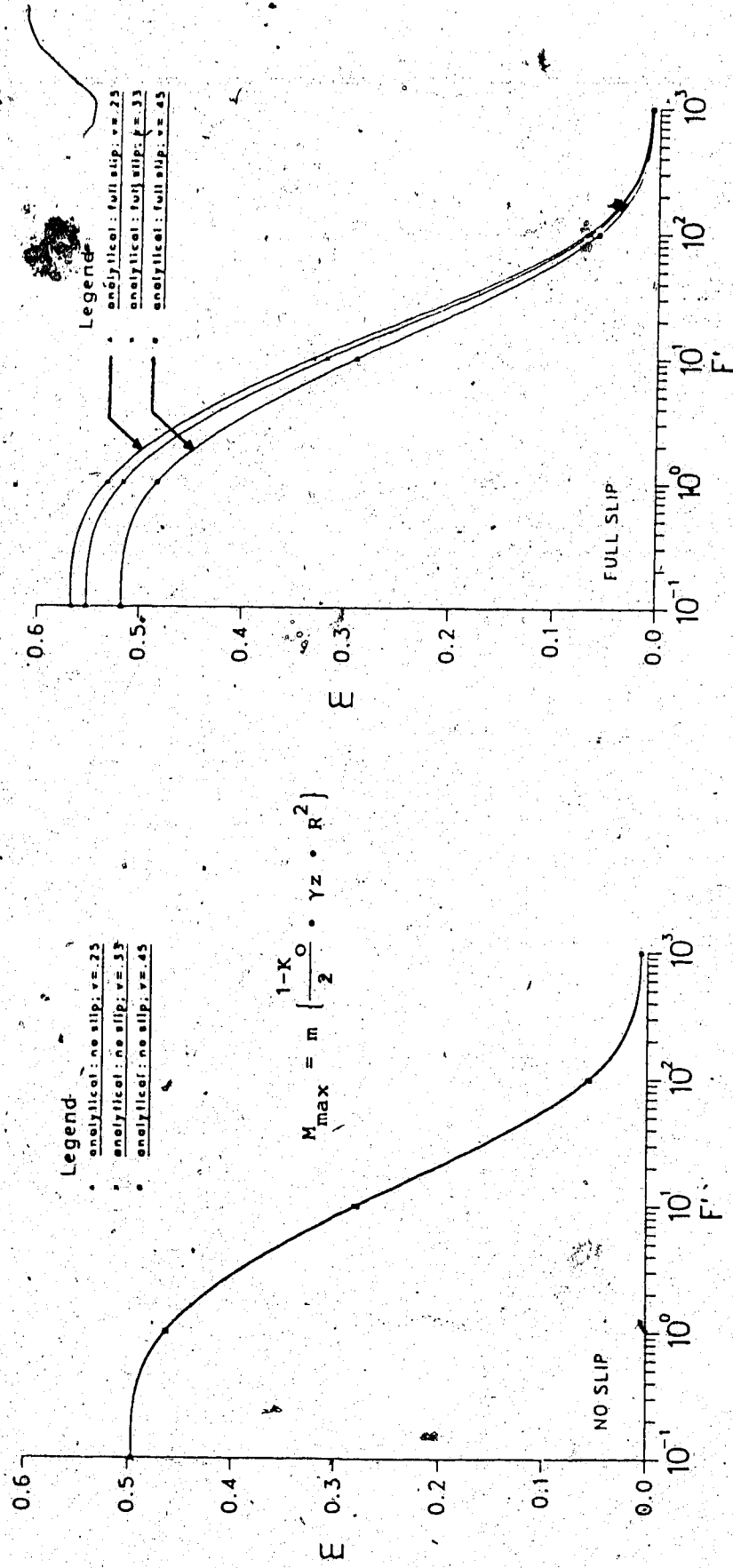
(a) no slip

(b) full slip

Figure 4.9 Variation of Maximum Moment Coefficient with
Flexibility Ratio

The curves in Figures 4.10(a) and (b) can be used to describe the vertical and horizontal diameter change coefficient, $\frac{\Delta D}{D} \cdot \frac{E}{\gamma z}$, by replacing u/R with $\Delta D/D$ in the radial displacement coefficient. For an incompressible liner and $K_o < 1$, the vertical diameter will become smaller and the horizontal diameter will increase by the same amount.

4.2.6 Summary

This concludes the description of the analytical solution for both the no slip and full slip loading conditions. The influence of the stiffness ratios, the in situ stress ratio and Poisson's ratio on the thrusts, moments and displacements are presented. These responses describe the standard which the results from the discrete ring and spring model are calibrated against.

4.3 Discrete Ring and Spring Model Analyses

4.3.1 General

Duddeck and Erdmann (1985) report that a full correspondence between the analytical plate solution and the continuous ring and spring solution is theoretically possible. This requires the ring and spring model to be fully embedded and have both radial and tangential springs. Different spring constants must be used to describe the soil response to each constituent component of the applied loading. The analyses are performed individually then

(a) no slip

(b) full slip
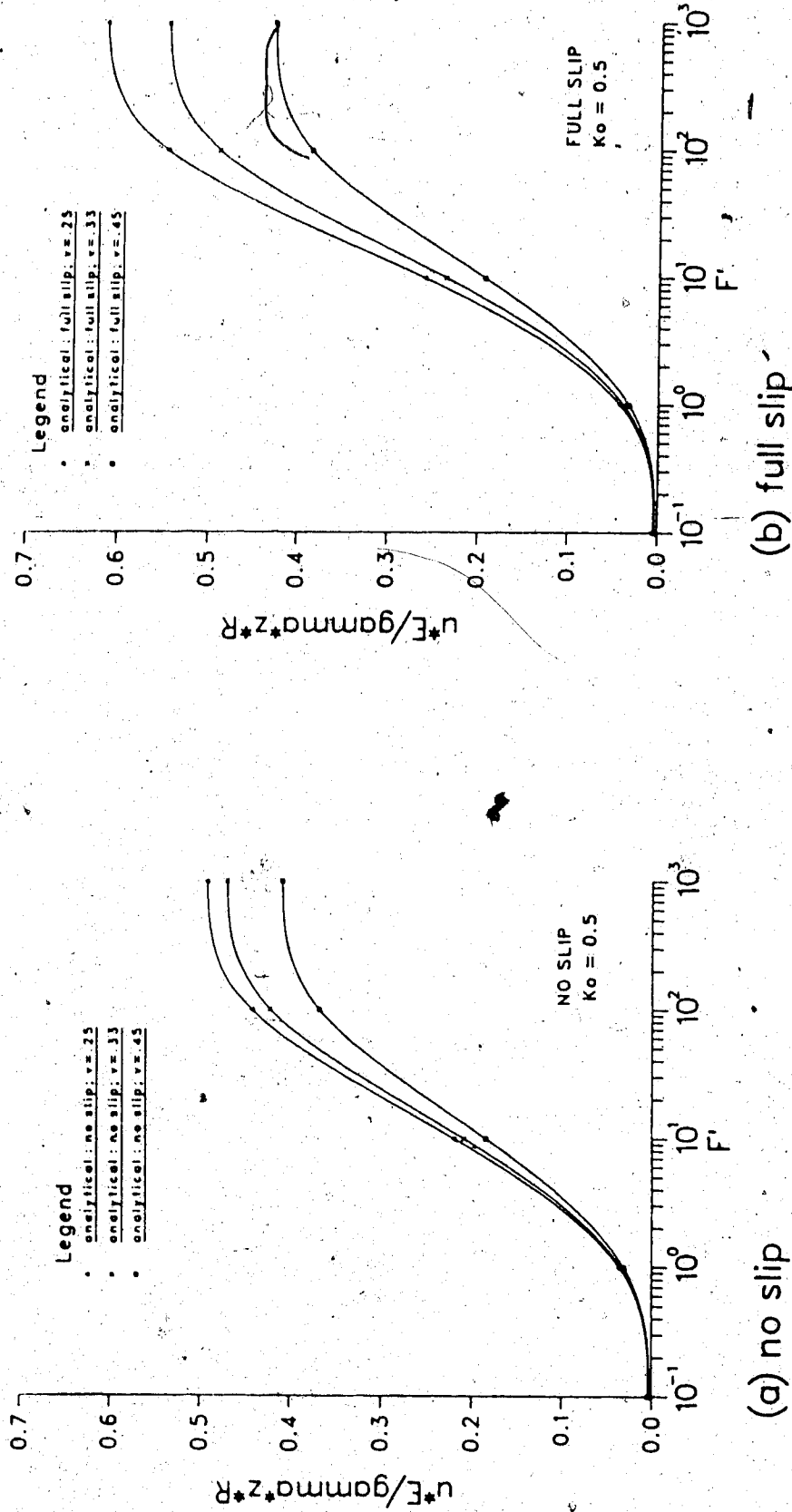
Figure 4.10 Variation of Maximum Radial Displacement
Coefficient with Flexibility Ratio for an incompressible
Liner

superimposed to provide the final results.

The spring constants used in this set of analyses are those given by Ahrens et.al. (1982) and shown in Table 3.: They have been derived fro the soil response around an incompressible liner, and are appropriate for the paramet: values used the studies of the variations of liner flexibility. This set of spring constants describes the "Lined Spring Constant Combination" discussed in Section 4.3.5.1. The presence of the liner constrains the soil deformations so that the soil response is more stiff compared with the stiffness associated with the deformati into an unlined opening.

A second set of analyses uses the soil response arou an unlined opening to define the spring constants. These provide the spring stiffnesses for the "Unlined Combinati analyses described in Section 4.3.5.2.

The third set of analyses uses radial springs only w spring stiffnesses defined by a soil response under unifo pressure. This it the "k_{ro} Only" series of analyses and details are seen in Section 4.3.5.3.

The full correspondence or "lined" spring constant combination simulates the analytical solution for full sl quite accurately, but is unconservative with respect to a aspects of the no slip solution.

The responses obtained by using the "unlined" spring constant combination are generally over conservative for moments and displacements but underestimate the no-slip

thrusts by up to 10%. The degree of error is quite pronounced with this approach.

The third and popular "k_{ro} Only" approach gives moments and thrusts within 5% of the analytical solution for common values of the Poisson's ratio of the soil, $0.3<\nu<0.4$. The radial displacements are closely simulated for $\nu\approx0.3$, but are increasingly overestimated as ν increases.

4.3.2 Geometry of the Model for Parametric Study

The general details of the fully embedded discrete ring and spring model are described in Section 3.4 and illustrated in Figure 3.5. The model in the parametric study is used both with and without tangential springs according to the combination of spring constants being investigated. These are described further in Section 4.3.5.

The fixed and variable parameters used in the parametric study are illustrated in Figures 4.11 (a) and (b) and explained in the following sections.

The tunnel opening has a radius, R = 1 m, and soil cover H = 10 m which gives the depth to the tunnel axis as z = 11 m. The results are normalized and so are applicable for any H/D ratio for deep conditions where no account of gravity is made.

The fixed soil parameters include the weight, $\gamma=20$ kN/m³, the Young's modulus, E = 1 MPa and the in situ stress ratio, K_o = 0.5. The Young's modulus for the liner is E_s = 10 000 MPa and the Poisson's ratio for the soil, ν, and

for the support, ν_s, are set equal to each other throughout.

The input co-ordinates for the computer program are defined by setting the origin (0,0) at the centre of the opening. The input procedure is given in Section 3.7 with a sample file provided in Appendix I.

For both the no slip and full slip interface conditions, the analyses consider the variation of the flexibility ratio, F', of Poisson's ratios $\nu = \nu_s$, and three different representations in the model for the soil response. The range of values investigated is tabulated in Figure 4.11(b).

4.3.3 Flexibility and Compressibility Ratios

4.3.3.1 Flexibility Ratio

The moment of inertia of the liner, I_s, is varied in the input data to provide the required flexibility ratios, F'. These are established in the following manner.

From the given fixed parameters in Figure 4.11(a), the flexibility ratio

$$F' = \frac{ER^3(1-\nu_s^2)}{E_s I_s(1-\nu^2)}$$ [2.1]

gives

$$I_s = \frac{10^{-4}}{F'} \ [m^4/m]$$ [4.5]

The computer program requires the cross sectional area of
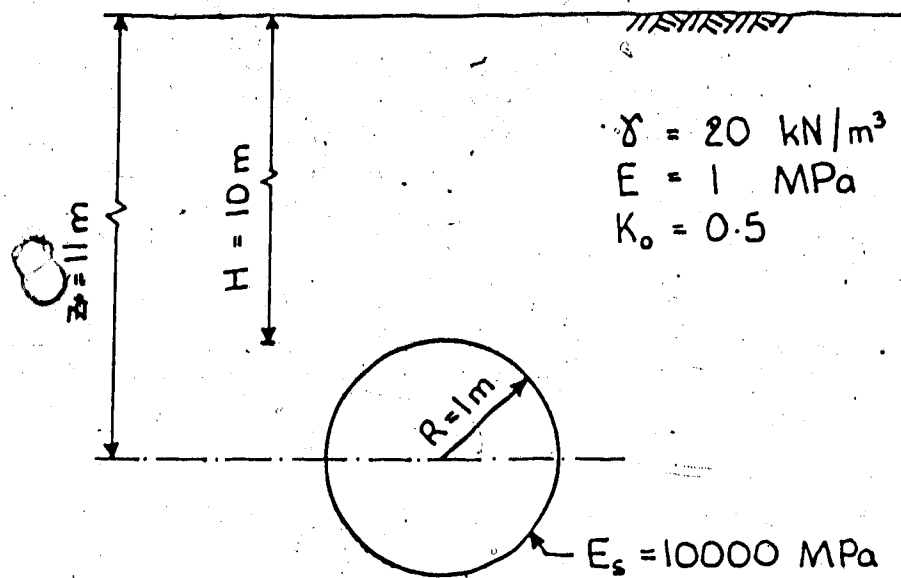
(a) fixed parameters

Parameter	Values				
F'	.1	1	10	100	1000
$v = v_s$	.25		.33		.45
soil response*	'unlined'	'lined'		'k_{ro} only'	
loading$	no slip	full slip			

* see Section 4.3.5

$ see Figure 2.7

(b) variable parameters

Figure 4.11 Parameters Used in the Spring Model Analyses for Deep Tunnels

the liner, A_s, to be defined as an input parameter. For a unit length, b = 1 m, and liner thickness, t,

$$A_s = bt = t \ [m^2/m]$$

The moment of inertia of the liner, $I_s = bt^3/12$, enables A_s to be calculated as

$$A_s = \sqrt[3]{12I_s} \ [m^2/m] \qquad\qquad [4.6]$$

Although A_s has negligible influence on the results and could be left as a constant value for all F', it is systematically altered according to equation [4.6] for each F' value investigated.

4.3.3.2 Compressibility Ratio

Because of the finite input values required for A_s, it is not possible to set C' identically equal to zero. An evaluation of the compressibility ratios used in this study reveals that the most compressible configuration is associated with F' = 1000, where

$$C' = \frac{ER(1-\nu_s^2)}{E_s A_s (1-\nu^2)} = 0.0094 \qquad\qquad [2.2]$$

This corresponds to C≈0.02 in Figure 4.5 so that the liner configurations can be considered as incompressible for the purpose of the analyses. This also justifies the use of the Ahrens et.al. (1982) expressions for the "lined" spring

constants.

A separate study described in Section 4.4.1 indicates
that the discrete ring and spring model is fairly accurate
in describing the response to compressibility effects.

4.3.4 Input Loads

As described in Section 3.7, the external soil stresses
are input as horizontal and vertical point loads at the
nodes of the frame representing the liner.

The interface shear conditions define the loading
pattern that is entered into the analyses. For the
conditions that no stress reduction or displacements occur
prior to the interaction process, the external stresses
required for the spring model are described by the loading
recognized by an incompressible and inflexible liner
($C=F=0$). In Section 2.2 and Figure 2.7 it is explained that
these stresses are the same as the in situ stress ratio for
a no slip interface conditions, and adjusted to account for
shear stress redistribution for the full slip situation.

The loads can be obtained by setting $C=F=0$ and
evaluating the equations for the external stresses in
Figures 4.2 and 4.3 for no slip and full slip respectively.

The appropriate constants in these figures indicate
that the no slip loading is independent of ν. For the full
slip condition, the shear stress redistribution is partly
influenced by ν so that the applied loads must be assessed
for each distinct value.

In summary, for C=F=0 and $\theta = 0°$ at the crown, the no slip external soil stresses are:

$$\sigma_r = \frac{\gamma z}{2} \{(1+K_o)+(1-K_o)\cos 2\theta\}$$ [4.7(a)]

$$\tau = \frac{\gamma z}{2}(1-K_o)\sin 2\theta$$ [4.7(b)]

Similarly, the full slip soil stresses are:

$$\sigma_r = \frac{\gamma z}{2} \{(1+K_o)+\lambda(1-K_o)\cos 2\theta\}$$ [4.8(a)]

$$\tau = 0$$ [4.8(b)]

where $\lambda = 3 - \frac{6(1-\nu)}{(5-6\nu)}$ is constant for a particular ν and is graphed in Figure 2.7.

As described in the following section, the majority of the analyses was performed with the response to the radial stress component (equations 4.7(a) and 4.8(a)) subdivided into two parts with different spring constants describing each. In these cases, each part is analysed separately because the stiffness for any member has only one value for a particular analysis. The final result is obtained by superposition.

For input loads, equations sets [4.7] and [4.8] are each rearranged into a uniform radial component, and a distortional component which includes both the distortional radial pressure and the shear stress. The latter combination

is possible since the radial and tangential spring

stiffnesses are assigned separately.

4.3.4.1 No Slip

The uniform component from equation set [4.7] is

$$\sigma_{ro} = \frac{\gamma z}{2} (1+K_o) \qquad [4.9]$$

The distortional component is

$$w = \frac{\gamma z}{2}(1-K_o)(\cos2\theta+\sin2\theta) \qquad [4.10]$$

4.3.4.2 Full Slip

The uniform component is the same for no slip and full

slip. The distortional component from equation set [4.8] is

$$\dot{w} = \frac{\gamma z}{2}(1-K_o)\lambda\cos2\theta \qquad [4.11]$$

4.3.5 Spring Constant Combinations

Three alternate soil response descriptions were used to

define the spring constant combinations. These in turn

enable the spring stiffnesses to be defined for the discrete

ring and spring model analyses. The terminology used to

describe the three sets is

    (i) Lined   (see Section 4.3.5.1)

    (ii) Unlined   (see Section 4.3.5.2)

    (iii) k_{ro} Only   (see Section 4.3.5.3)

In all three cases the uniform component of loading is

analysed using a model with radial springs only. The spring stiffness is evaluated from the spring constant, k_{ro}.

For the "unlined" and the no slip version of the "lined" case, the model used in computing the effects of the distortional loads has both radial and tangential springs. The stiffnesses of these springs are calculated from the radial, k_{r2}, and tangential, k_{t2}, spring constants respectively.

The full slip "lined" case has no distortional shear component and is modelled using radial springs only.

In the "k_{ro} Only" case, the total loading is applied to a model with radial springs only. These have a stiffness calculated from k_{ro}. It is established in Figure 3.4 that the spring constants of the soil, k, are related to the assumed modulus of elasticity of the spring member, E_{sp}, and the length of the spring member, L. It is usual to set L equal to the tunnel radius, R, so that $k = E_{sp}/R$. The derivation applies equally to radial or tangential stresses and their associated displacements.

The input for the computer analysis requires the definition of the spring member stiffness. For $R = 1$ m,

$$E_{sp} = k \qquad\qquad [4.11]$$

so that the spring stiffnesses for the radial or tangential spring members are equal in value to the selected spring constant.

A summary of the spring constant combinations and their associated input data is provided in Table 4.1. The details regarding each combination are given in the following subsections.

The uniform component of the loading in each case is run with the radial spring member stiffness, $E_{sp} = k_{ro}$. This analysis is performed using a model which has radial springs only. It can equally be run with a model having both radial and tangential springs. The required tangential spring stiffness is zero, but since the program uses zero as a default value in this instance, the tangential springs are assigned a stiffness equal to 0.001.

4.3.5.1 "Lined" Spring Constant Combination

The spring constants in this analysis are given by the expressions derived by Ahrens et.al. (1982) shown in Table 3.2.

The no slip analyses requires a discrete ring and spring model which includes both radial and tangential springs. Two separate runs are performed and then superimposed for the final results.

(i) uniform load component with radial spring stiffness = k_{ro}

(ii) distortional load component calculated from equation [4.10] with the radial spring stiffness defined by k_{r21-ns} and the tangential stiffness by k_{t21-ns}.

The spring model for the full slip condition does not require tangential springs, but once again, the analyses are

Table 4.1 Summary of the Spring Constant Combinations and Ring and Spring Geometry

	NO SLIP				FULL SLIP			
	Load Component[2]	Radial	Tangential	Model[3]	Load Component[2]	Radial	Tangential	Model[3]
LINED	(i) uniform [4.9]	k_{ro}		A	(i) uniform [4.9]	k_{ro}		A
	(ii) distortional [4.10]	$k_{r2\ell-NS}$	$k_{t2\ell-NS}$	B	(ii) distortional [4.11]	$k_{r2\ell-FS}$		A
UNLINED	(i) uniform [4.9]	k_{ro}		A	(i) uniform [4.9]	k_{ro}		A
	(ii) distortional [4.10]	k_{r2u}	k_{t2u}	B	(ii) distortional [4.11]	k_{r2u}		A
k_{ro} ONLY	(i) total [4.9] + [4.10]	k_{ro}		A	(i) total [4.9] + [4.11]	k_{ro}		A

Notes:
1. Expressions for spring constants given in Table 3.2.
2. Load Components – see Equations [4.9], [4.10], [4.11].
3. A: Model with Radial Springs only   B: Model with Radial and Tangential Springs

run in two parts because of the separate responses of the radial components.

(i) uniform load component with k_{ro} defining the radial spring stiffness.

(ii) the distortional load component [equation 4.11] is associated with a $\odot$radial spring stiffness $E_{sp} = k_{r21-ts}$

4.3.5.2 "Unlined" Spring Constant Combination

This approach follows the same procedure outlined in Section 4.3.5.1 except the lined spring constants are replaced by the unlined spring constants given in Table 3.2.

4.3.5.3 k_{ro} Only

This approach assumes that the entire load response for both no slip and full slip is described by the stiffness associated with uniform convergence. The model has radial springs only with stiffnesses defined by k_{ro}.

For the no slip calculations, equations [4.9] and [4.10] are combined to provide the load input, so only one run is necessary to provide the final results.

Similarly, the full slip solution combines equations [4.9] and [4.11] for the input loads.

4.4 Results of the Discrete Ring and Spring Model Analyses

This section presents the reduced output data for the discrete ring and spring model provided by the computer analyses. The results are compared in each case with the analytical solutions.

1 The Influence of the Compressibility Ratio

With the parameters described in Section 4.3 it is shown that the compressibility ratio is zero for the purpose of comparison with the analytical solution. Consequently the influence of C' is not discernible for the series already described.

A separate analysis was performed to ascertain the capability of the discrete spring model to simulate the effect of liner compressibility on the average thrust term, $\bar{T}$. It is seen in Section 4.2.3 that this component of the total thrust induced by the uniform load component is the one most influenced by the compressibility ratio. The geometry for this series remained unchanged, but the material properties were altered to provide a soil-liner configuration that was more dominated by the compressibility ratio. These are listed below:

$E = 100$ MPa

$E_s = 100$ MPa

$\nu = \nu_s$ (0.25, 0.33, 0.45)

$K_o = 0.5$

$F' = 10$

$I_s = 0.1 \ m^4/m$

$A_s = 1/C' \ m^2/m$

An inspection of available output data and the equations in Figures 4.2 and 4.3 indicate that the average thrust term is independent of the flexibility ratio, F'. For this reason, a value of $F' = 10$ was arbitrarily selected so

that the moment of inertia of the liner was fixed at 0.1 m^4/m.

The average thrust is a consequence of the uniform load component [equation 4.9] with a soil response described by $k_{ro} = \frac{1}{1+\nu} \cdot \frac{E}{R}$. It is independent of the interface slip conditions. The cross sectional area of the liner, A_s, was varied in the input data to provide the required compressiblity ratio values. Note that the model only needed to have radial springs.

Figure 4.12 illustrates the variation of the average thrust coefficient, $\bar{T}/\gamma zR$, with the compressibility ratio. The spring model is able to simulate the variation associated with changing Poisson's ratio, ν, but slightly underestimates the average thrust. This is accentuated as C increases, but for common soil-liner systems, this discrepancy amounts to less than 2%.

The spring model provides an accurate response under a uniform radial pressure with the stiffness of the radial springs defined by k_{ro}.

4.4.2 Influence of the Flexibility Ratio on Moments

The results for this subsection are addressed individually for each spring constant combination since the response in each instance is slightly different.
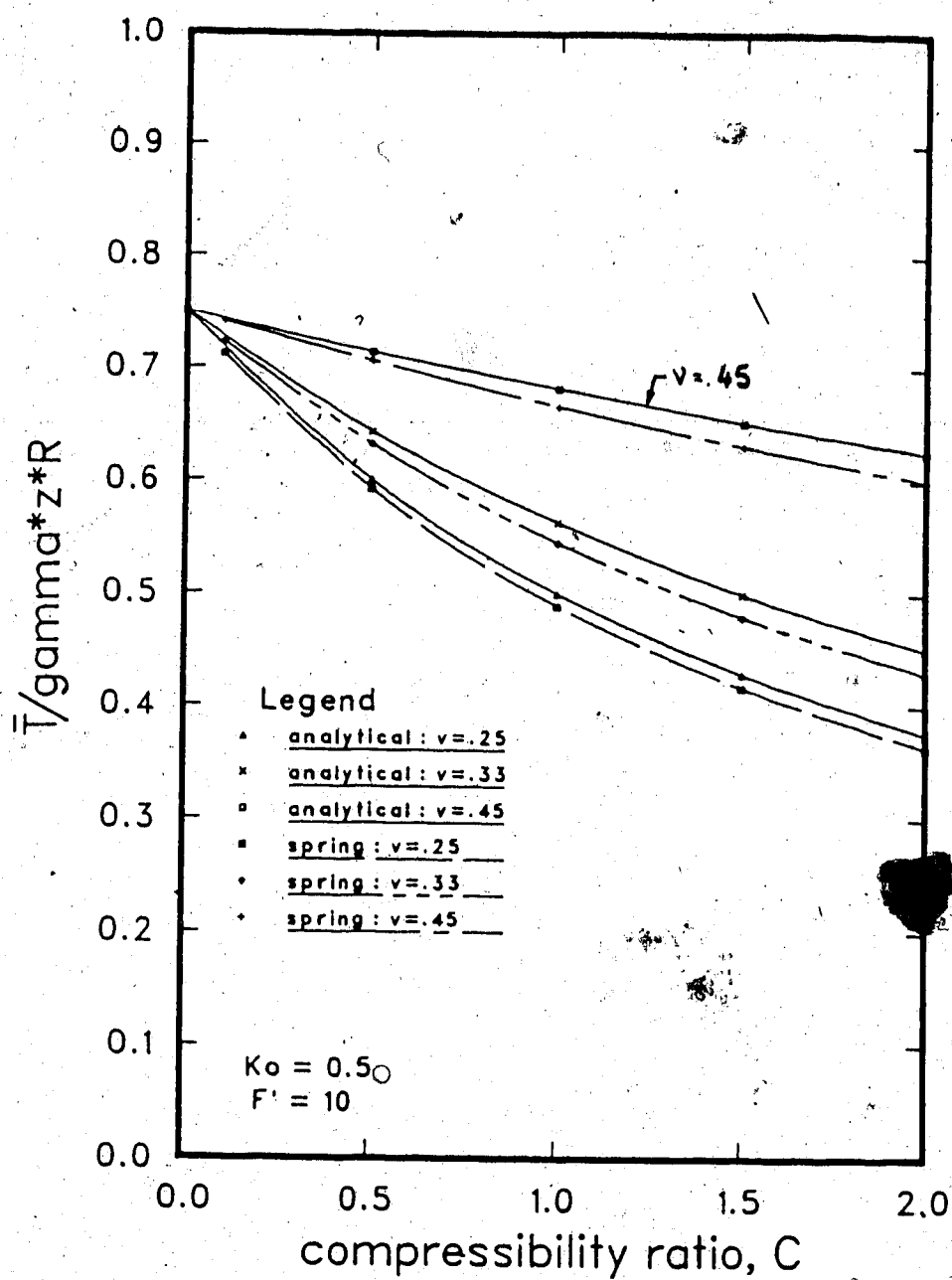
Figure 4.12 Variation of Average Thrust Coefficient with Compressibility Ratio

4.4.2.1 Lined Combination

The variation of the moment coefficient, m, with the flexibility ratio, F', is given in Figures 4.13(a) and (b) for no slip and full slip respectively.

For no slip conditions, the "lined" spring constant combination produces a response which is essentially independent of ν and although it imitates the general trend in behaviour, it consistently underestimates the analytical solution. Typically the largest deviation in the curves is associated with F' = 10 and falls short of the target values by up to 15%.

For clarity, only the results for ν = 0.25 and ν = 0.45 are plotted in Figure 4.13(b). The response for ν = 0.33 falls in the range provided by the given curves. The analytical and numerical curves are seen to correspond reasonably well, altering with ν as required. The closeness of fit decreases as ν increases, but the maximum discrepancy at F'=10 only amounts to 8% for ν = 0.45.

4.4.2.2 Unlined Combination

The variation of the moment coefficient, m, with the flexibility ratio, F', is given in Figures 4.14(a) and (b) for no slip and full slip respectively.

The overall pattern for the no slip response to the variation in the flexibility ratio is well matched, but the spring model indicates a dependence on the changing Poisson's ratio which is not a feature of the analytical counterpart. The spring model overestimates the analytical

$$M_{max} = m \left(\frac{1-K_o}{2} \cdot \gamma_z \cdot R^2 \right)$$
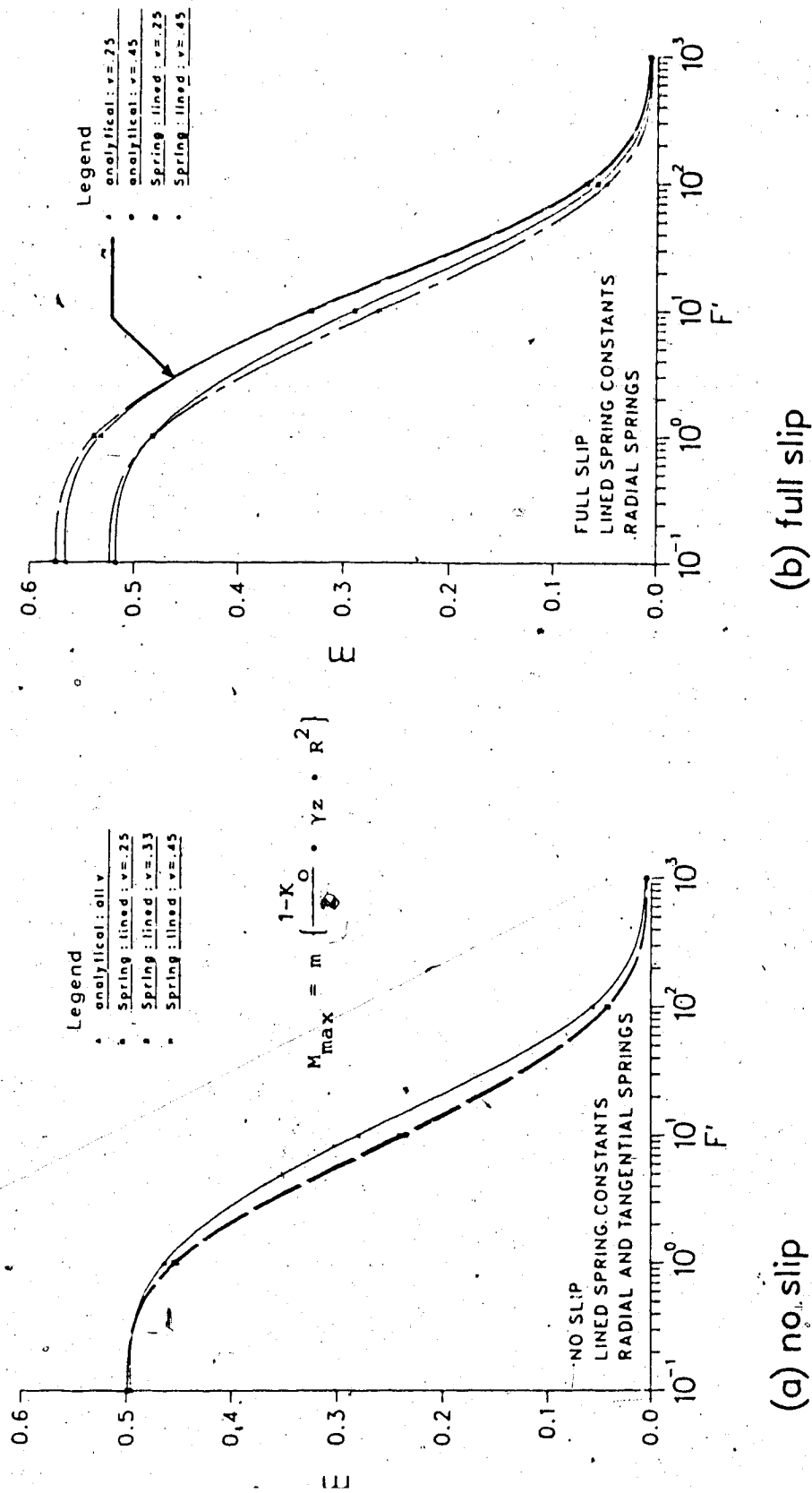
(a) no slip

(b) full slip

Figure 4.13 Variation of Moment Coefficient with Flexibility

Ratio: "Lined" Combination
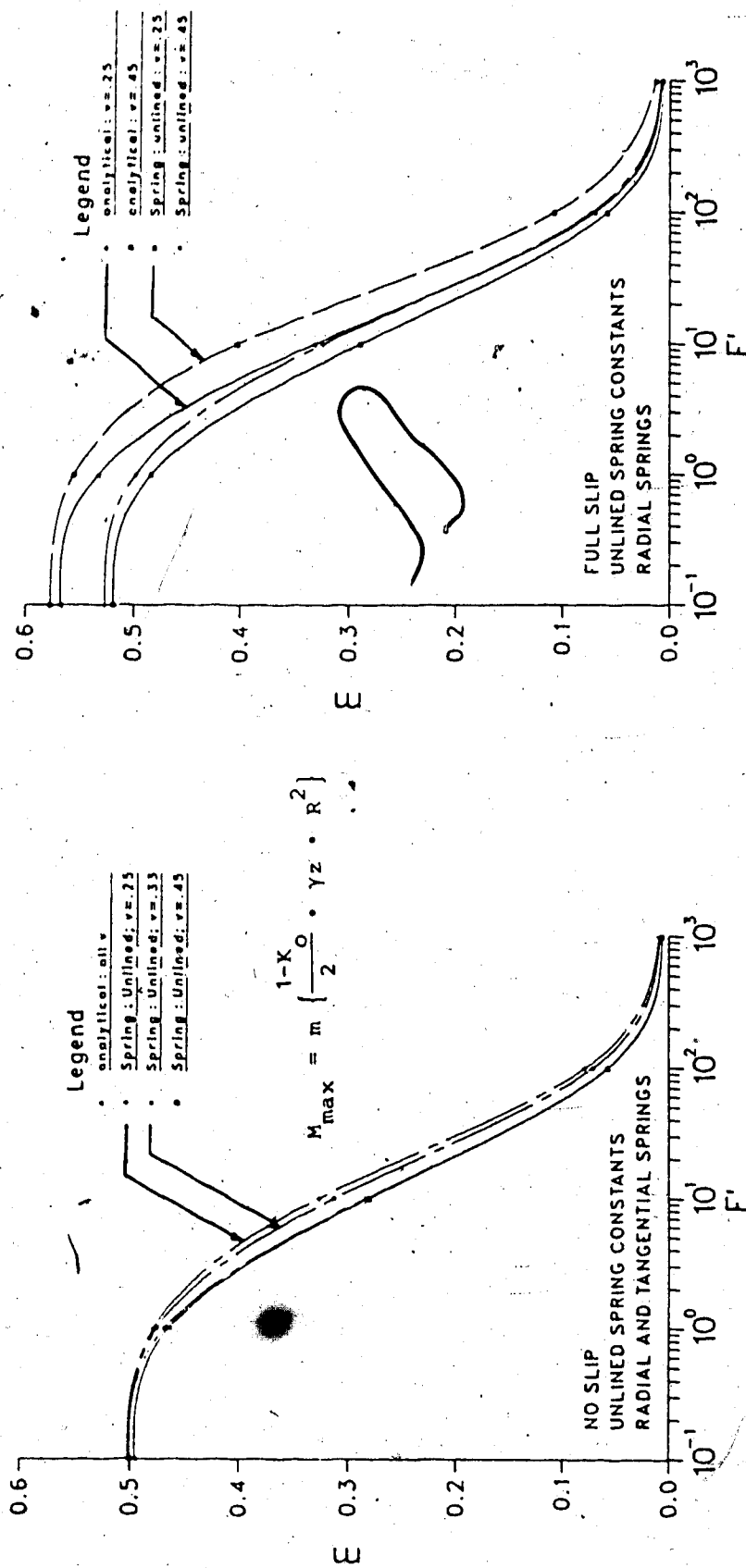
(a) no slip

(b) full slip

Figure 4.14 Variation of Moment Coefficient with Flexibility

Ratio: "Unlined" Combination

solution for all values of ν, with a maximum of 16% occurring for $\nu = 0.25$ and F' = 10.

Although the overall pattern of behaviour is simulated in the full slip conditions, the tendency to overestimate the analytical solution is more pronounced as seen in Figure 4.14(b). The maximum deviation occurs for F' = 10 where the values are overestimated by 21% for $\nu = 0.25$. This amount decreases to 12% for $\nu = 0.45$. The curves for $\nu = 0.33$ which are omitted from the figure describe a behaviour contained within the range provided by $\nu = 0.25$ and $\nu = 0.45$.

4.4.2.3 k_{ro} Only

The variation of the moment coefficient, m, with the flexibility ratio, F', is given in Figures 4.15(a) and (b) for no slip and full slip respectively.

Under no slip conditions, the "k_{ro} Only" assumption for the spring model provides a good simulation of the analytical solution. The response is only slightly affected by the different Poisson's ratio values and all three curves lie within ±4% of the analytical solution.

The full slip condition is also reasonably well simulated with $\nu = 0.25$ giving the least accurate results by underestimating the moments for F' = 10 by 7%. For simplicity, the curves for $\nu = 0.33$ are omitted, but once again, the response is bounded by the curves for $\nu = 0.25$ and $\nu = 0.45$.

This approach appears to provide the best match for the moment response, providing values within ±7% of the

Legend
analytical: r=25
analytical: r=45
Spring : Kro only r= 25
Spring : Kro only r= 45

FULL SLIP
kro ONLY SPRING CONSTANT
RADIAL SPRINGS ONLY

(b) full slip

Legend
analytical: all v
Spring : Kro only; v=.25
Spring : Kro only; v=.35
Spring : Kro only; v=.45

$$M_{max} = m \left\{ \frac{1-K_o}{2} \cdot \gamma_z \cdot R^2 \right\}$$

NO SLIP
kro ONLY SPRING CONSTANT
RADIAL SPRINGS ONLY

(a) no slip
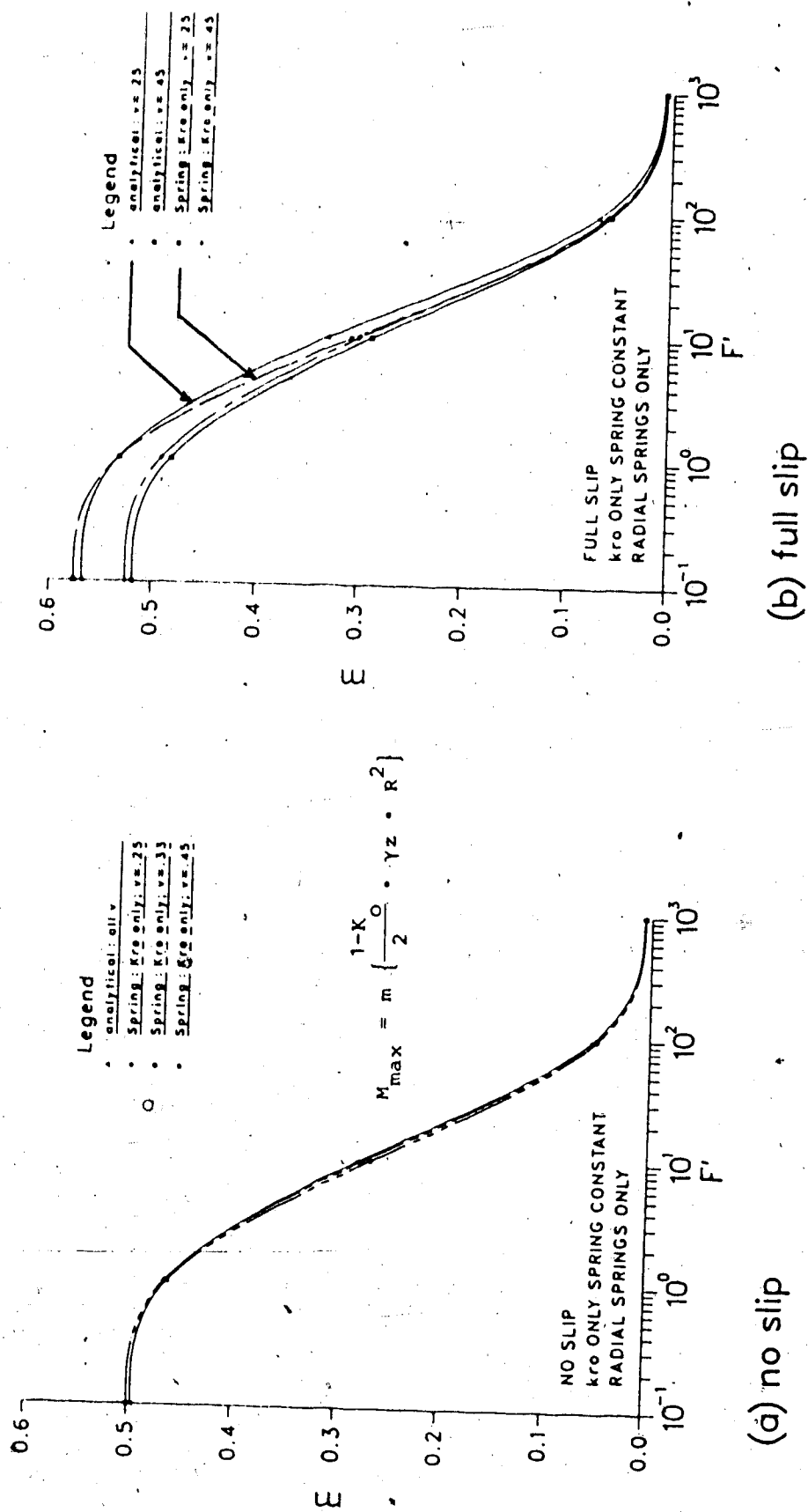
Figure 4.15 Variation of Moment Coefficient with Flexibility

Ratio: "k_{ro}" only Combination

analytical. Although the k_{ro} only combination does not provide values which are consistently on one particular side of the analytical solution for all ν, a pattern does emerge for both no slip and full slip. For $\nu = 0.25$, the results are always slightly smaller than the analytical and for $\nu = 0.45$, the values are slightly higher. For $\nu = 0.33$, the match for both interface conditions is very close.

4.4.3 Influence of the Flexibility Ratio on Thrust

4.4.3.1 Total Thrust

It is seen in Section 4.4.1 that the average thrust, $\bar{T}$, is essentially independent of the flexibility ratio, F', so that the variation in response shown in this section is due to the differential thrust induced by the distortional component of the loading.

Figures 4.16(a) and (b) illustrate the influence of the various spring constant combinations on the total thrust coefficient, $T/\gamma zR$, for no slip and full slip respectively. The curves are given for specifically $F' = 10$, $\nu = 0.33$, but the response is similar for all F' and ν. The deviation from the analytical solution is condensed or expanded depending on the particular values.

For no slip conditions, the deviations increase as F' increases, and as ν decreases. For any pair, F' and ν, all three spring constant combinations underestimate the maximum thrust $(K_o < 1)$ at the springline to some extent. The approach

using k_{ro} only consistently provides the closest value to the analytical solution with discrepancies that underestimate by up to 8% for the worst pairing of $F' = 1000$ and $\nu = 0.25$. The worst pairings in the lined and unlined combinations provide unconservative values in the order of 15%.

For the full slip simulation, all approaches provide curves which are very close to the analytical solution with no one combination producing a closer fit than the others. The maximum deviation of less than 2% occurs for $F' = 10$ and decreases for all other F' values. Figure 4.16(b) indicates the full slip response for the specific conditions of F' and ν given in Figure 4.16(a) and typifies the general behaviour for total thrust under full-slip conditions.

4.4.3.2 Differential Thrust

A closer inspection of the distortional, component of the thrust term, ΔT (deviation from the average thrust, $\bar{T}$), indicates that the spring model is poor at simulating the thrust response to the distortional load component.

Figures 4.17(a) and (b) illustrate this point for no slip and full slip respectively. These show the variation of the maximum thrust differential coefficient, n, with the flexibility ratio, F', for $\nu = 0.33$. The curves highlight the effect of the different spring constant combinations and describe a pattern of response which is generally similar for $\nu = 0.25$ and $\nu = 0.45$.
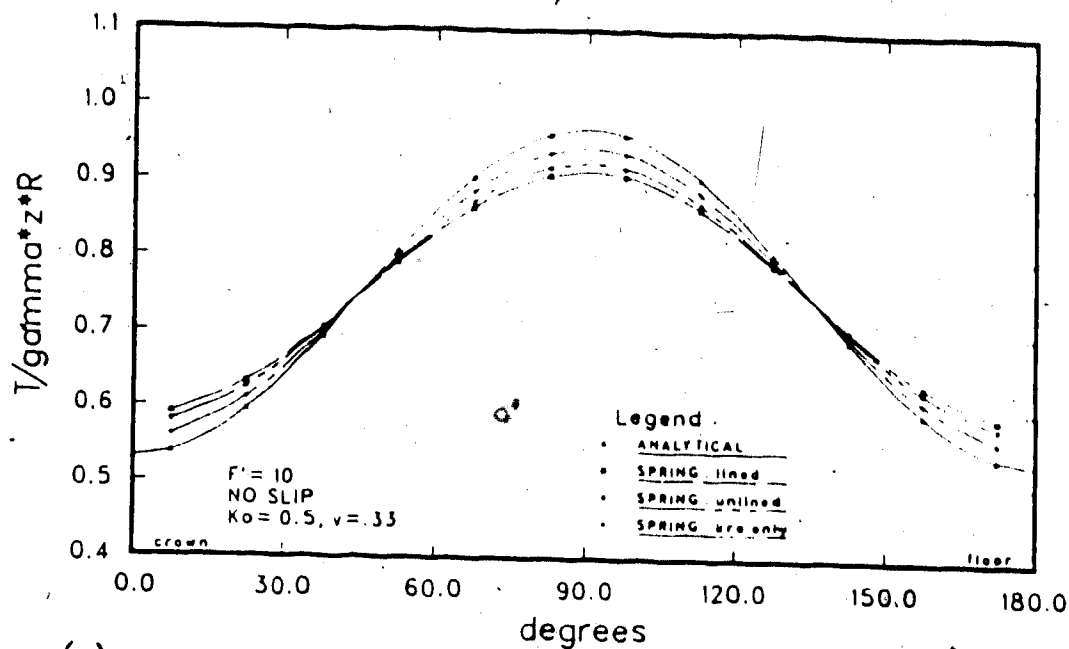
(a) no slip
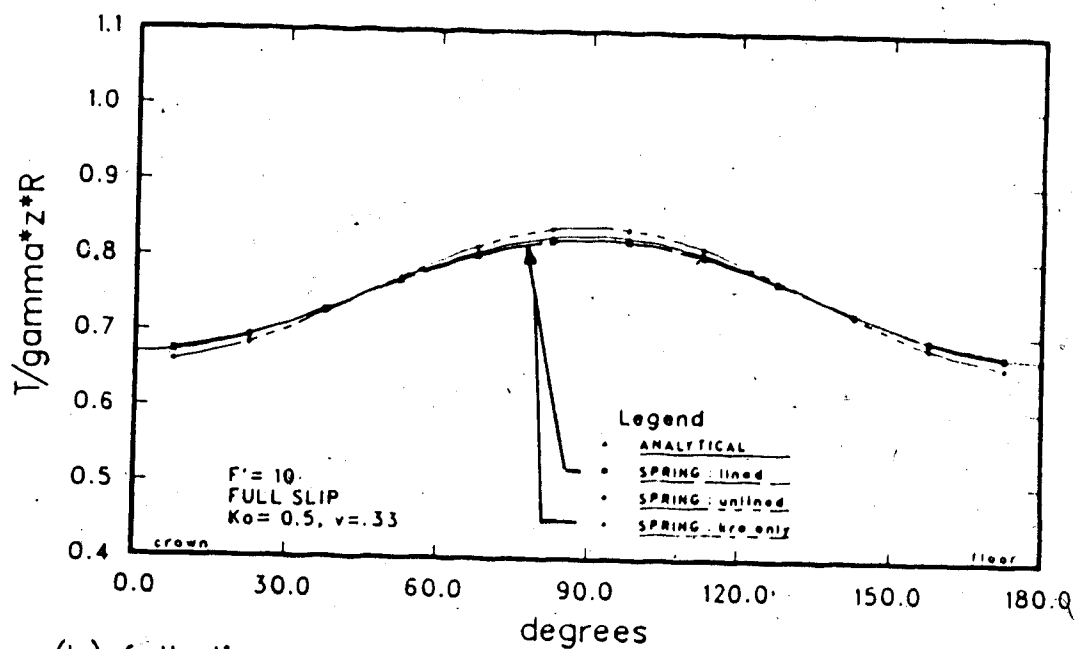
(b) full slip

Figure 4.16 Variation of Total Thrust Coefficient with

$$\Delta T_{max} = n \left[\frac{1-K}{2} \sigma \cdot \gamma z \cdot R \right]$$

(a) no slip

(b) full slip
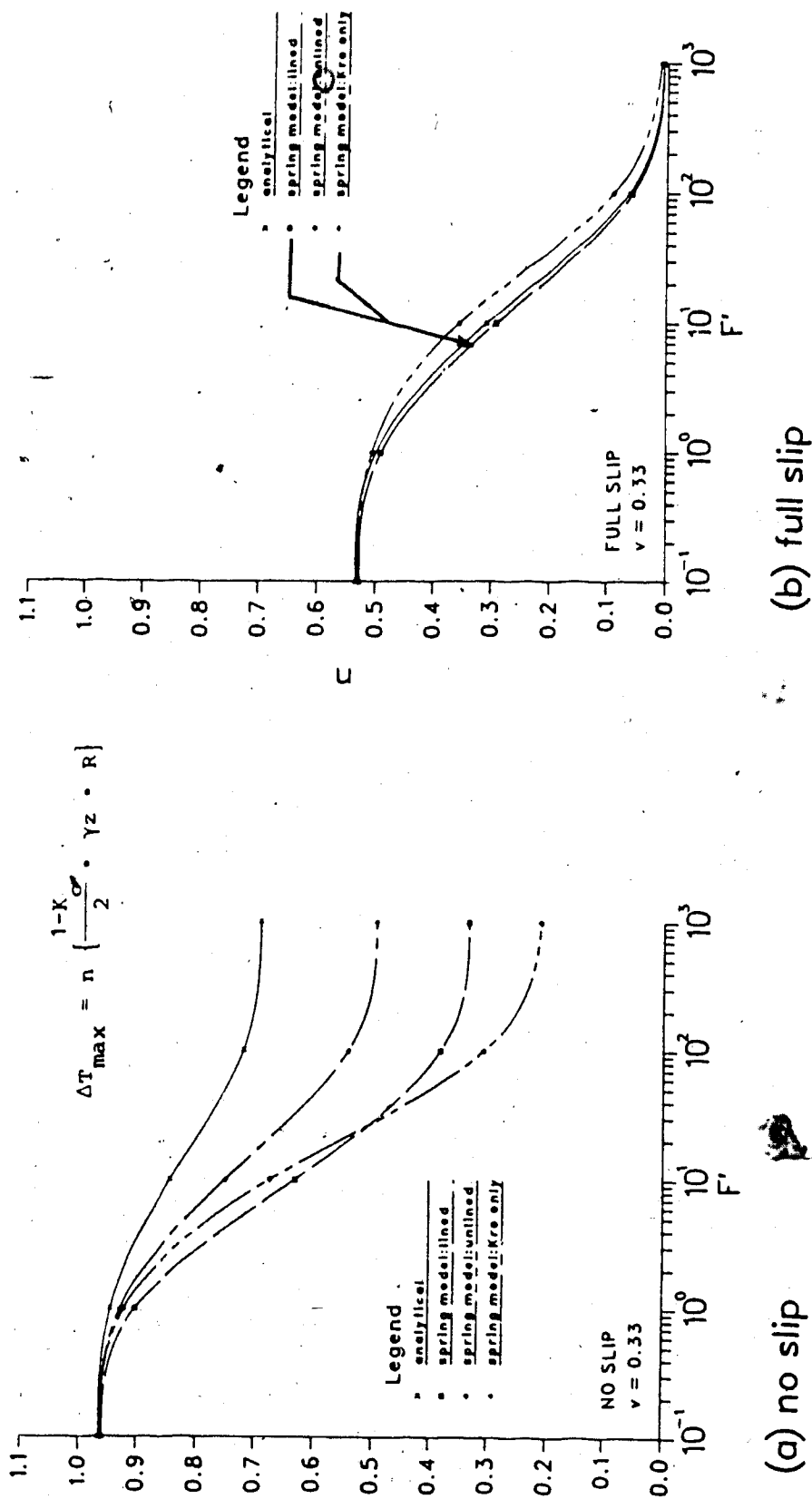
Figure 4.17 Variation of Maximum Thrust Differential
Coefficient with Flexibility Ratio

The influence of these inadequate simulations however, do not have the same major impact on the total thrust term described in Section 4.4.3.1.

The no slip condition shown in Figure 4.17(a) indicates that the discrepancies are strongly pronounced for F' values greater than 10, for which values the differential thrust component, ΔT, is less than about 20% of the total thrust, T. The net influence of the lack of match agreement in the ΔT simulation is a much reduced effect on the overall thrust term. For example, the curve for only in Figure 4.17(a) indicates that ΔT is underestimated by 28% for $F' = 1000$. This is combined with the average thrust, $\bar{T}$, to produce a value of total thrust, T, which underestimates the analytical solution by only 6%.

The full slip condition given in Figure 4.17(b) illustrates a lesser effect that ΔT has on the total thrust term. The large relative discrepancies which occur as F' increases are indiscernible since ΔT itself is negligible. This results in a minimal adjustment to the average thrust to obtain the total thrust. The outcome is that any of the three approaches simulate the full slip thrust conditions very well since the differential thrust effect is almost completely suppressed.

4.4.4 Influence of the Flexibility Ratio on Displacements

The analyses used to assess the influence of the flexibility ratio have a soil-liner configuration in which

the liner is virtually incompressible ($C' \approx 0$). This dictates that the constant inward displacements resulting from the uniform load component are essentially zero.

The displacement patterns illustrated in Figures 4.18 and 4.19 show the response to the distortional load component and are very much influenced by the spring constant combination selected to represent the soil behaviour in the model.

The shape of the curve for each spring constant combination and Poisson's ratio is similar in form to the analytical solution but the magnitude of the displacements differ considerably with the same parameters.

Figures 4.18 and 4.19 show the variation of the maximum displacement coefficient with the flexibility ratio for no slip and full slip respectively. Within each figure the responses for $\nu = 0.25$ and $\nu = 0.45$ are given. The model responses for $\nu = 0.33$ are not shown, but lie about midway between those given for $\nu = 0.25$ and $\nu = 0.45$ for each spring constant combination.

The in situ stress ratio, K_o, is 0.5 so that the maximum inward displacement occurs at the crown (and floor), and the maximum outward displacement occurs at the springline. For $C' = 0$, the magnitude of the maximum inward and outward displacements are equal.
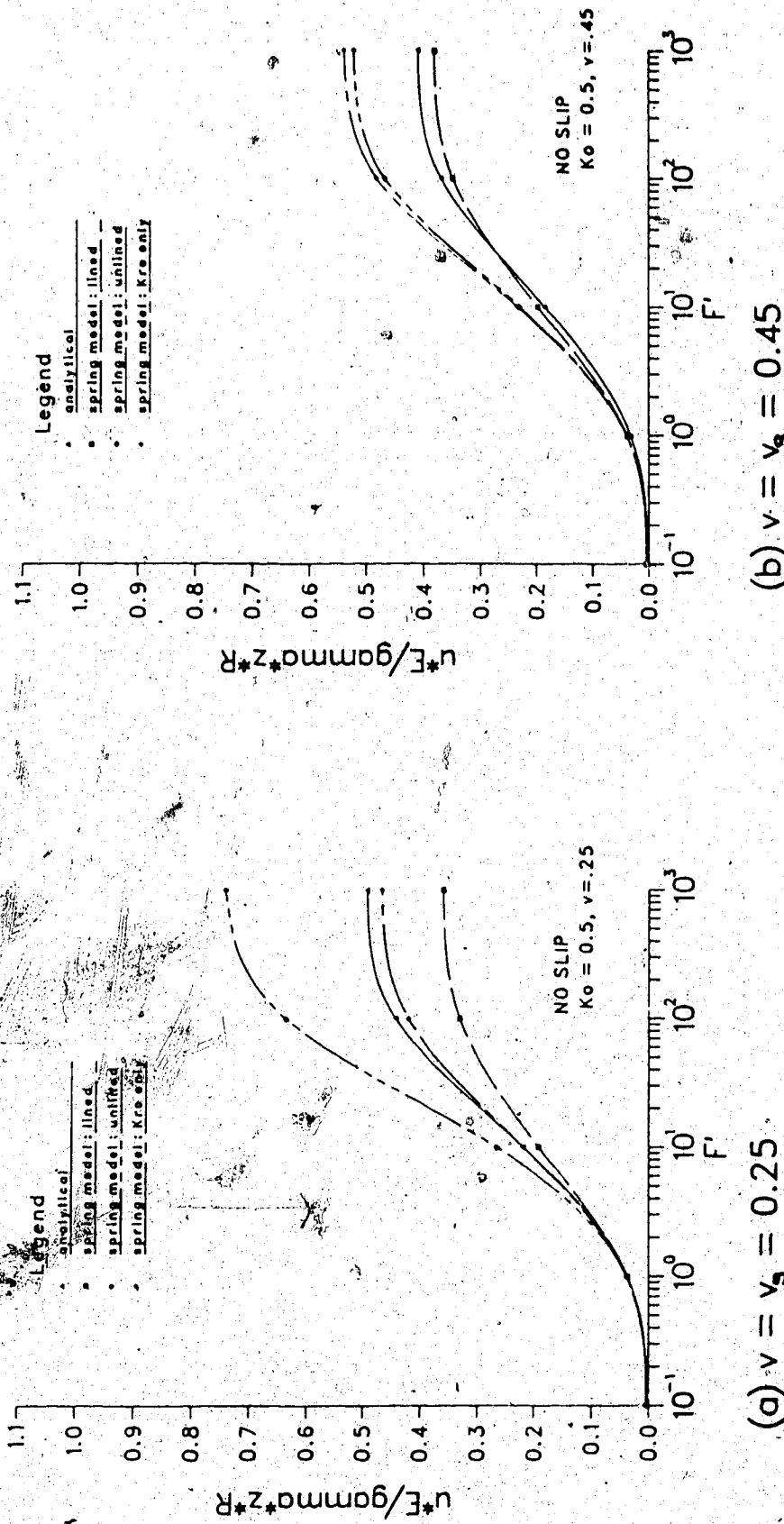
Figure 4.18 Variation of Maximum Displacement Coefficient with Flexibility Ratio : No Slip

(a) $v = v_s = 0.25$

(b) $v = v_s = 0.45$

(a) $v = v_s = 0.25$

(b) $v = v_s = 0.45$
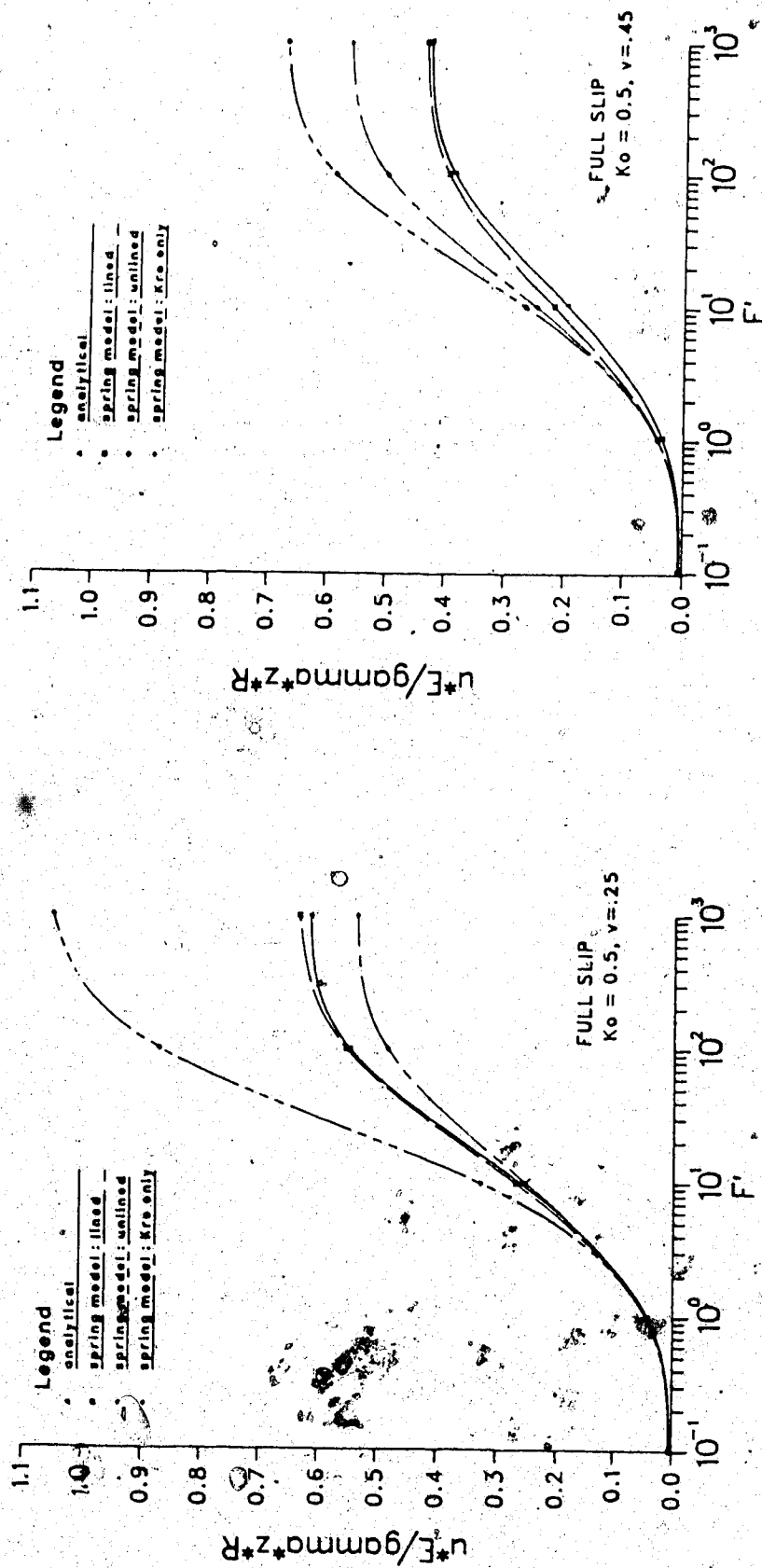
Figure 4.19 Variation of Maximum Displacement Coefficient
with Flexibility Ratio : Full Slip

4.4.4.1 Effect of Poisson's Ratio

For both no slip and full slip conditions, the influence of increasing $\nu = \nu_s$ is to decrease the overall range of displacements produced by the different assumptions for the spring representations. This indicates that the sensitivity of the displacements to the choice of soil representation decreases as ν increases.

For $\nu = 0.25$, Figure 4.18 shows that for F' = 1000, the no slip curves lie between +50% and -30% of the analytical solution. This range is more than halved for ν = 0.45 with bounds of +30% to -8% as seen in Figure 4.18(b). The range of displacements for the full slip conditions show a similar 50% decrease as ν increases. This is seen in Figures 4.19(a) and (b).

4.4.2 Lined Combination

The no slip response portrayed in Figure 4.18 indicates that the use of the lined spring constant combination always produces displacements which are usually less conservative than the analytical. The underestimate decreases as ν increases.

The full slip conditions given in Figure 4.19 show that a reasonably good match is possible with the lined combination. The model provides values which are within 13% greater than the corresponding analytical solution for all ν.

4.4.4.3 Unlined Combination

It can be seen in Figure 4.19 for no slip that the unlined spring constant combination always generates an extremely conservative response. The conservatism is exaggerated for the full slip conditions shown in Figure 4.19.

4.4.4.4 k_{ro} Only

As for the moment response described in Section 4.4.2.3, the use of k_{ro} only to describe the soil response does not consistently provide conservative or unconservative values according to the interface condition. Once again, it rather depends on the value of ν, and for $\nu = 0.25$ the model provides less than a 10 % underestimate of the analytical solution for both no slip and full slip. This is seen in Figures 4.18(a) and 4.19(a). Although not shown, the responses for $\nu = 0.33$ produce good simulations for both no slip and full slip with curves which deviate up to 6% more than the analytical.

For $\nu = 0.45$, the radial displacements in both the full slip and no slip cases are overestimated in the order of 30%.

4.5 Summary

A detailed description of an analytical solution for an excavation loading in deep conditions is provided. The response expected for variations with the flexibility and compressibility ratios provides the basis for comparison of

the discrete ring and spring model.

Three spring constant combinations representing the soil behaviour in the spring model are individually assessed to determine the approach which provides the closest simulation of the analytical solution.

Although individual aspects of the responses are better in some instances than the other approaches can provide, no one approach becomes particularly dominant for every part of the simulation.

The soil representation assuming "k_{ro}" only perhaps provides the best overall response since, although the results are not consistently on one side of the analytical solution, they are usually acceptably close. An advantage in favour of this approach is that the model uses only radial springs whose stiffnesses are defined by the spring constant associated with uniform convergence, $k_{ro} = \frac{1}{1+\nu} \cdot \frac{E}{R}$. The entire input load is subject to this spring stiffness and the results are therefore obtained with one computer run.

The lined spring constant combination produces results which underestimate the analytical solution in all respects, except for providing an essentially perfect match for the full slip displacements. Although these lined spring constants are the expressions derived for the full correspondence between the analytical solution and the continuous ring and spring approach, the discrete spring representation responds in a more rigid manner and attracts some load which should be carried by the liner. The presence

of the tangential springs enhances this rigidity.

The unlined approach typically produces results which
overestimate the analytical solution. Although a
conservative approach might be preferred, the actual degree
of conservatism is quite excessive in some instances.

5. ANALYSIS OF DISCRETE RING AND SPRING MODEL FOR SHALLOW TUNNELS

5.1 Introduction

The results of the deep tunnel simulations in Chapter 4 indicate that of the three models tried, the discrete spring model with radial springs only provides a response closest to Ranken's (1978) analytical solution. In Chapter 5, this particular model is compared with the analytical Hartmann (1970, 1972) solution which accounts for the additional stresses due to gravity which prevail in a shallow tunnel.

The formulation of the Hartmann solution assumes the soil is represented by an infinite plate the soil and so does not model the shallow tunnel effects of being close to the stress free ground surface. However, in comparison with an appropriate finite element analysis, the analytical approach is very similar for relative depth ratios, H/D > 1.5 (Negro, 1988), indicating that the ground surface effects may be ignored below this depth.

In this Chapter it will be shown that the fully embedded model with radial springs only, compares reasonably well with these models.

The commonly promoted partially embedded spring model for shallow tunnels (Duddeck and Erdmann, 1982, 1985) assumes that the liner in the crown region is not supported by active springs. It will be shown that this approach provides results which are very conservative for good ground

control conditions (Negro, 1986:166), even though a stiff spring constant is adopted to describe the soil response away from the unsupported crown.

The assumption of full overburden is usually applied for the design of the final support, mainly because sensible criteria are not available to make some estimate of permanent ground stress relief.

In recognition of the stress release and the stiffness reduction which occurs in the tunnelling process, it is normal to take account of reduced loads for the primary liner design. Until the design process proposed by Negro (1988) however, the reduced loads and stiffnesses for application in ring and plate or ring and spring models were obtained empirically. Negro's (op.cit.) design process is described briefly and the modifications necessary to implement the ring and spring model as an alternate approach for the ground-liner interaction phase are presented.

A case history indicates that the ring and spring model provides a reasonable alternate for the analytical approach originally suggested by Negro (op.cit.).

5.2 Analytical Solution for Shallow Tunnels - Hartmann

5.2.1 General

The analytical ring and plate solution by Hartmann (1970, 1972) fully accounts for the non uniform stress field existing in a shallow tunnel. This stress field results from

an in situ stress ratio, K_o, different from unity and from gravitational effects.

The solution neglects the effects of proximity to the ground surface because the ground is represented by an infinite plate. The consequences of this assumption were investigated by Negro (1988:1126) and are recorded in Section 5.2.3.

The full details of the Hartmann solution are provided by Negro (op.cit.:1117), but briefly, the general assumptions given in Section 4.2.1 for the analytical solution in deep conditions, apply also for the shallow conditions, except that the lining is activated by the excavation loading conditions described in Figure 2.8.

Negro (op.cit.:99) indicates that the ratio of mobilized shear stress to acting normal stress at the soil-lining interface is a measure of the shear strength mobilization. Generally this ratio shows that small zones of localized slip might occur, but that a full slip condition around the tunnel profile would not exist. The shear strength mobilization decreases as H/D increases, as K_o approaches unity and as the lining becomes more flexible. For this reason, only the no slip solution is considered.

5.2.2 Summary of the Hartmann Solution

The notations and positive sign conventions used in Hartmann's solution are given in Figure 5.1. A summary of the no slip solution is presented in Figure 5.2.

As for the deep conditions, the final form of this thin liner solution is simplified by using a compressibility ratio, $\hat{a}$, and a flexibility ratio, β, where

$$\hat{a} = \frac{E_s A_s (1+\mu)}{E \ r_o (1-\mu_s^2)} \qquad [5.1]$$

$$\beta = \frac{E_s I_s (1+\mu)}{E \ r_o^3 (1-\mu_s^2)} \qquad [5.2]$$

E_s, A_s, I_s and E are as defined earlier, r_o is the tunnel radius and μ and μ_s are the Poisson's ratios for the soil and the support (liner) respectively.

As in Chapter 4, the results of the analyses are mostly presented using the Einstein and Schwartz (1979) stiffness ratios, C' and F'. The expressions for $\hat{a}$ and β are related to equations [2.1] and [2.2] defining C' and F' respectively, as follows.

$$\hat{a} = \frac{1}{C'(1-\nu)} \qquad [5.3]$$

$$\beta = \frac{1}{F'(1-\nu)} \qquad [5.4]$$

5.3 Discrete Ring and Spring Models

Both fully embedded and partially embedded discrete ring and spring models are investigated for the shallow tunnel conditions.
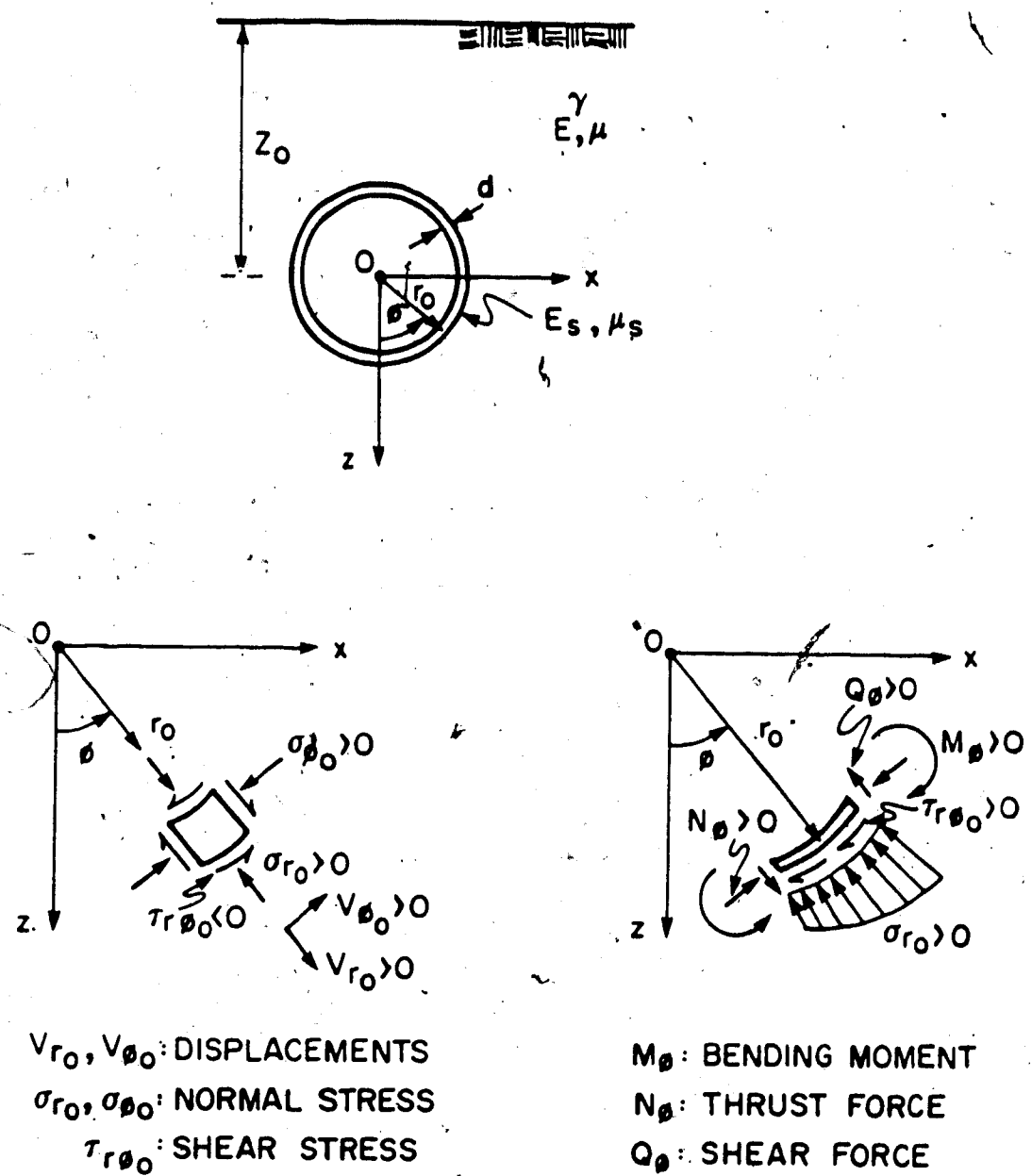
Figure 5.1 Notations and Conventions used in Hartmann's
Solution (after Negro, 1988)

$$(5.1)$$

$$(5.2)$$

(5.3)

(5.4)

(5.5)

(5.6)

(5.7)

(5.8)

(5.9)

(5.10)

(5.11)

(5.12)

(5.13)

Figure 5... ining Stresses, Displacements and Internal
Forces Given by Hartmann's Solution (after Negro, 1988)

The circular configuration shown in Figure 3.5 which has radial springs at 15° intervals is used for both approaches. For the fully embedded condition, all the springs are assumed to be effective. The partially embedded condition is achieved by assigning zero stiffness to the springs in the crown region where the partially embedded model assumes the soil is not contributing to the resistance of the soil-liner system. This would be appropriate if the dead weight of the soil was transferred entirely to the liner. Note that if full overburden is assumed in the loading then the partially embedded configuration represents a column of soil extending from the tunnel crown to the ground surface bounded by vertical failure surfaces which have zero shear strength. This condition is not encountered in reality, except if the material itself has no shear strength.

In tunnelling operations where good ground control is maintained, the soil could reasonably be expected to always participate in load sharing with the liner. This condition is represented in the discrete ring and spring model by assigning a non zero stiffness to all of the springs as done in the fully embedded model.

5.3.1 Fully Embedded Model

The geometry and fixed parameters of the fully embedded model for shallow conditions are given in Figure 5.3(a) and the variable parameters are tabulated in Figure 5.3(b). The ring and spring model geometry is as shown in Figure 3.8

with radial springs only.

Essentially the details for the geometry, material properties and input variables defining the stiffness ratios C' and F,' are as described in Sections 4.3.2 and 4.3.3 for the deep conditions. The effect of gravity is assessed through introducing variations in the soil cover to diameter ratio, H/D.

An inspection of the output data indicates that the patterns established for the effect of variations in Poisson's ratio on the deep solution also apply when the effect of gravity is included. For this reason, the results are typically shown for $\nu = \nu_s = 0.33$.

5.3.1.1 Spring Constant Combinations

The results recorded in Chapter 4 indicate that, of the three different ground response representations investigated, the values provided by the "k_{ro} only" model simulate the analytical solution most closely. This model has radial springs only with stiffnesses determined from the spring constant, $k_{ro} = \frac{1}{1+\nu} \cdot \frac{E}{R}$, defining the soil convergence response to uniform pressure. This approach is used for the parametric studies and is seen to provide good results for moments, thrusts and displacements.

The expressions established by Negro (1988:375) for the equivalence between the continuous ring and spring model(i.e. a model with an infinite number of springs) and analytical ring and plate solution for an unlined circular opening in a gravitational stress field are seen in Figure

(a) fixed parameters

γ kN/m³

E   MPa

$K_o = 0.5$

R=1m

$E_s = 10000$ MPa
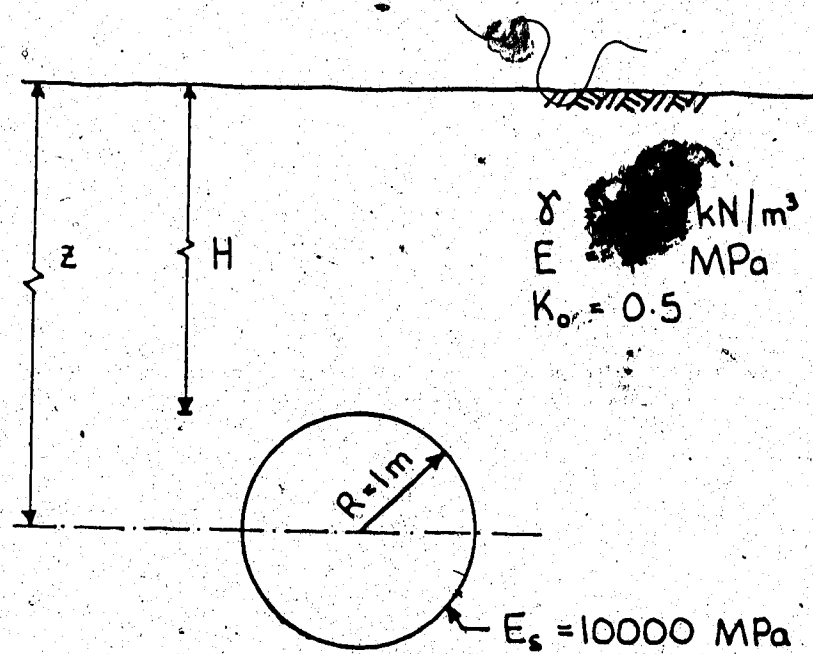
Parameter	Values				
F'	.1	1	10	100	1000
$\nu = \nu_s$	.25		.33		.45
spring constant	'k$_{rb}$ only'				
H/D	0.5	1.0	2.0	3.5	5.0
loading$	no slip				

$ See Figure 2.8

(b) variable parameters

Figure 5.3 Parameters Used in the Spring Model Analyses for Shallow Tunnels

3.7. For common values of the variables in the expression for the radial spring constant, k_r, Negro (op. cit.) shows that the average radial spring constant is

$$\bar{k}_r = (1.05 \pm 0.06) k_{ro}$$
[5.5]

Equation 5.5 indicates that generally the unlined expression describes a stiffer soil response than obtained by setting $\bar{k}_r = k_{ro}$. This in turn provides a less conservative estimate of the liner actions since more of the load will be carried by the soil.

If the tangential springs are also introduced into the system with stiffnesses described by the tangential spring constant k_t in Figure 3.7, the stiffness of the soil is further enhanced and the liner is required to support even less load.

It is anticipated that the equivalence between the continuous spring model and analytical solution for a lined circular opening in a gravitational stress field would produce estimates for the liner actions which are less conservative than the unlined values. The introduction of a liner into the opening constrains the soil displacements and alters the associated stress distribution in the soil in such a way that the soil response is described by a stiffer spring constant. Although the development of the full correspondence for the lined opening would be interesting in terms of the complete picture, the anticipated

unconservatism for liner actions render this exercise unnecessary for use in the discrete ring and spring models.

5.3.1.2 Input Loads

As described in Section 2.2.5.1, the installation of a rigid liner (C=F=0) into an excavated opening in a gravitational stress field results in a redistribution of the in situ stresses even for the no-slip interface condition. Accounting for this buoyancy effect provides the stress distribution illustrated in Figure 2.8. The equations for the radial stress, σ_r, and the shear stress, τ, are combined to provide the input loads recognized by the liner.

For the given radius of R=1 m, the gravity components, σ_g and τ_g, of each expression remain constant, where for ϕ measured from the crown,

$$\sigma_g = -\frac{\gamma R}{4} \{(1+K_o)\cos\phi + (1-K_o)\cos3\phi\} \tag{5.6}$$

$$\tau_g = \frac{\gamma R}{4} \{(1+K_o)\sin\phi - (1-K_o)\sin3\phi\} \tag{5.7}$$

The resulting interaction provides the moments, thrusts and relative deformations of the liner.

If an assessment of the absolute displacements is required, then the original in situ stresses with gravity effects as described in Figure 2.2 are applied as input loads and the vertical upward displacement at the springline provides an estimate of the heave.

For a given R, K_o and γ, the estimate for the vertical heave at the springline is virtually constant for any value of H/D.

This provides an advantage over the Hartmann solution in which the heave component, v_{zo}, varies according to the value of r_1, as seen in Figure 5.2. The parameter, r_1, is the distance to a boundary where zero displacements occur or to the ground surface.

Values of H/D = 0.5, 1.0, 2.0, 3.5 and 5.0 are used to assess the influence of the gravitational components given in equations 5.6 and 5.7.

5.3.2 Partially Embedded Model

The geometry of the model is identical to that used for the fully embedded model with radial springs at 15° for the full contour. The partially embedded assumption is realized by assigning zero stiffness to the springs in the regions where the soil is assumed to not provide any self support.

This approach is recommended by Duddeck and Erdmann (1982, 1985) for designing very shallow tunnels as shown in Figure 3.1. It is seen in the results in Section 5.4 that the influence of gravity on the maximum liner actions is still evident for H/D ratios larger than the 1.5 value Duddeck and Erdmann (op.cit.) indicate as sufficient for including these effects, but the discrepancies are not substantial.

The investigations applied to this model assess a range
of H/D values between 0.5 and 5.0. These depths result in
very little difference in the various expressions
approximating the gravity loading condition. Examples of
these stress distributions are those by Schulze and Duddeck
(1964) and Windels (1966), and these are presented in Table
3.1 along with the equations for the shallow conditions
which they approximate.

5.3.2.1 Effect of Unsupported Arch Span on Crown Moments

The unsupported arch is generally taken to be 90°, but
other angles have been assumed. The shallow stress
distribution given in Figure 2.8 is used for the
investigation of the effect of progressively "disconnecting"
the springs in the crown region as shown in Figure 5.4.

The crown moment, M_c, is the critical action resulting
from the partially embedded assumption and in Figure 5.4 it
is normalized to the crown moment, M_{co}, of the fully
embedded model. Figure 5.4 illustrates the response of the
crown moment as the unsupported arch span is increased from
0° to 90°.

The curves indicate that the 90° unsupported arch
region is not the most critical in terms of crown moment.
The geometry of the unsupported span mobilizes sufficient
resistance from arching effects that the crown moments
actually decrease after reaching a maximum at about a 70°
arc.

At present, it is not uncommon that a prerequisite of
tunnel construction is to ensure good ground control
conditions. Negro (1988:166) defines tentative criteria to
assess these quantitatively in terms of a normalized
displacement, U. If these conditions hold, then the crown
soil provides some self support, and a design approach such
as the fully embedded ring and spring model is appropriate.
Under these circumstances, the increase in magnitude of the
crown moments by six to ten times the fully embedded
equivalent indicates that the partially embedded assumption
is extremely conservative.

The absolute values obtained by using the partial
spring model are compared with other approaches in the
discussion of the influence of the stress free ground
surface in Section 5.4.3.

5.4 Calibration of the Fully Embedded Spring Model

5.4.1 General

By inspecting the no slip equations for the radial and
tangential stresses in Figures 2.2 and 2.8, it is seen that
the shallow tunnel conditions are an extension of the deep
tunnel conditions with the inclusion of terms accounting for
the effect of gravity.

The investigation of the fully embedded discrete ring
and spring model in shallow conditions is concentrated on
simulating the gravitational influence since the portion of
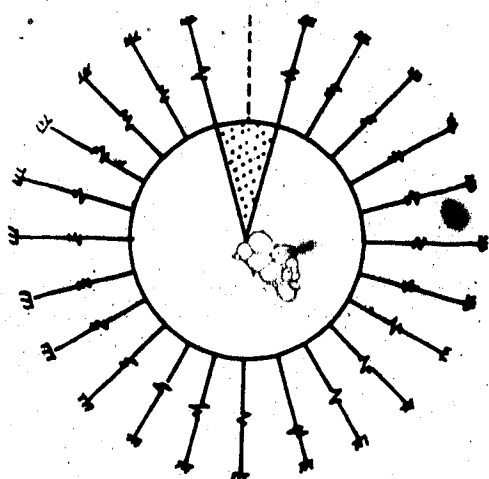
(a) 30° unsupported arch   (b) 90° unsupported arch

Mc: unsupported crown moment
Mco: fully supported moment
Ko = 0.5, v=.33

Legend
- H/D = 0.5
- H/D = 1.0
- H/D = 2.0
- H/D = 3.5
- H/D = 5.0

Mc/Mco
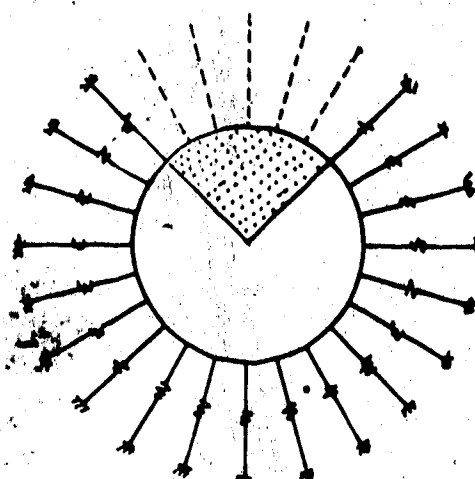
unsupported crown arch
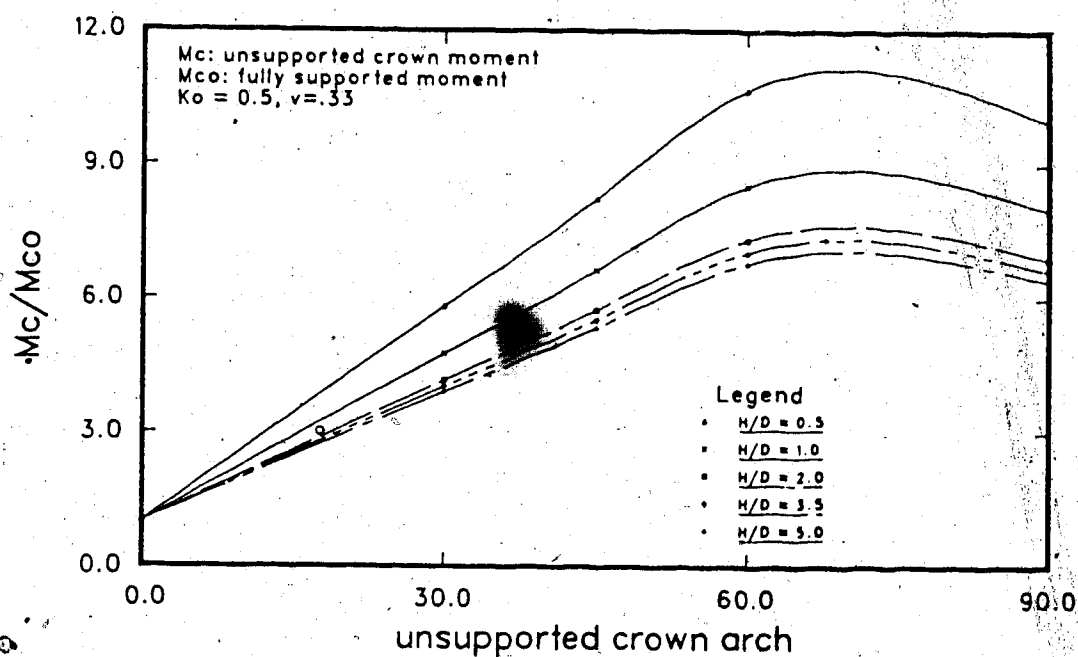
(c) effect on crown moment

Figure 5.4 Effect of Unsupported Arch on Crown Moment

the response defined by deep conditions is discussed in detail in Chapter 4.

For a given excavated tunnel radius, the gravitational stress contribution is constant for any depth. Its influence is more strongly felt as the cover depth, H, decreases because it comprises an increasingly larger percentage of the overall stresses applied to the lining.

From the results given in Chapter 4, it is seen that the distortional components of the applied loading are susceptible to variations in the flexibility ratio, F', and that the response to changes in the common range of compressibility ratios, C', is of much smaller consequence.

Since the gravitational stress contribution is of a non-uniform nature, the effect of variations in the liner flexibility is emphasized.

Comparisons performed in this chapter consider the overall response pattern to the no slip excavation loading condition. A separation of the components would not provide any further information to the material presented in Chapter 4. It is seen there that the discrepancies which appear in the discrete ring and spring model results are mainly due to the poorer simulation of the response to the distortional components. The general patterns of response to variations in stiffness ratios and Poisson's ratio established in Chapter 4 also apply in the shallow conditions.

5.4.2 The Influence of Gravity

The influence of gravity is assessed by varying the cover depth/diameter ratio, H/D. Values of H/D = 0.5, 1.0, 2.0, 3.5 and 5.0 are considered, but for clarity, the results of some of these curves are omitted in various figures.

5.4.2.1 Thrust Variation with Compressibility Ratio

An assessment of the response of the maximum total thrust coefficient to variations in the compressibility ratio, C, including the effect of gravity is shown in Figure 5.5.

The input parameters for the study are the same as those used for the deep conditions described in Section 4.4.1. However, for the shallow conditions, the variation in H/D plotted only for a Poisson's ratio of $\nu = \nu_s = 0.33$.

The model has radial springs only with a stiffness defined by $k_{ro} = \frac{1}{1+\nu} \cdot \frac{E}{R}$.

The maximum thrust occurs away from the springline and the analytical and spring model approaches do not necessarily peak at the same location, although this difference is only a matter of a few degrees. The curves in Figure 5.5 were produced using the maximum thrust values regardless of their location.

As expected, an increase in the compressibility ratio produces a reduction in the maximum total thrust. When compared with Figure 4.12, it is deduced that this reduction is predominantly in response to the uniform component of the
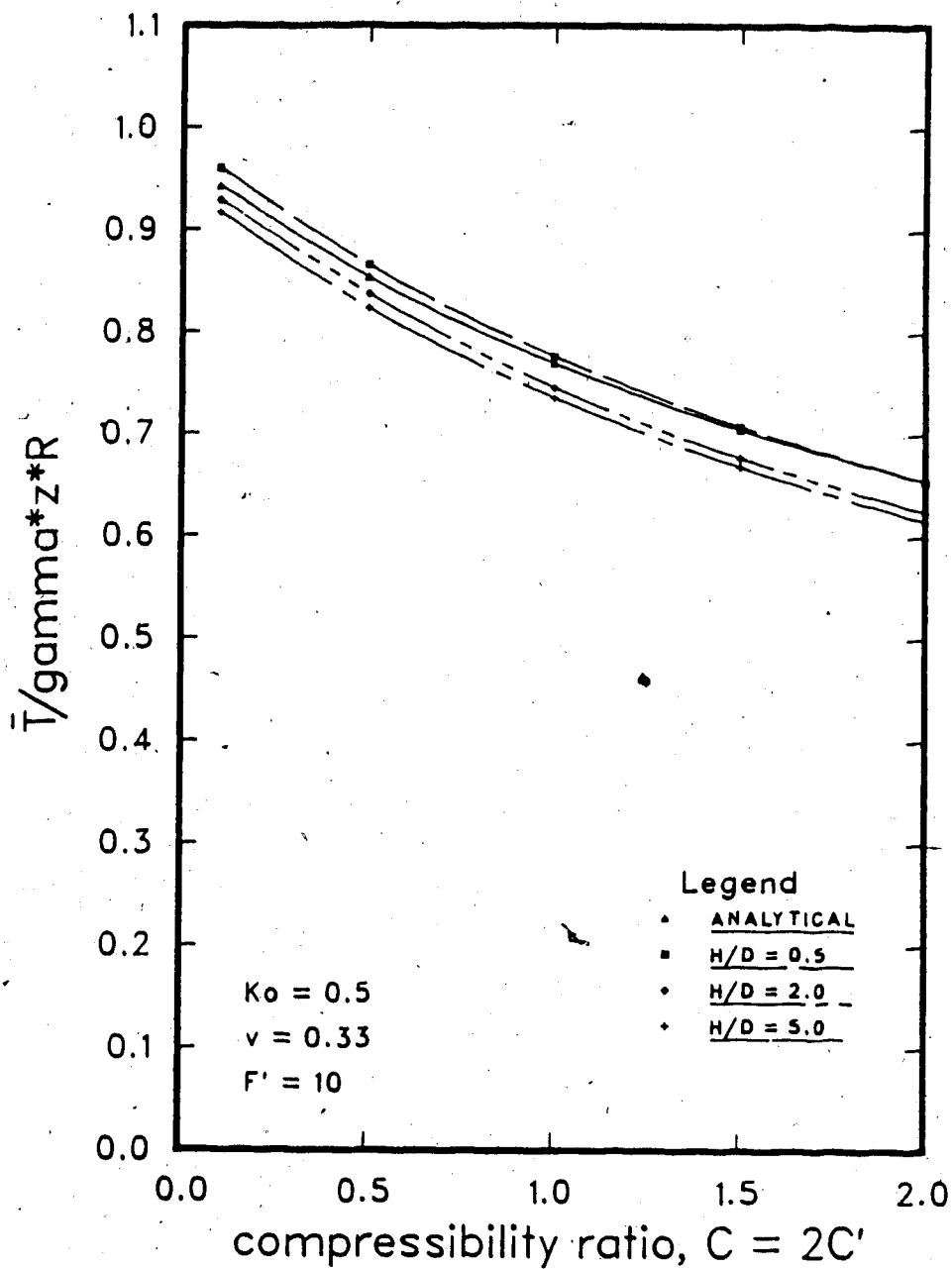
Figure 5.5 Influence of Gravity on the Variation of Total Thrust Coefficient with Compressibility Ratio

input load and is affected very little by the gravitational component.

5.4.2.2 Moment Variation with Flexibility Ratio

Figure 5.6(a) illustrates for the analytical solution, the influence of gravity on the moment coefficient response for $F'=10$ and $K_o=0.5$. It is seen that there is not a major alteration in the response by including the effect of gravity. For H/D = 3.5, the shift in the distribution from the deep tunnel solution is negligible.

The maximum increase in the moment occurs at the floor with a corresponding decrease of similar magnitude affecting the moments at the crown. For H/D = 0.5, the maximum adjustment in crown moment due to gravity effects for all F' values is 11%.

The conditions in the springline region are virtually identical to the deep solution except the local maximum moment is relocated to slightly below the springline. Figure 4.6(b) provides the comparison of the fully embedded ring and spring model results with the analytical solution.

Although the curves are presented only for $F'=10$ and $H/D=0.5$, the response to the input loads including gravity is well simulated for all variations in F' and H/D. The maximum deviation for any combination underestimates the shallow tunnel analytical solution by 4%.

Figure 5.7 provides a more general representation for the moment coefficient response with variations in the flexibility ratio, F'. Both the moment coefficient for the
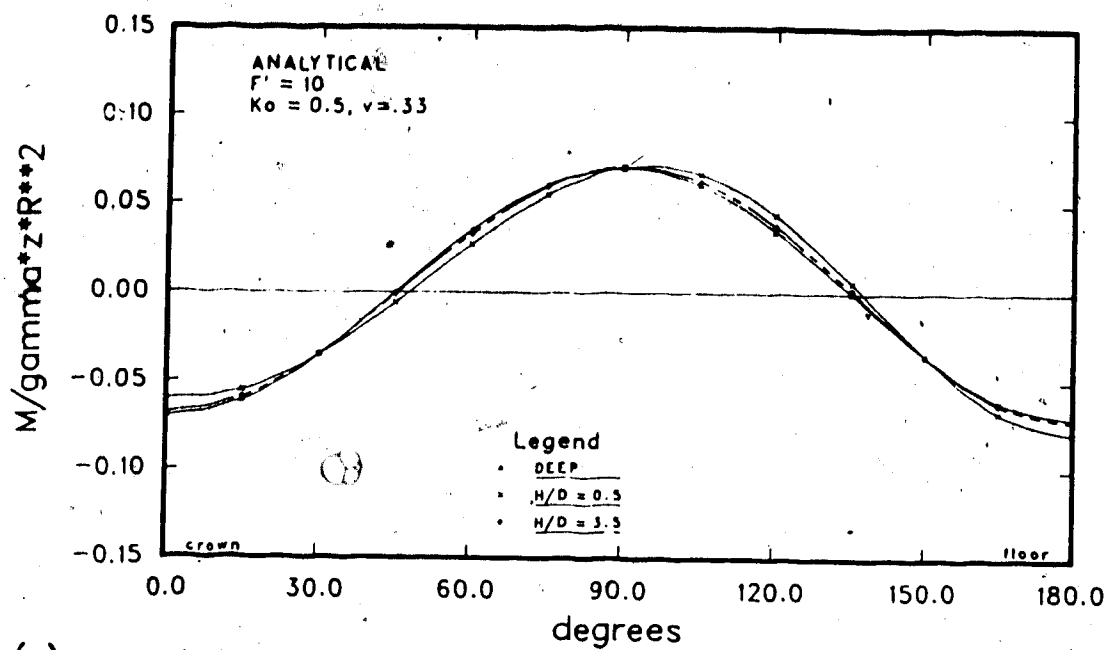
(a) analytical solution
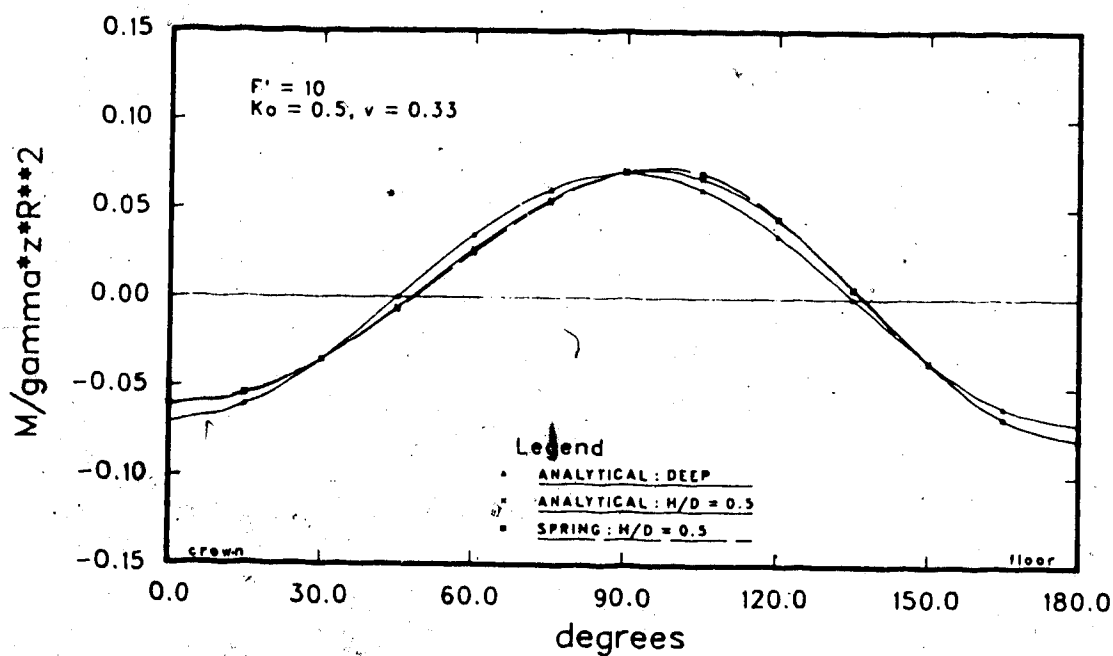
(b) comparison of spring model with analytical solution

Figure 5.6 Influence of Gravity on the Distribution of the Moment Coefficient

crown and the floor are illustrated for H/D=0.5 and 2.0 and $\nu=0.33$.

It is seen that as H/D increases, the difference between the crown and floor moment coefficients rapidly decreases, and both values converge towards the single value associated with the deep solution. The simulation provided by the discrete spring model agreed very closely with the corresponding analytical and for this reason, the analytical curves are not included here.

5.4.2.3 Thrust Variation with Flexibility Ratio

Figure 5.8(a) illustrates the gravitational effects on the distribution of the thrust coefficient for the analytical solution. It is seen that the relative depth, H/D, of the tunnel exerts a strong influence on the distribution of thrust throughout the contour with a relocation of the maximum thrust, for $K_o<1$, away from the springline towards the floor. However, the increase in maximum thrust, regardless of circumferential location, is relatively small and in the order of 5% for any value of F'.

Figure 5.8(b) shows the reasonable simulation that is possible with the fully embedded spring model. Although for clarity the figure illustrates curves only for F'=10, the maximum underestimate of the analytical equivalent for any value of F' is 5%.

$$M_{max} = m_0 \left\{ \frac{1-K_0}{2} \cdot \gamma z \cdot R^2 \right\}$$

Legend

ANALYTICAL : DEEP

SPRING Mc: H/D = 0.5

SPRING Mf: H/D = 0.5

SPRING Mc: H/D = 2.0

SPRING Mf: H/D = 2.0

Mf : moment at floor
Mc : moment at crown
v = 0.33
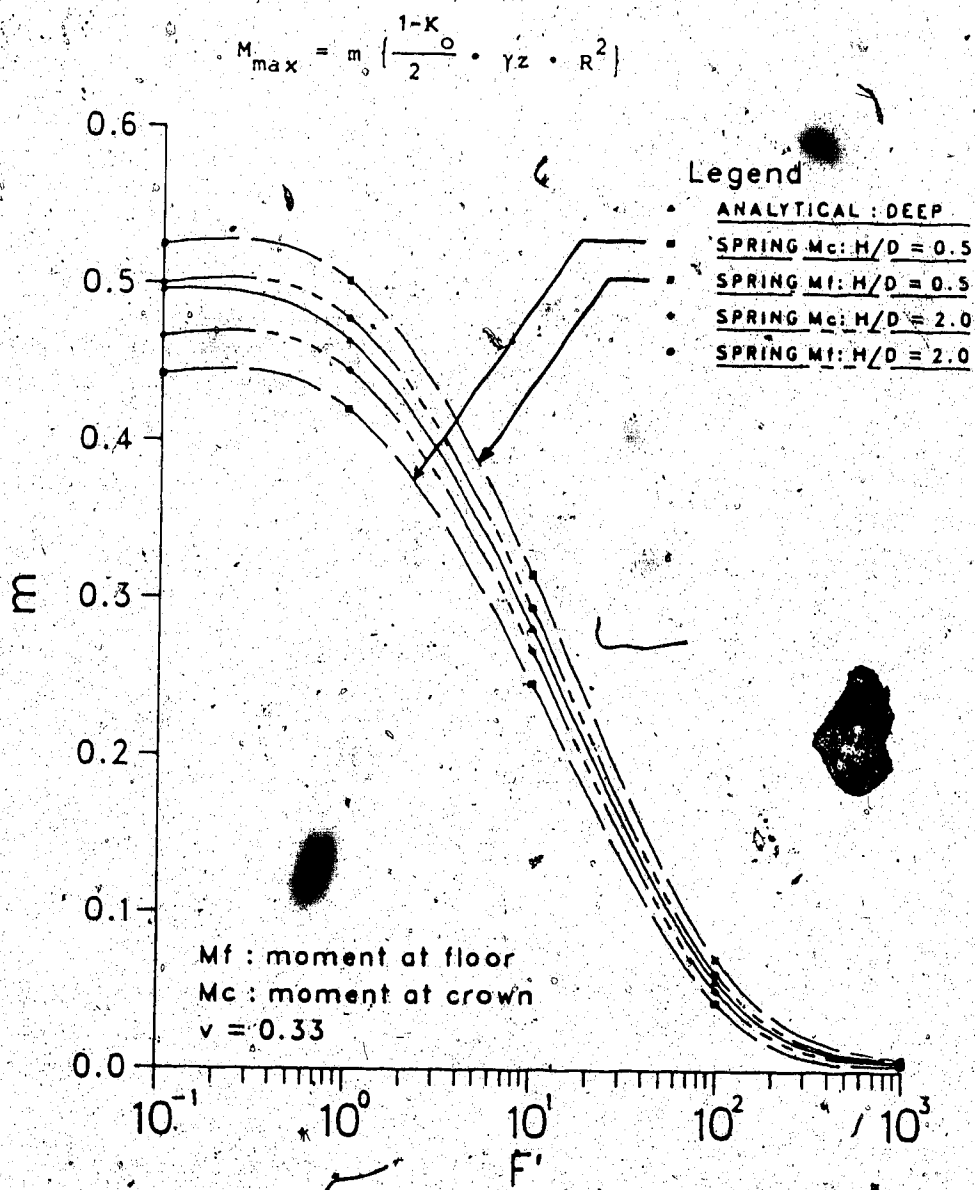
Figure 5.7 Influence of Gravity on the Variation of Moment
Coefficient with Flexibility Ratio
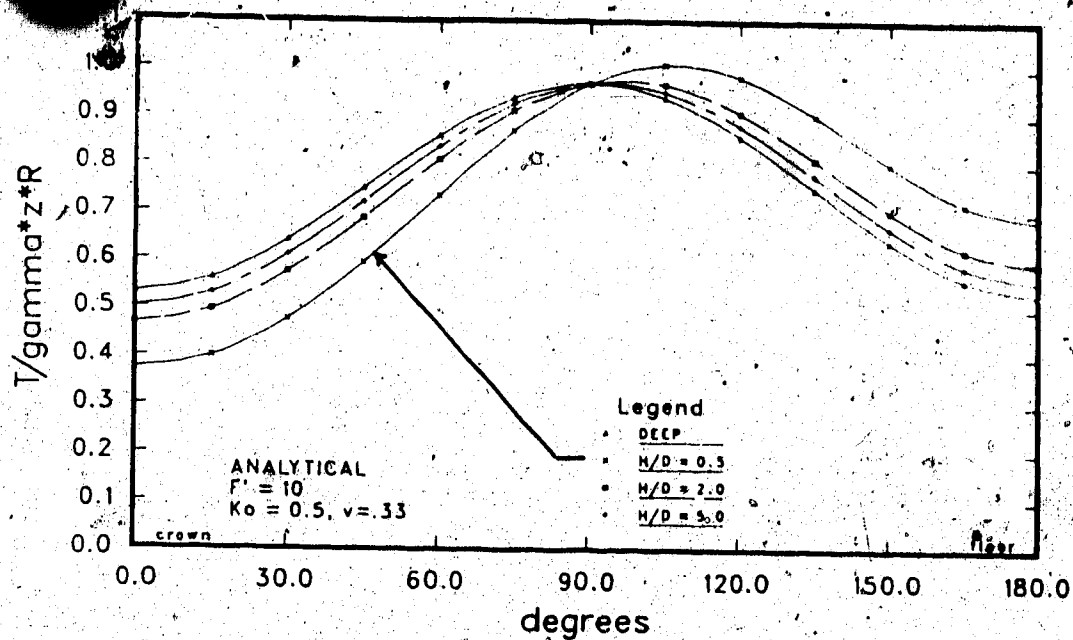
(a) analytical solution
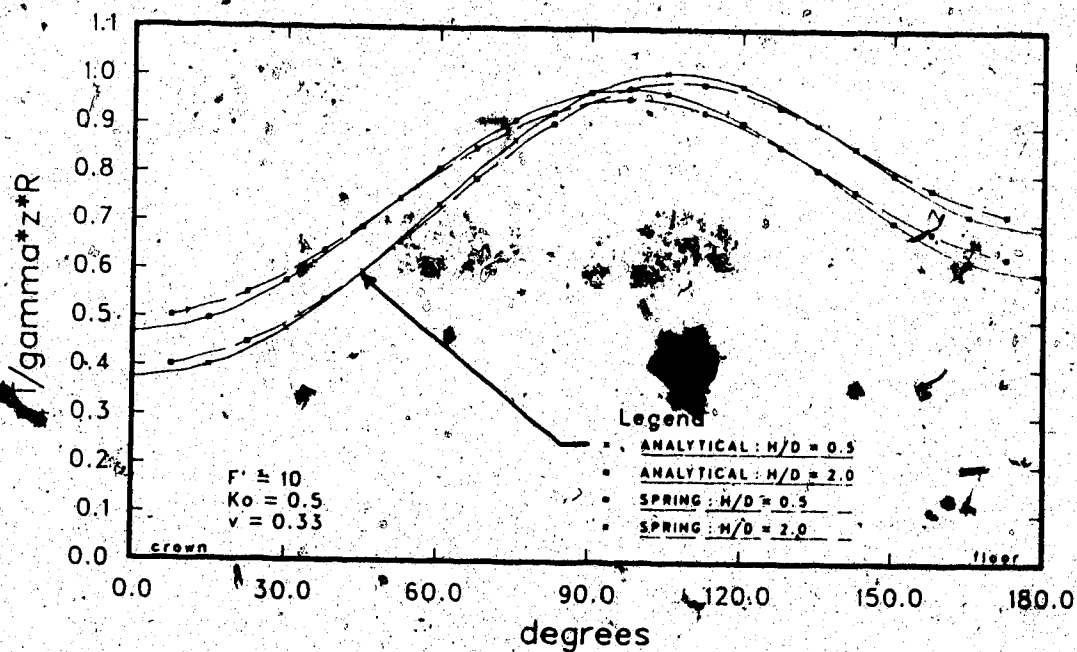
(b) comparison of spring model with analytical solution

Figure 5.8 Influence of Gravity on the Distribution of the Total Thrust Coefficient

5.4.2.4 Displacement Variation with Flexibility Ratio

Using the equations in Figure 2.8 for the input loads for the spring model will provide the relative displacements occurring around the lining. The heave at the springline is excluded in these analyses because of the adjusted format of the loading stress distribution from the in situ conditions.

The crown displacement coefficient curves illustrated in Figure 5.9 indicate once again the reasonably good match between the analytical solution and the spring model which has only radial springs with stiffness defined by k_{ro}. The curves are shown for $\nu=0.33$, but in Section 4.4.4, the sensitivity of the deep tunnel displacements to the choice of Poisson's ratio is noted. Similar trends occur in the shallow conditions.

The influence of the gravitational stress component is to reduce the vertical loads and consequently the displacements at the crown. As the gravity fraction of the total input load decreases, its effect on reducing crown displacements is also decreased.

This is reflected in the curves of Figure 5.9 where the increase in the crown displacement coefficient with increasing relative depth is seen. Note also for increasing H/D, the profiles rapidly converge towards the solution without gravity effects included.

CROWN DISPLACEMENTS
kro ONLY, RADIAL SPRINGS
Ko = 0.5, v=.33

Legend
▲ ANALYTICAL : DEEP
× ANALYTICAL : H/D=0.5
□ ANALYTICAL : H/D=2.0
■ SPRING MODEL : H/D=0.5
♦ SPRING MODEL : H/D=2.0
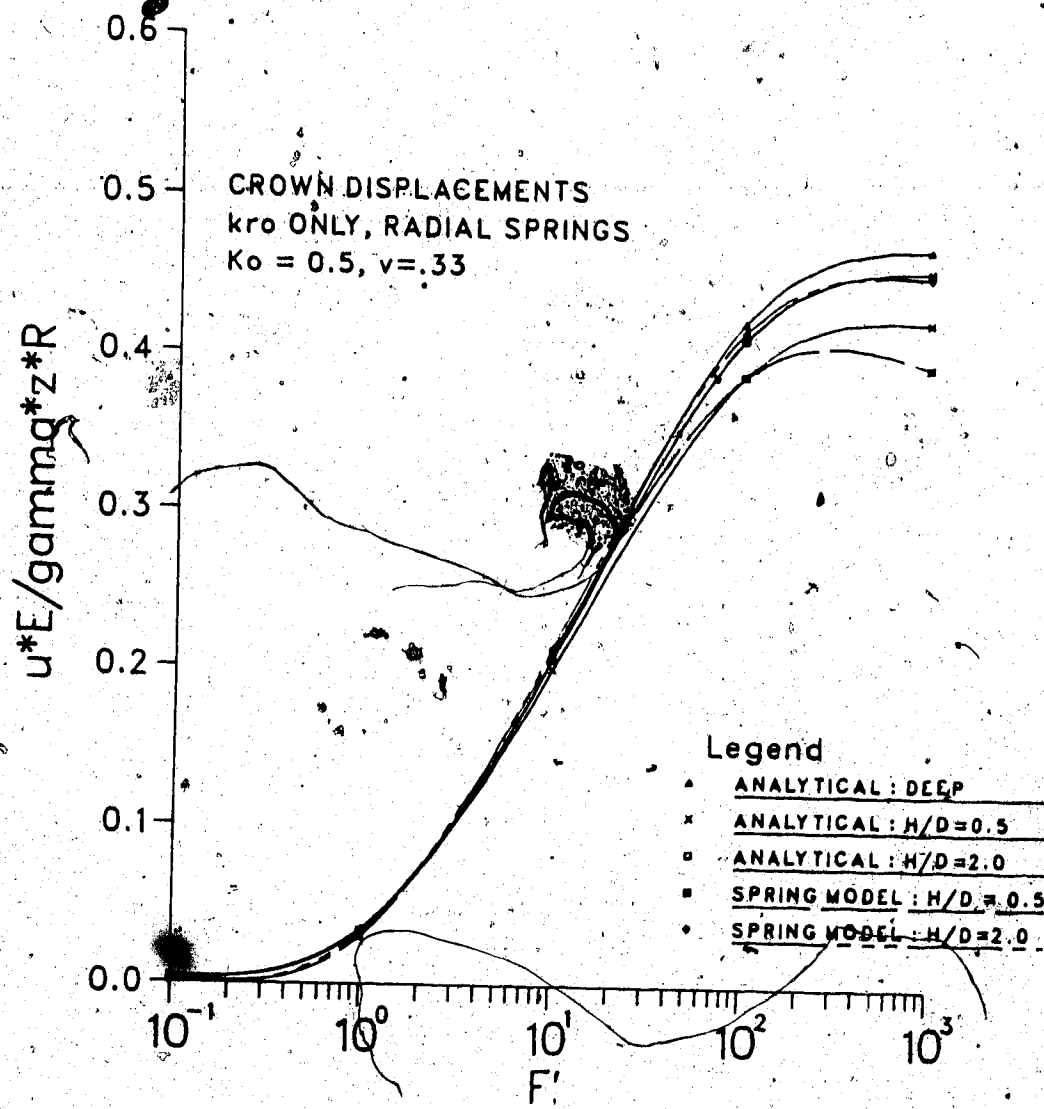
Figure 5.9 Influence of Gravity on the Variation of Relative
Crown Displacement Coefficient with Flexibility Ratio

5.4.3 Consequence of Neglecting Ground Surface Effects

The analytical Hartmann (1970, 1972) solution does not consider the influence of the stress free ground surface, because in this formulation the ground is represented by an infinite plate. Negro (1988:1126) investigated the effect of this assumption by comparing the analytical solution with results from a finite element analysis of a shallow tunnel. In both cases, the action of gravity was included and, apart from any numerical inaccuracies, any differences were attributed to the influence of the stress free ground surface modelled by the finite element analysis.

The numerical and analytical solutions were found to give similar results for relative depth ratios, H/D > 1.5, and for H/D < 1.5, the analytical solution typically provided conservative estimates of the lining response.

Figures 5.10, 5.11 and 5.12 portray the crown response for the no slip conditions, along with comparable analyses performed using both the fully and partially embedded ring and spring models.

The finite element Ranken curve refers to a solution which allowed for the effect of the ground surface. As stated earlier, the Hartmann and the fully embedded model with active crown region springs did not account for ground surface effects. The partially embedded model could arguably be attempting to take some account of this in that a column of soil is assumed to sit on the liner with slip surface boundaries reaching the surface. But this increased load

assumption is in conflict with the finite element results which tend to show signs of a load shedding process.

Figure 5.10 illustrates the variation in the crown moment coefficient in response to the changing relative depth ratio. Figure 5.11 records the variation in the crown thrust coefficient and Figure 5.12 illustrates the displacement response in terms of absolute crown displacement, u_c (includes heave), and of vertical and horizontal diameter changes, $\Delta D/D$.

5.4.3.1 Input Parameters

The input parameters which are common to all the models are

Soil: $E = 20.09$ MPa

$\nu = 0.25$

$K_o = 0.5$

$\gamma = 20$ kN/^{3}

Liner: $E_s = 980$ MPa

$\nu_s = 0.1562$

$R = 1.0$ m

$t = 0.1 R$

$I_s = 8.33 \times 10^7$ mm^4/m

Springs:

$A_{sp} = 0.2611$ mm^2/m

$I_{sp} = 1 \times 10^2$ mm^4/m
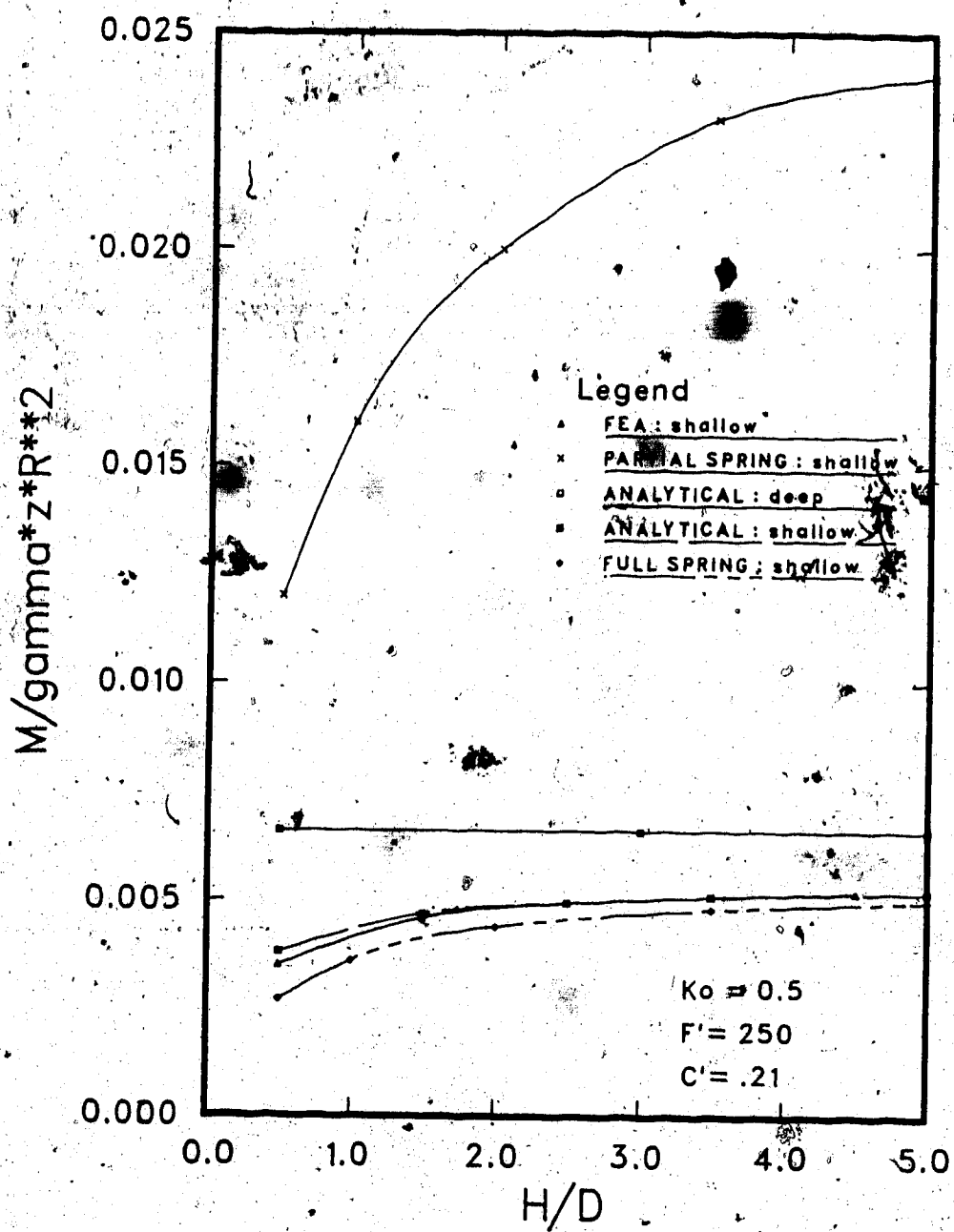
Figure 5.10 Comparison of Crown Moment Response with Varying Relative Depth
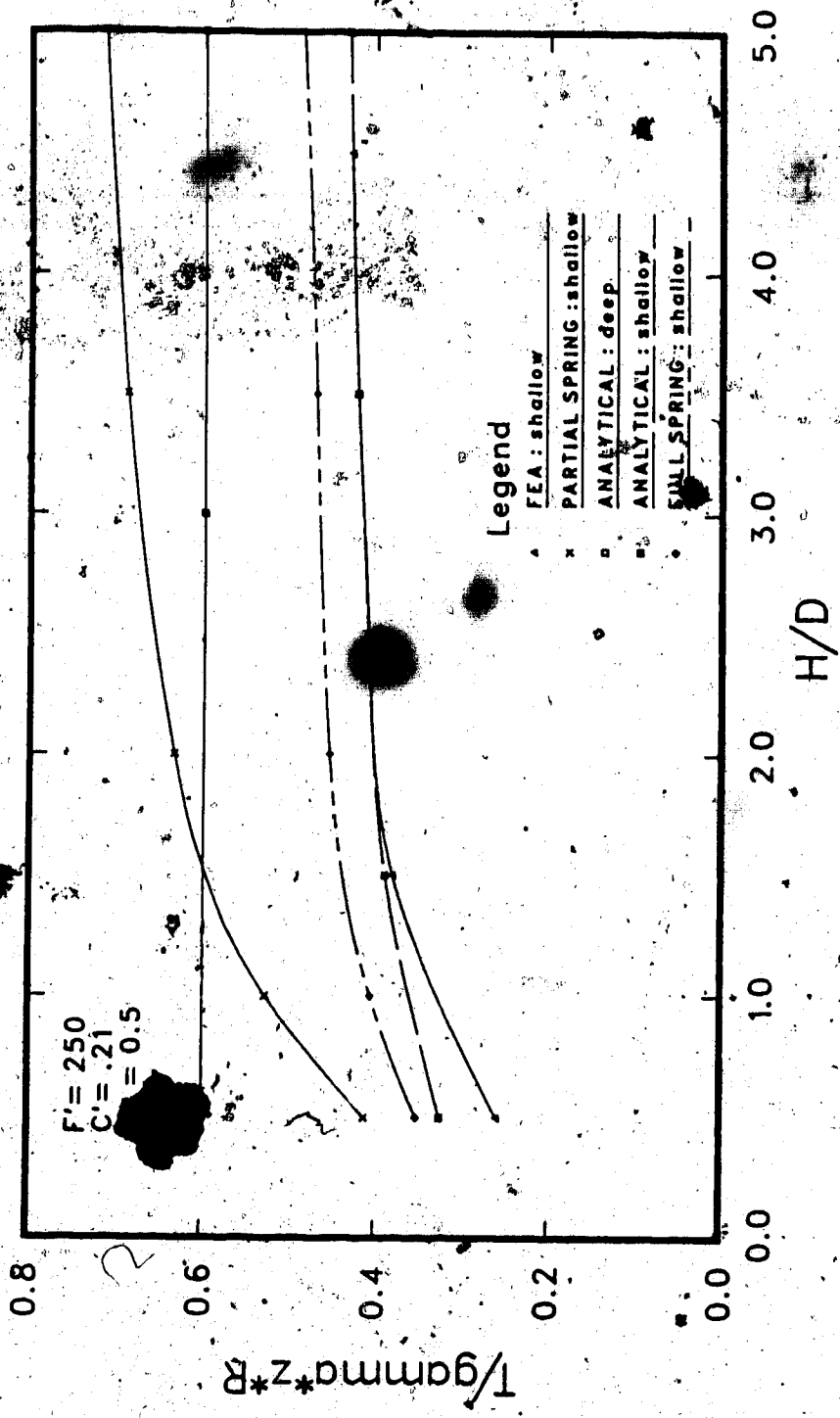
Figure 5.11 Comparison of Crown Thrust Response with Varying
Relative Depth
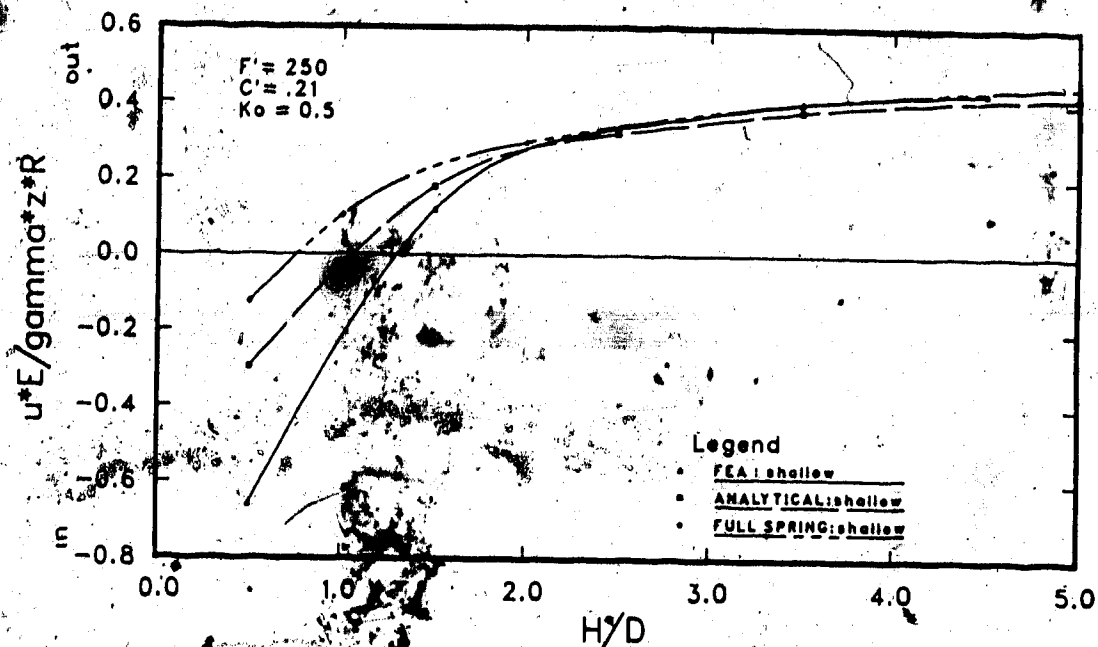
(a) absolute crown displacements
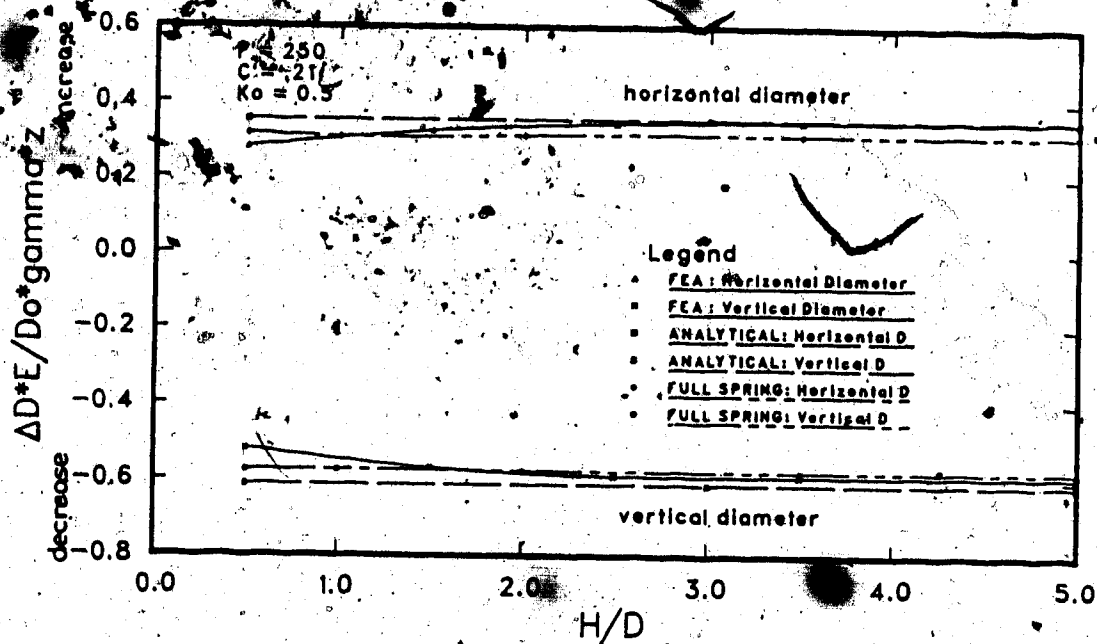
(b) diameter changes

Figure 5.12 Comparison of Deformations for Variation in Relative Depth

5.4.3.2. Input Loads and Responses for Partially Embedded
Model

This investigation provides the opportunity to assess
the conservatism of the partially embedded model approach
using the suggested input loads of Schulze and Duddeck
(1964) given in Table 3.1. Note however, the Schulze and
Duddeck (op.cit.) model assumes an unsupported arch of 100°.
The calculations given in this section are for a 90°
unsupported arch, which may exaggerate the crown moments
slightly if the trends in Figure 5.4 are inferred. It is
common in this approach to assume that the radial spring
constant $k_r = E_{sp}/R = D/R$ where D is the constrained soil
modulus. The stiffness of the springs is therefore

$$E_{sp} = D = \frac{(1-\nu)}{(1+\nu)(1-2\nu)} \cdot E \qquad [5.8]$$

and using the given input parameters, $E_{sp} = 24.1$ MPa.

By inspecting the constant, $\frac{(1-\nu)}{(1+\nu)(1-2\nu)}$, in equation
[5.8] and comparing with the expressions in Figure 3.5, it
is seen that the use of the constrained modulus as the
spring stiffness assumes the soil response is very much
stiffer than the other expressions provide, especially for
values of ν approaching 0.5.

This, to some small extent, offsets the conservatism of
assuming partial embedment which is seen particularly for
the crown moments shown in Figure 5.10.

The partially embedded model approach is shown in Figures 5.10 and 5.11 for H/D between 0.5 and 5.0, but observing the recommendations of Duddeck and Erdmann (1982, 1985) recorded in Section 3.2, the appropriate results for the deep analytical solution are also recorded.

At some H/D about 1.5, the partially embedded solution plotted in Figure 5.10 jumps down to the deep analytical solution. The combination is seen to provide a rather curious discontinuity of design moments for increasing relative depths. The thrust envelope suggested by Duddeck and Erdmann (op.cit.) and shown in Figure 5.11, provide conservative design values for all H/D values when comp with the finite element results.

5.4.3.3 Input Loads and Responses for Fully Embedded Model

The moment and thrust actions for the liner are obtained by imposing the no slip stress distribution which accounts for the heave as given in Figure 2.8.

The absolute displacements required for the comparison in Figure 5.12 demand that the vertical heave component be included and this is obtained by applying the in situ stress distribution given in Figure 2.2 directly to the model.

The moment response provided by the fully embedded spring model is seen to slightly underestimate the finite element and analytical solutions and this is more pronounced for H/D < 1.5.

This is mostly explained by the model response to the lower values of the Poisson's ratios, ν and ν_s used in the analyses. According to Section 4.4.2.3, these provide slightly smaller moments that the analytical values.

Figure 5.11 indicates that the full spring model slightly overestimates the thrusts, but is seen to follow the trends very acceptably. The slight conservatism for the crown thrust is not unexpected, especially for F'=250 and Poisson's ratios used in this study. This is explained in Section 5.4.3.

Similar to the moment response, a small error is seen for the diameter change and absolute crown displacement responses given in Figure 5.12. Once again, from the explanation describing the displacement response for deep conditions in Figure 4.18, this is not unexpected in view of the lower Poisson's ratio values used.

5.5 Account of Three Dimensional Effects

Erdmann and Duddeck (1985) report that for long term resistance it is general practice to assume that the active soil pressures on the liner are equal to the primary stresses in the undisturbed ground. They qualify this however, by conceding that this assumption is too conservative in some instances depending, for example, on soil type and relative tunnel depth.

The two-dimensional plane strain models discussed in Chapters 4 and 5 assume in their formulation that the full

overburden loads are imposed on the liner. This assumes that no stress release or ground displacement occurs prior to lining activation and implicitly requires that the soil stiffness is also described by the undisturbed conditions. Typically then, this loading system is used for the design of the final support since historically no criteria are available to assume otherwise.

Physically these conditions are not realized, as discussed in Section 2.2.3. Radial displacements and associated stress reduction occur ahead of the tunnel face as part of the three-dimensional activity occurring close to the excavation zone. Further radial displacements occur due to the physical delay in time and space before the liner itself can be activated against the ground. This aspect can be represented in the two-dimensional model as ground stress relaxation.

The non linear response of the ground to the altered stress distribution generated by the excavation indicates that the ground around the opening "softens". The interaction process will not be controlled by the initial ground stiffness, E_{ti}, but by the "current" stiffness, E_t, existing at the time of liner activation. This can be represented by the ground stiffness degradation.

The cumulative effect is that the initial support is required to carry only a portion of the in situ stresses. Some permanent stress reduction and ground softening may also be justified in the considerations for the design of

the final support.

The input parameters of the 2-D design models enable
consideration of a reduced ground stress and stiffness
degradation to be included.

Typically the procedures for this have been fully
empirical. No solution existed to account for the
three-dimensional effects in ring and plate or ring and
spring models for shallow tunnels (Negro, 1988:500) prior to
the design method proposed by Negro (op.cit.).

5.5.1 Shallow Tunnel Design - Negro

The suggested sequence of steps for the design of
initial supports for shallow soft ground tunnels is
reproduced from Negro (1988:1161) as Figure 5.13. Although
the approximate nature and limits of applicability are
stressed, the procedure is shown to provide good simulations
of the 3-D models, laboratory tests and many case histories
investigated (Negro, op.cit.).

The purpose of utilizing Negro's design approach is to
establish the reduced loads and stiffness degradations in a
logical procedure and to implement the ring and spring model
as an alternate method for the ground-liner interaction
phase.

The steps which establish the presupport ground
response shown in Figure 5.13 involve assessing the amount
of stress release, Σ, which occurs up until liner
activation, and evaluating the reduced ground stiffness, E_t,
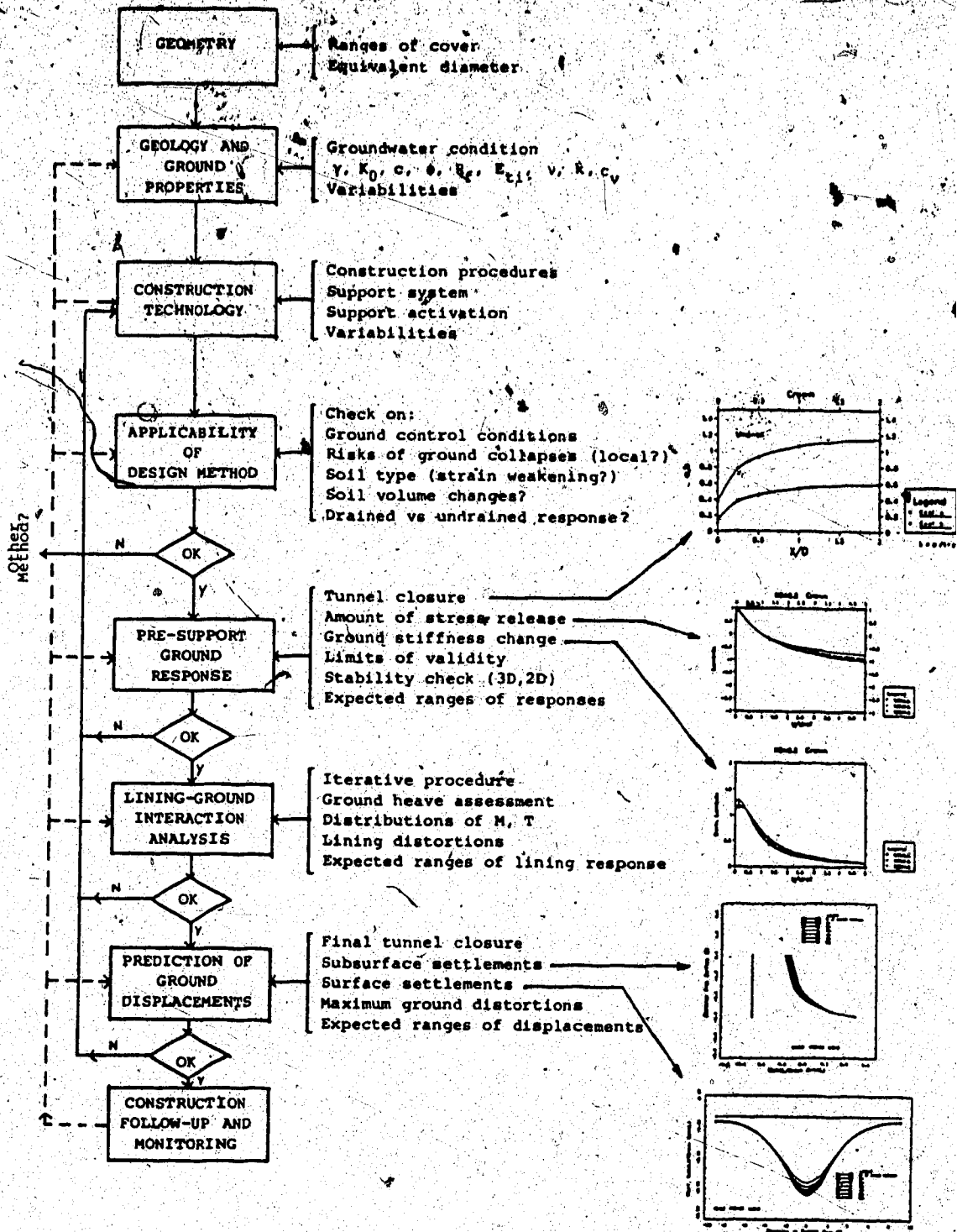
Figure 5.13 Suggested Sequence of Steps for Shallow Tunnel Design (after Negro:1988)

associated with this stress release. This corresponds to completing step 5 of the calculation sheet presented by Negro (op.cit.:1170) and modified as Figure 5.14.

5.5.1.1 Evaluation of Stress Release

Initially an estimate is made of the radial displacement occurring at the point of liner activation for the crown, springline and floor.

These displacements are assumed to be univocally related to the stress release occurring at these locations through the appropriate ground reaction curves describing the ground response to the excavation loading.

This establishes the amount of stress release, Σ. The reduced soil unit weight $\gamma_{red} = \gamma\Sigma$ is entered into the interaction analysis and allows account of the reduced ground loads due to delayed liner activation.

For both the analytical and spring models, this approach is appropriate to assess the ground stress release.

5.5.1.2 Evaluation of Ground Stiffness Degradation

The next calculation is to establish the degradation of the in situ soil stiffness, E_{ti}, which is assessed from the slope, $\Delta\sigma/\Delta u$, of the ground reaction curve. This is recognized as the radial spring constant, k_r of the soil and can be evaluated at any stage of the tunnel unloading process by differentiating the expression representing the ground reaction curve.

4. REFERENCE VALUES (steps 1. to 3. in Figure 5.16)

H/D = [＿＿＿＿] k_o = [＿＿＿＿] (m $\cdot$) $_3$ [＿＿＿＿]

	$1-\Sigma_{ref} = \alpha_{ref}$	α_{ref}/U_{ref}	U_{ref}
C			
S			
F			

5. STRESS RELEASE AND STIFFNESS CHANGE AT LINING ACTIVATION

	U	U/U_{ref}	Beyond Limit?	λ	λ'
C					
S					
F					

STRESSES : $\Sigma = 1-(1-\lambda)\alpha_{ref}$

	$(1-\lambda)$	Σ
C		
S		
F		

$\bar{\Sigma} = (\Sigma_C + 2\Sigma_S + \Sigma_F)/4$ = [＿＿＿＿]

$\bar{\alpha} = 1-\bar{\Sigma}$ = [＿＿＿＿]

$\gamma_{red} = \gamma \cdot \bar{\Sigma}$ = [＿＿＿＿]

* SPRING CONSTANT : $k_r = (\alpha_{ref}/U_{ref}) \cdot (E_{ti}/D) \cdot \lambda'$

STIFFNESS : $E_t = (\lambda'/\lambda'_i) E_{ti}$

	λ'_i	E_{ti}/λ'_i	E_t	* k_r
C				
S				
F				

$\bar{E}_t = (E_{tC} + 2E_{tS} + E_{tF})/4$ = [＿＿＿＿]

* $\bar{k}_r = (k_{rC} + 2k_{rS} + k_{rF})/4$ = [＿＿＿＿]

Figure 5.14 Stress Release and Ground Stiffness at the Section the Lining is Activated (after Negro, 1988:modified)

For the cohesionless soil model for which the procedure (Negro, op.cit.) is given, the current spring constant, k_r is assessed through the derivative functions of the twice normalized ground reaction curves (λ' curves), so that

$$k_r = \frac{a_{ref}}{U_{ref}} \cdot \frac{E_{ti}}{D} \cdot \lambda' \qquad\qquad [5.9]$$

This is evaluated at the crown, springline and floor and may be incorporated in regions, or averaged to provide a single constant value, $\bar{k}_r$, as input for the ring and spring model.

Figure 5.14 includes minor modifications to the original calculation sheet by including the necessary details required to evaluate the spring constants for the ring and spring model. These are indicated by asterisks in the figure.

For the analytical solution, the required input variable with respect to soil stiffness degradation, is the reduced average tangent modulus of elasticity, $\bar{E}_t$. This is obtained by assuming that this modulus is directly proportional to the spring constant such that

$$\frac{E_t}{E_{ti}} = \frac{k_r}{k_{ri}} \qquad\qquad [5.10]$$

and substituting equation [5.9] gives

$$E_t = \frac{\lambda'}{\lambda'_i} \cdot E_{ti} \qquad\qquad [5.11]$$

for the discrete spring model, three options are
investigated, two of which use the modifications introduced
in Figure 5.14. Note that all options have models that are
fully embedded with radial springs only.

Option A:

It has been shown in Chapter 4 that acceptable
simulations of the analytical solution in shallow conditions
are obtained with the discrete spring model by using radial
springs only whose stiffness is defined by $k_{ro} = \frac{E_s}{R}$.
Option A simply substitutes the average reduced elastic
modulus, $\bar{E}_t$, shown in Figure 5.14 directly into this
expression for k_{ro}, thereby defining the spring stiffness as

$$E_{sp} = \frac{\bar{E}_t}{1+\nu}$$

[5.12]

Option B:

This approach assumes a single valued spring constant,
$\bar{k}_r$, which is obtained by averaging the values of the spring
constants at the crown, springline and floor, including the
appropriate double weighting of the springline value. This
is shown in Figure 5.14.

Option C:

An advantage of the ring and spring model is that the
stiffnesses of the spring representing the soil response can

be varied in magnitude around the tunnel contour. For the investigation performeds in Section 5.6, the distinct k_r values for the crown, springline and floor define the spring stiffnesses in the appropriate 90° regions. Springs on the boundaries between two regions are assigned the lower of the two possible values.

Other options are possible, for example interpolating linearly between crown, springline and floor, but these are not evaluated here.

The input parameters for the ground-liner interaction phase are therefore defined.

5.5.1.3 Ground-Liner Interaction Analysis

The calculation sheet (Negro 1988:1171) was developed for using with the Hartmann solution. Modifications are required to this for using with the discrete ring and spring model, but once again these are minor and typically relate to terminology. These are presented in Figure 5.15 with alterations indicated by asterisks.

The estimation of the heave, h, is provided by applying the reduced soil unit weight, γ_{red}, into the equations in Figure 2.2 which do not eliminate the heave component from the calculations.

The moments, thrusts and relative displacements, Δu_r, are output data from using γ_{red} in the equations for σ_r and τ in Figure 2.8. It is possible to iterate the solution by updating the spring constant values until convergence is

7. LINING-GROUND INTERACTION

GEOMETRY: $Z'=$ [ ]   *$R=$ [ ]

SOIL: *$k_r=$ [ ]   *$\nu=$ [ ] $\gamma_{red}=$ [ ] $k_o=$ [ ]

LINING: $E_s=$ [ ]   *$\nu_s=$ [ ]   *$t=$ [ ] $I_s=$ [ ]

*$k_r=$ _____   *$E_{sp}=$ [ ]

ITERATION No:

	u_r	Δu_r	$u_{rf}=u_r+\Delta u_r+h$	u	U/U_{ref}	λ'	*k_r	σ_r
C								
S								
F								

*HEAVE, $h=$ [ ]   *$(k_r)_{new}=(k_{r-c}+2k_{rs}+k_{rF})/4=$ [ ]

Figure 5.15 Calculation Step for Lining-Ground Interaction
Analysis (after Negro, 1988: modified)

solution.

The final radial stresses, σ_r, can be calculated from the forces in the springs resulting from the interaction analysis.

5.6 Case History Using Discrete Ring ⬛⬛⬛⬛ Model for Liner Interaction Phase

The purpose of the example is to illustrate the use of the discrete ring and spring model for the design of the primary lining. It is used as an alternate approach to the analytical Hartmann solution which Negro (1988:1117) adopts for the ground-liner interaction phase of the design process.

The ring and spring model is assessed using the three different options for defining the spring constants as described in Section 5.5.

Negro (op.cit.) uses the Alto da Boa Vista Tunnel built in Sao Paulo, Brazil, as an example for using his design procedure. The case history is described in detail by Negro (op.cit.) and only the parameters relevant to the ring and spring approach are recorded here.

The tunnel has a soil cover of 6.2 m and an equivalent circular profile with an excavated diameter of 4 m.

The ground properties and geometric data are incorporated into the calculation sheet detailed by Negro

(op.cit.) and reproduced in Figure 5.16.

The parameters are processed through the design approach to obtain the amount of stress release and the stiffness reduction at liner activation as indicated in Figure 5.17. The modified calculation sheets show the values estimated for the spring constants, k_r. Three separate analyses following the options presented in Section 5.5.1 were then run and the results compared with both the Hartmann solution and the appropriate results from field measurements. The common input parameters for all three options are listed first, then the individual details are described for each.

Soil : $\nu = 0.3$

              $K_o = 0.8$

              $\gamma_{red} = 7.356$ kN/m^3

Liner : $E_s = 10$ GPa

              $\nu_s = 0.25$

              $R = 1.95$ m

              $z = 8.15$ m

              $t = 0.1$ m

              $I_s = 8.33 \times 10^{-5}$ m^4/m

Springs : $A_{sp} = 0.5091$ m^2/m

              $I_{sp} = 1.0 \times 10^{-10}$ m^4/m

1. GEOMETRY

H = $\boxed{6.2\,m}$ D = $\boxed{4.0\,m}$ H/D = $\boxed{1.55}$

2. GROUND PROPERTIES

$\gamma = \boxed{16\,KN/m^3}$ $K_0 = \boxed{0.6}$

$(\sigma_3)_{axis} = \boxed{104.12\,K\textbf{A}}$ c = $\boxed{0}$ $\phi = \boxed{29°}$ $R_f = \boxed{1.0}$

$\phi_a = arc\ sin\left[\dfrac{1 + (\sigma_3/c)\tan\phi}{1 + (\sigma_3/c)\sec\phi}\right]$ = $\boxed{29°}$

$\phi_e = arc\ sin\ (1 - R_f + R_f\ csc\phi_a)^{-1}$ = $\boxed{29°}$

$(m-1) = \dfrac{2\sin\phi_e}{1-\sin\phi_e}$ = $\boxed{1.662}$

K = $\boxed{400}$ n = $\boxed{0.25}$ $p_a = \boxed{101.33\,k\textbf{A}}$ $\mu = \boxed{0.3}$

$E_{ti} = K\,p_a\left(\dfrac{\sigma_3}{p_a}\right)^n\left[1 - \dfrac{R_f(1-\sin\phi)(\sigma_1-\sigma_3)}{2c\cos\phi + 2\sigma_3\sin\phi}\right]^2 = 30477.682 \cdot (\sigma_3/101.33)^{0.25}$

Location	$\sigma_3\ kPa$	$\sigma_1\ kPa$	$E_{ti}\ MPa$
1/2 D above C	53.76	67.20	26.01
at S	104.32	130.40	30.70
1/2 D below F	154.88	193.60	33.89

av. 30.325

3. TUNNEL CLOSURE AT LINING ACTIVATION

X = $\boxed{2.6\,m}$ X/D = $\boxed{0.65}$ $K_0 = \boxed{0.6}$ $u_r = (D\sigma_{ro}/E_{ti})U$

Location	U	$\sigma_{ro}\ kPa$	$D\,\sigma_{ro}/E_{ti}$	$u_r\ mm$
C	0.587	99.20	0.015255	8.95
S	0.469	104.32	0.013592	6.37
F	0.352	161.60	0.019026	6.70

Figure 5.16 ABV Tunnel - Input Data and Tunnel Closure at Lining Activation (after Negro, 1988)

4. REFERENCE VALUES (steps 1. to 3. in Figure 5.16)

$H/D =$ [1.55] $K_o =$ [0.6] $(m-1) =$ [1.892]

	$1-\Sigma_{ref}=\alpha_{ref}$	α_{ref}/U_{ref}	U_{ref}
C	0.529	0.87	0.603
S	0.465	1.12	0.415
F	0.435	2.02	0.215

5. STRESS RELEASE AND STIFFNESS CHANGE AT LINING ACTIVATION

	U	U/U_{ref}	Beyond Limit?	λ	λ'
C	0.587	0.973	No	0.03	0.62
S	0.469	1.130	No	-0.05	0.45
F	0.352	1.637	No	-0.45	0.65

STRESSES : $\Sigma = 1-(1-\lambda)\alpha_{ref}$

	$(1-\lambda)$	Σ
C	0.97	0.491
S	1.05	0.512
F	1.45	0.369

$\overline{\Sigma} = (\Sigma_C + 2\Sigma_S + \Sigma_F)/4 =$ [0.491]

$\overline{\alpha} = 1 - \overline{\Sigma}$ = [0.529]

$\gamma_{red} = \gamma \cdot \overline{\Sigma}$ = [7.536] kN/m^3

SPRING CONSTANT : $k_r \cdot (\alpha_{ref}/U_{ref}) \cdot (E_{ti}/D) \cdot \lambda'$

STIFFNESS : $E_t = (\lambda'/\lambda'_i) E_{ti}$

	λ'_i	E_{ti}/λ'_i	E_t	k_r
C	1.278	20.352	12.618	3.507
S	1.425	21.544	9.695	3.868
F	1.005	33.721	21.919	12.766

$\overline{E}_t = (E_{tC} + 2E_{tS} + E_{tF})/4 =$ [13.482] MPa

$\overline{k}_r = (k_{rC} + 2k_{rS} + k_{rF})/4 =$ [6.002] MPa/m

Figure 5.17 ABV Tunnel – Stress Release and Ground Stiffness at Lining Activation (after Negro, 1988: modified)

Option A

The spring constant for this option is assumed to $k_{ro} = \frac{1}{1+\nu} \cdot \frac{E_t}{R}$ where from Figure 5.17, $E_t = 13.482$ MPa. This provides the single valued spring stiffness to be

$$E_{sp} = R \cdot k_{ro} = \frac{E_t}{1+\nu} = 10.371 \text{ MPa}.$$

Option B

The spring stiffness is defined by the average spring constant, $\bar{k}_r = 6.002$, given in Figure 5.17. In this case,

$$E_{sp} = \bar{k}_r \cdot R = 11.704 \text{ MPa}$$

Option C

The spring constants, k_r are defined for the crown, springline and floor as seen in Figure 5.17. These translate into spring stiffnesses for the appropriate locations as

crown E_{sp} : $3.507 \times 1.95 = 6.84$ MPa.

springline E_{sp} : $3.868 \times 1.95 = 7.54$ MPa.

floor E_{sp} : $12.766 \times 1.95 = 24.89$ MPa.

The distribution over the associated 90° regions is illustrated in Figure 5.18.

The results of this analysis are presented in the modified calculation sheet in Figure 5.19 to illustrate the details of the interaction process using the ring and spring model option. The figure shows only the first round of the iteration process but the values of σ_r are within 3% of the values at the end of the converged, final solution given in Table 5.1.

The input and output files for this case can be found in Appendix A.

5.6.1 Comparisons Between Measured and Calculated Results

Table 5.1 summarizes the comparisons between the ring and spring results and the measured and calculated performance (Negro, 1988:1191) for the ABV Tunnel for the results available from the interaction analyses. Negro (1988:op.cit.) reports that the comparisons provided by the calculated approach taking into account the reduction due to the three dimensional nature of the tunnelling process are quite reasonable. Bearing this comment in mind, it is seen also that the fully embedded ring and spring model also supplies reasonable estimates of the parameters in question. It is of interest to note that the varied input values of k_r (Option C) do not alter the response system to any significant degree.

crown 90° region
$E_{sp} = 6.84$ MPa

springline regions
$E_{sp} = 7.54$ MPa

$R = 1.95m$

$E_{sp} = 7.54$ MPa

floor region
$E_{sp} = 24.89$ MPa
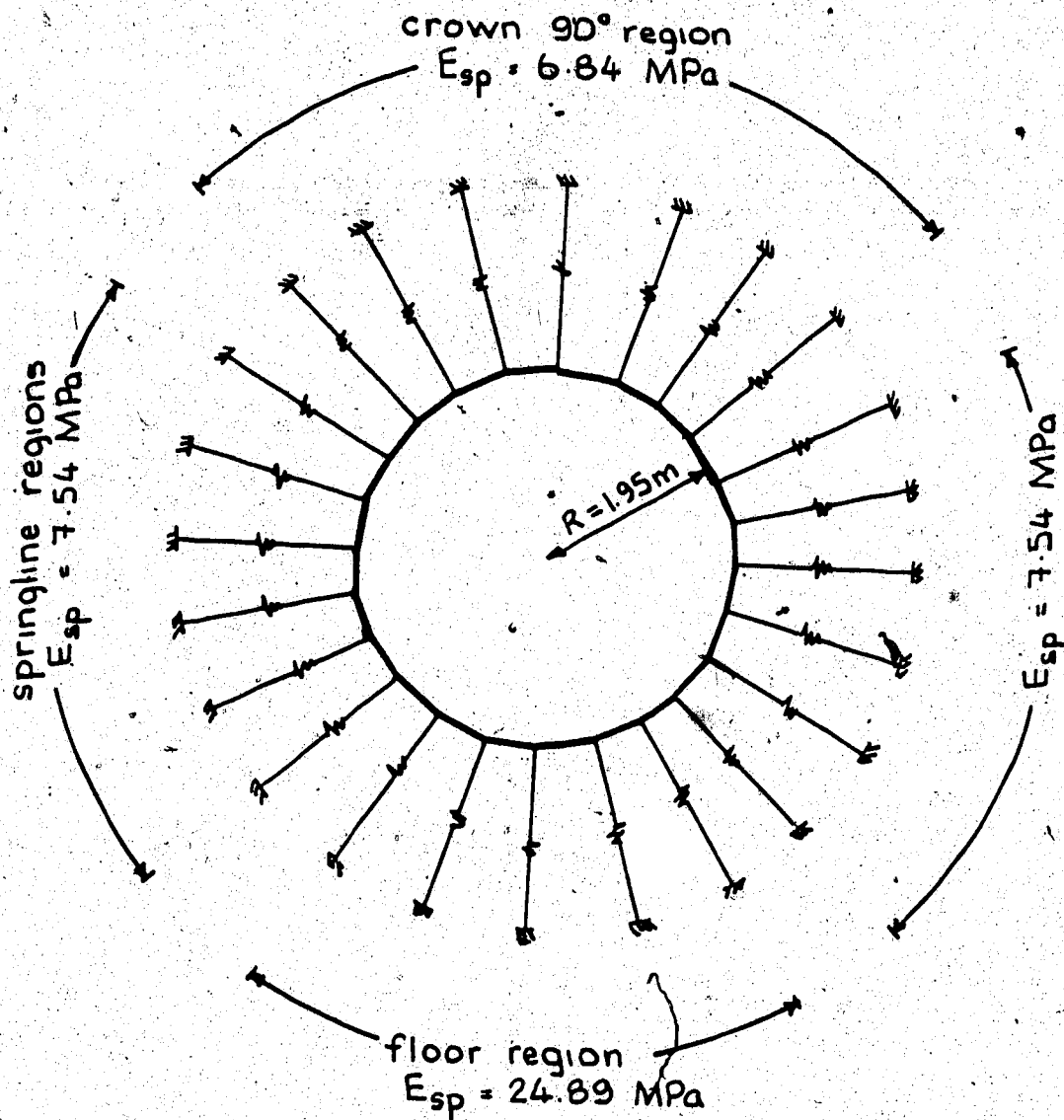
Figure 5.18 Spring Stiffness Used in Analysis Option C for ABV Tunnel

$\bar{\alpha} = \boxed{0.529}$

$\therefore P_\ell/\gamma D = \boxed{0.35}$

$\bar{\sigma}_{ro} = \dfrac{1+k_0}{2}\gamma(H+\dfrac{D}{2}) = \boxed{117.36 \ kPa}$ $\phi' = \boxed{30°}$ $c/\gamma D = \boxed{0}$ $H/D = \boxed{1.55}$

$P_\ell = \boxed{22.4 \ kPa}$ $\alpha = 1 - P_\ell/\sigma_{ro} = \boxed{0.809}$

$FS = \dfrac{[(1-k_0)/(1+k_0)+\alpha_\ell]}{[(1-k_0)/(1+k_0)+\bar{\alpha}]} = \boxed{1.437}$

7. LINING-GROUND INTERACTION

GEOMETRY: $Z = \boxed{8.15 \ m}$ $R = \boxed{1.95 \ m}$

SOIL: $\bar{k}_r = \boxed{6.002}$ $\nu = \boxed{.3}$ $\gamma_{red} = \boxed{7.536}$ $k_0 = \boxed{.8}$

LINING: $E_s = \boxed{10 \ GPa}$ $\nu_s = \boxed{.25}$ $t = \boxed{.1 \ m}$ $I_s = \boxed{6.33 \times 10^7} \ mm^4/m$

$k_r = \boxed{6.002}$ $E_{sp} = \boxed{11.704}$

ITERATION No. $\underline{01}$

	u_r	Δu_r	$u_{rf}=u_r+\Delta u_r+h$	U	U/U_{ref}	λ'	k_r	σ_r
C	8.95	1.54	8.01 (10.49)	.525 (.688)	.871 (1.140)	.67 (.52)	3.790 (2.942)	37
S	6.37	-1.27	5.10	.375	.904	.60	5.158	57
F	6.70	1.79	10.97 (8.49)	.577 (.446)	2.682 (2.075)	.44 (.56)	7.530 (9.413)	59

HEAVE, $h = \boxed{2.48}$ (zero)

$(k_r)_{new} = (k_{rc} + 2k_{rs} + k_{rF})/4 = \boxed{5.402}$ (5.668)

(no heave)

Figure 5.19 ABV Tunnel - Option B Lining-Ground Interaction

Analysis (after Negro, 1988: modified)

Performance Aspect	Ring and Spring Model			Measured (Negro 1988:1191)	Calculated (Negro 1988:1191)
	Option A	Option B	Option C		
Final Floor Heave (mm)	(8.7)* 11.4	(8.7)* 11.4	(8.1)* 10.7	5-9	(8.5)* 11.0
Maximum Horizontal Convergence of Lining (mm)	2.8	2.8	3.0	0.85	2.7
Final Crown Settlement (mm)	(10.6)* 7.9	(10.6)* 7.9	(11.3)* 8.7	8.0	(10.6)* 8.1
Pressure on Lining at Crown (kPa)	38	38	39	30	44
Pressure on Lining at Springline (kPa)	57	57	57	35	58
Pressure on Lining at Floor (kPa)	66	66	66	55	57

(heave excluded)*

Table 5.1 Comparison of Results for ABV Tunnel - Final Convergence

5.7 Summary

A brief description is given of an analytical solution which fully accounts for the non-uniform stress field existing in a shallow tunnel. This provides a basis for comparing the fully embedded discrete ring and spring model proposed in earlier chapters.

It is seen that the expressions for the stress distributions in shallow conditions are an extension of the deep solution by including additional terms to describe the gravitational stress component.

The responses to variations in the relative depth of the tunnel provide the main focus on the model comparisons in order to assess the ability of the spring model to simulate the influence of gravity.

The model using radial springs only with stiffness, $E_{sp}=R.k_{ro}$ where $k_{ro} = \frac{1}{1+\nu}.\frac{E}{R}$, is used due to its successful debut in Chapter 4. This model provides good results for all aspects of the shallow tunnel simulation for the chosen Poisson's ratio of 0.33. The variation in response to different Poisson's ratio follows the same patterns as seen for the deep conditions and are not presented pictorially.

The partially embedded ring and spring model with its associated input stress distribution is seen to provide very conservative estimates of the liner actions in the crown in spite of the very stiff soil response representation using the constrained modulus.

For the initial support liner, the decrease in loads and stiffnesses has prompted empirical reductions in the stresses producing the actions for the initial support. Negro (1988) proposes a design method for the initial supports in shallow tunnels which provides a logical procedure for establishing appropriate reduced loads and stiffnesses. Although the approximate nature of the procedure is stressed (Negro, op.cit.), it does account for many features relevant to shallow tunnel conditions and is seen to provide a good correlation with case histories, three-dimensional finite element studies and laboratory tests.

A case history is investigated using the method, but implementing the discrete ring and spring model as an alternate approach for the ground-lining interaction phase. It is seen that the approach provides very acceptable results.

The design loads for the final support conditions are usually those created by full overburden. In many situations this approach is conservative, but prevails because no sensible criteria are available to accept otherwise.

It is of interest to note that varying the stiffness around the contour does not significantly change the results from just assuming a constant value of the spring stiffnesses. This needs further investigation however, because it may be an appropriate conclusion only for this configuration.

6. SUMMARY AND CONCLUSIONS

Many approaches are available for the design of tunne linings in shallow or deep soft ground conditions. Each method has its own merits and disadvantages. They range in complexity from the simple analytical models which are inherently restrictive in their application, to complicate computer models which have tremendous facilities to simula many varied aspects of the parameters involved. A brief summary of the various classes of approaches is given.

A synopsis from a survey of tunnel liner design practice revealed that, in spite of the increasing capadit to model complex configurations, a preference was show, towards using the simpler discrete ring and spring model i practical design situations.

A summary of the commonly adopted assumptions for lin design in soft ground is given. These recommendations are seen to have drawbacks which include the assumption of ful overburden for the design load, the exclusion of gravitational stress effects below a relative depth ratio H/D of 1.5, the use of a partially embedded model for very shallow tunnels and the way in which the full slip interfa loading condition is applied in the ring and spring model.

Good ground control conditions assume that the soil i the crown region provides some resistance to the stress changes caused by the tunnel excavation process. This can modelled by a fully embedded discrete ring and spring mode In this case, all of the springs are actively sharing the

imposed loads with the lining as a result of the ground-lining interaction process.

The partially embedded model assumes that the springs in the crown region do not contribute to the resistance. This results in relatively large crown bending moments, even though the approach usually adopts a very stiff soil response in the regions away from the crown.

The fully embedded discrete ring and spring model is compared with available analytical solutions for both deep and shallow conditions. These ring and plate solutions account for non-uniform stress fields resulting from an in situ stress ratio different from unity (deep and shallow) and from the gravitational stress gradient across the tunnel opening (shallow only).

The calculations are numerically processed using a computer program set up to solve two dimensional frame configurations.

For the deep tunnel conditions, three separate ground response descriptions are defined ("unlined", "lined" and "k_{ro} only"). These differ in terms of the loading the soil applies to the support system.

Although it is possible to include both radial and tangential springs in the model, the simplest configuration with radial springs only is seen to provide the best, but not perfect, simulation of the analytical solution. This model uses the soil response, k_{ro}, which is defined by the ground convergence into a circular opening under uniform

conditions which account for the effect of gravity across the tunnel opening. In order to obtain the moments, thrust and relative displacements using the spring model, the heave of the tunnel liner must be accounted for. The absolute displacements of the liner are obtained by applying the unadjusted in situ stresses in the model.

The input loads for the system are defined by the ground-liner interface conditions of "no slip" or "full slip". The recommended procedure for full slip (Duddeck and Erdmann, 1985) is to simply ignore the shear stress component of the input loads. While it is reasonable to define the interface shear stress as zero for the full slip conditions, the ring and spring model is unable to redistribute the in situ soil stresses to account for the change in boundary conditions from no slip to full slip.

Because the springs in the model represent individual radial columns of soil which are not connected to each other, no shear transfer between columns can be effected. This means that the alteration of the radial stress which is necessary to obtain the full slip condition cannot occur. The input loads for the full slip condition must account for this redistribution prior to being included in the analysis.

No criteria are available to justify reducing the full overburden loads for designing the final support, although it is appreciated that this assumption can be very conservative.

For the initial support design, the stress reduction and stiffness degradation which occur in the tunnelling excavation can logically be accounted for through a design procedure proposed by Negro (1988).

The minor modifications necessary to use the method with a ring and spring model are implemented in Negro's procedure and tested against a case history. It is seen that the spring model provides an acceptable alternative approach for the ground-liner interaction phase of the design procedure.

In conclusion, a ring and spring model with radial springs only can provide a useful simulation of the ground-liner interaction process for both deep and shallow soft ground conditions.

It is essential that the input loads reflect the interface conditions to be modelled and care should be exercised in interpreting the response with respect to the value of the Poisson's ratio involved.

REFERENCES

Ahrens, H., Linder, E. and Lux, K.H., 1982. Zur Dimensionierung von Tunnelausbauten nach den Empfehlungen zur Berechnung von Tunneln im Lockergestei (1980). Die Bautechnik, 50, pp.260-273; 303-311 (see also 'Taschenbuch fur den Tunnelbau' 1983, Verlag Gluckauf, Essen).

Andraskay, E., Hofmann and Jenalka, P., 1972. Berechnung de Stahlbetontubbinge fur den Heitersbergtunnel, Los West. Schweizerische Bauzeitung, Jahrgang, Heft 36 (September), pp. 664-668.

Branco, P., 1981. Behaviour of a shallow tunnel in till. M.Sc. Thesis, Department of Civil Engineering, University of Alberta, 351p.

Bull, A., 1946. Stresses in the linings of shield-driven tunnels. American Society of Civil Engineers, Proceedings, Nov. 1944.

Craig, R.N. and Muir Wood, A.M., 1978. A review of tunnel lining practice in the United Kingdom. Department of th Environment, Department of Transport, TRRL Supplementar Report 335: Crowthorne, (Transport and Road Research Laboratory).

Curtis, D.J., 1976. The circular tunnel in elastic ground. Discussion. Geotechnique, Vol. 26, pp.231-237.

Duddeck, H., 1972. Zu den Berechnungsmethoden und zur Sicherheit von Tunnelbauten. Bauingenieur 47. H.2, pp. 43-52.

Duddeck, H., 1980. Empfehlungen zur Berechnung von Tunneln im Lockergestein (1980). Die Bautechnik, 10, pp. 349-356.

Duddeck, H., 1980. On the basic requirements for applying the Convergence Confinement Method. Underground Space, Vol. 4, No. 4, pp. 241-247.

Duddeck, H., 1981, Views on structural design models for tunnelling. Synopsis of answers to a questionnaire

(ITA). Advances in Tunnelling Technology and Subsurface
   Use. Vol. 2, No. 3, pp. 155-228.

Duddeck, H. and Erdmann, J., 1982. Structural design models
   for tunnels. Proceedings, Tunnelling '82 (edited by M.J.
   Jones), The Institution of Mining and Metallurgy,
   London, pp. 83-91.

Duddeck, H. and Erdmann, J., 1985. On structural design
   models for tunnels in soft soil. Underground Space, Vol.
   9, pp. 246-259.

Einstein, H.H., and Schwartz, C.W., 1979. Simplified
   analysis for tunnel supports. Journal of the
   Geotechnical Engineering Division, American Society of
   Civil Engineers, V. 106, pp. 499-518 (Discussion with
   corrections on the original paper in the same journal,
   July, 1980, pp. 835 838).

Eisenstein, Z. and Negro, A., 1985. Comprehensive design
   method for shallow tunnels. ITA/AITES, International
   Conference, Underground Structures in Urban Areas,
   Prague, Czechoslovakia, pp. 7-20.

Eisenstein, Z., Heinz, H. and Negro, A., 1984. On
   three-dimensional ground response to tunnelling.
   Proceedings, Geotech' 84, American Society of Civil
   Engineers (edited by K.Y. Lo), pp. 107-127.

Erdmann, J., 1983. Vergleich ebener und Entwicklung
   raumlicher Berechnungsverfahren fur Tunnel. Bericht Nr.
   83-40, Institut fur Statik der Technischen Universitat
   Braunschweig, 220 p.

Erdmann, J. and Duddeck, H., 1983. Statik der Tunnel im
   Lockergestein-Vergleich der Berechnungsmodelle.
   Bauingenieur, 58 Jahrgang, pp. 407 - 414.

Erdmann, J. and Duddeck, H., 1984. Stress-displacement
   fields at the face of rock tunnels. Proceedings, 1st
   Latin-American Congress of Underground Construction -
   ITA (Caracas), Vol. I, pp. 177-183.

Hartmann, F., 1970. Elastizitatstheorie des ausgekleideten
   Tunnelhohlraumes und des eingebohrten kreisformigen

Rohres. Strasse Brucke Tunnel 22 (1970), Heft 8,
209-215, Heft 9, 241-246, und Jg. 24 (1972), Heft 1,
13-20, Heft 2, 39-45.

Hartmann, F., 1985. Einfache Berechnung uberschuttetter
kriesformiger Rohre von beliebiger Steifigkeit
Elastizitatstheorie des uberschutteten Rohres.
Bautechnik, 62, Heft 7, pp. 224-235.

MacGregor, J.G., 1988. Personal Communication.

Morgan, H.D., 196C A contribution to the analysis of stres
in a circular tunnel. Geotechnique, Vol. 11, pp. 37-46.

Muir Wood, A.M., 1975. The circular tunnel in elastic
ground. Geotechnique, Vol. 25, pp. 115-127.

Negro, A., 1988. Design of Shallow Tunnels in Soft Ground.
Ph.D. Thesis, Department of Civil Engineering,
University of Alberta, 1480 p.

O'Rourke, T.D. et.al., 1984. Guidelines for Tunnel Lining
Design. Prepared by the UTRC Technical Committee on
Tunnel Lining Design. ASCE Geotechnical Engineering
Division. 82 p.

Paul, S.L., Hendron, A.J., Cording, E.J., Sgouros, G.E. and
Saho, P.K., 1983. Design recommendations for concrete
tunnel linings. Volume II: Summary of research and
proposed recommendations. Report UMTA-MA-06-0100 83-3.
National Technical Information Service, Springfield,
Virginia, 22161.

Peck, R.B., Hendron, A.J. and Mohraz, B., 1972.
State-of-the-Art of soft ground tunnelling. Proceedings
1st North American Rapid Excavation and Tunnelling
Conference, Vol. 1, pp. 259-286.

Pender, M.J., 1980. Elastic solution for a deep circular
tunnel. Geotechnique, Vol. 30, pp. 216-222.

Pender, M.J., 1980. Simplified analysis for tunnel.
Discussions. ASCE, GT7, pp. 833-835.

Ranken, R.E., 1978. Analysis of ground liner interaction for tunnels. Ph.D. Thesis. Univeristy of Illinois. (Urbana-Champaign), 427 p.

Schmidt, B., 1984. Tunnel lining design - do the theories work?, Proceedings, 4th Australia-New Zealand Conference on Geomechanics, (Perth), May.

Schulze, H., and Duddeck, H., 1964(a). Statische Berechnung schildvorgetriebenen Tunneln. Festschrift "Beton-und Monierbau AG 1889-1964", Dusseldorf, pp. 87-114.

Schulze, H., and Duddeck, H., 1964(b). Spannungen in Schildvorgetriebenen Tunneln. Beton-und Stahlbetonbau (Berlin), Heft 8, 59 Jahrgang, pp. 169-175.

Sgouros, G.E., 1982. Structural behaviour and design implications of concrete tunnel linings based on model tests and parameter studies. Ph.D. Thesis, University of Illinois at Urbana-Champaign., 385 p.

Simmonds, S.H., 1981. User Manual for Computer Program (PFT). Internal Note, Department of Civil Engineering, University of Alberta.

A. PFT EXAMPLE: INPUT AND OUTPUT FILES

(i) INPUT FILE

```
 1      H ••••••••••••••••••••••••••••••••••••••••••
 2      H ALTO DA BOA VISTA CASE HISTORY          : LINER ACTIONS
 3      H .                                        : OPTION B
 4      H .                                        : ITERATION 01
 5      H SOIL PROPERTIES :
 6      H .                      REDUCED SOIL WEIGHT • 7.536 kN/m•3
 7      H .                     ' INSITU STRESS RATIO • 0.8
 8      H .                       H/D • 1.55
 9      H .                       EXCAVATED D • 4.0 m
10      H .                       H • 6.20 m
11      H .                       POISSONS RATIO • 0.3
12      H .                       AVERAGE INITIAL E • 30.325 MPa
13      H .    •                  AVERAGE REDUCED E • 13.482 MPa
13.1    H .                       AS : 100000 mm••2/m
13.2    H .                       IS : 8.33E7 mm••4/m
13.3    H
13.4    H
27      H .       OPTION B    : FROM AVERAGE SPRING CONSTANT Kr
28      H .                           : Kr • 6.002  MPa/m
29      H .                       .   : Es • 11.704 MPa
30      H
31      H .              LINER LOADS COME FROM EXCAVATED DIAMETER OF 4.0m
32      H .              LINER RADIUS • 1.95m. SHOTCRETE LINER T • .10m
33      H .              SPRING LENGTH • 1.95m
34      H ••••••••••••••••••••••••••••••••••••••••••
35      S.F,48,48,1,24,
36      J,1,0.000,1.950,
37      J,2,0.505,1.884,
38      J,3,0.975,1.689,
39      J,4,1.379,1.379,
40      J,5,1.689,0.975,
41      J,6,1.884,0.505,
42      J,7,1.950,0.000,
43      J,8,1.884,-0.505,
44      J,9,1.689,-0.975,
45      J,10,1.379,-1.379,
46      J,11,0.975,-1.689,
47      J,12,0.505,-1.884,
48      J,13,0.000,-1.950,
49      J,14,-0.505,-1.884,
50      J,15,-0.975,-1.689,
51      J,16,-1.379,-1.379,
52      J,17,-1.689,-0.975,
53      J,18,-1.884,-0.505,
54      J,19,-1.950,0.000,
55      J,20,-1.884,0.505,
56      J,21,-1.689,0.975,
57      J,22,-1.379,1.379,
58      J,23,-0.975,1.689,
59      J,24,-0.505,1.884,
60      J,25,0.000,3.900,
61      J,26,1.009,3.767,
62      J,27,1.950,3.377,
63      J,28,2.758,2.758,
64      J,29,3.377,1.950,
65      J,30,3.767,1.009,
66      J,31,3.900,0.000,
67      J,32,3.767,-1.009,
```

```
68   J.33,3.377,-1.950,
69   J.34,2.758,-2.758,
70   J.35,1.950,-3.377,
71   J.36,1.009,-3.767,
72   J.37,0.000,-3.900,
73   J.38,-1.009,-3.767,
74   J.39,-1.950,-3.377,
75   J.40,-2.758,-2.758,
76   J.41,-3.377,-1.950,
77   J.42,-3.767,-1.009,
78   J.43,-3.900,0.000,
79   J.44,-3.767,1.009,
80   J.45,-3.377,1.950,
81   J.46,-2.758,2.758,
82   J.47,-1.950,3.377,
83   J.48,-1.009,3.767,
84   D.100000,8.33E7,10000,
85   M.1,1,2,0,
86   M.2,2,3,0,
87   M.3,3,4,0,
88   M.4,4,5,0,
89   M.5,5,6,0,
90   M.6,6,7,0,
91   M.7,7,8,0,
92   M.8,8,9,0,
93   M.9,9,10,0,
94   M.10,10,11,0,
95   M.11,11,12,0,
96   M.12,12,13,0,
97   M.13,13,14,0,
98   M.14,14,15,0,
99   M.15,15,16,0,
100  M.16,16,17,0,
101  M.17,17,18,0,
102  M.18,18,19,0,
103  M.19,19,20,0,
104  M.20,20,21,0,
105  M.21,21,22,0,
106  M.22,22,23,0,
107  M.23,23,24,0,
108  M.24,24,1,0,
109  D.509050,1.00E2,11.704,
110  M.25,1,25,1,
111  M.26,2,26,1,
112  M.27,3,27,1,
113  M.28,4,28,1,
114  M.46,22,46,1,
115  M.47,23,47,1,
116  M.48,24,48,1,
117  D.509050,1.00E2,11.704,
118  M.29,5,29,1,
119  M.30,6,30,1,
120  M.31,7,31,1,
121  M.32,8,32,1,
122  M.33,9,33,1,
123  M.34,10,34,1,
124  M.40,16,40,1,
125  M.41,17,41,1,

126  M.42,18,42,1,
127  M.43,19,43,1,
128  M.44,20,44,1,
129  M.45,21,45,1,
130  D.509050,1.00E2,11.704,
131  M.35,11,35,1,
132  M.36,12,36,1,
133  M.37,13,37,1,
134  M.38,14,38,1,
135  M.39,15,39,1,
136  B.25,1,1,1,
137  B.26,1,1,1,
138  B.27,1,1,1,
139  B.28,1,1,1,
140  B.29,1,1,1,
141  B.30,1,1,1,
142  B.31,1,1,1,
143  B.32,1,1,1,
144  B.33,1,1,1,
145  B.34,1,1,1,
146  B.35,1,1,1,
147  B.36,1,1,1,
148  B.37,1,1,1,
149  B.38,1,1,1,
150  B.39,1,1,1,
151  B.40,1,1,1,
152  B.41,1,1,1,
153  B.42,1,1,1,
154  B.43,1,1,1,
155  B.44,1,1,1,
156  B.45,1,1,1,
157  B.46,1,1,1,
158  B.47,1,1,1,
159  B.48,1,1,1,
160  P.1,0,-27.621,0.20,0.,0.,0.,
161  P.2,-4.978,-27.063,0.,0.,0.,0.,
162  P.3,-9.925,-25.325,0.,0.,0.,0.,
163  P.4,-14.726,-22.244,0.,0.,0.,0.,
164  P.5,-19.136,-17.647,0.,0.,0.,0.,
165  P.6,-22.774,-11.464,0.,0.,0.,0.,
166  P.7,-25.166,-3.836,0.,0.,0.,0.,
167  P.8,-24.790,4.820,0.,0.,0.,0.,
168  P.9,-24.186,13.811,0.,0.,0.,0.,
169  P.10,-20.864,22.244,0.,0.,0.,0.,
170  P.11,-15.241,29.161,0.,0.,0.,0.,
171  P.12,-8.048,33.707,0.,0.,0.,0.,
172  P.13,0.,35.293,0.,0.,0.,0.,
173  P.14,8.048,33.707,0.,0.,0.,0.,
174  P.15,15.241,29.161,0.,0.,0.,0.,
175  P.16,20.864,22.244,0.,0.,0.,0.,
176  P.17,24.186,13.811,0.,0.,0.,0.,
177  P.18,24.790,4.820,0.,0.,0.,0.,
178  P.19,25.166,-3.836,0.,0.,0.,0.,
179  P.20,22.774,-11.464,0.,0.,0.,0.,
180  P.21,19.136,-17.647,0.,0.,0.,0.,
181  P.22,14.726,-22.244,0.,0.,0.,0.,
182  P.23,9.925,-25.325,0.,0.,0.,0.,
183  P.24,4.978,-27.063,0.,0.,0.,0.,
184
```

```
ALTO DA BOA VISTA CASE HISTORY          : LINER ACTIONS
                                          OPTION B
                                        : ITERATION 01

    SOIL PROPERTIES :
                     REDUCED SOIL WEIGHT = 7.536 kN/m**3
                     INSITU STRESS RATIO = 0.8
                     H/D = 1.55
                     EXCAVATED D = 4.0 m
                     H = 6.20 m
                     POISSONS RATIO = 0.3
                     AVERAGE INITIAL E = 30.325 MPa
                     AVERAGE REDUCED E = 13.482 MPa
                     AS : 100000 mm**2/m
                     IS : 8.33E7 mm**4/m


    OPTION B   : FROM AVERAGE SPRING CONSTANT Kr
                     Kr = 6.002 MPa/m
                     Es = 11.704 MPa

                 LINER LOADS COME FROM EXCAVATED DIAMETER OF 4.0m
                 LINER RADIUS = 1.95m.   ....  LINER T = 10m
                 SPRING LENGTH = 1.95m


---  Input / output units: SI by default
---  Problem control variables:
 O   Type of structure       = Frame
     Number of joints        = 48
     Number of elements      = 48
     Number of load cases    = 1
     Number of bdy. joints   = 24
---  Nodal geometry as input (metres)

Node  X-coordinate  Y-coordinate
  1     0.0            1.95000
  2     0.505000       1.88400
  3     0.975000       1.68900
  4     1.37900        1.37900
  5     1.68900        0.975000
  6     1.88400        0.505000
  7     1.95000        0.0
  8     1.88400       -0.505000
  9     1.68900       -0.975000
 10     1.37900       -1.37900
 11     0.975000      -1.68900
 12     0.505000      -1.88400
 13     0.0           -1.95000
 14    -0.505000      -1.88400
 15    -0.975000      -1.68900
 16    -1.37900       -1.37900
 17    -1.68900       -0.975000
 18    -1.88400       -0.505000
 19    -1.95000        0.0
 20    -1.88400        0.505000
 21    -1.68900        0.975000
```

```
             -1.37900    1.37900
             -0.975000   1.68900
             -0.505000   1.88400
              0.0        3.90000
              1.00900    3.76700
              1.95000    3.37700
              2.75800    2.75800
              3.37700    1.95000
              3.76700    1.00900
              3.90000    0.0
              3.76700   -1.00900
              3.37700   -1.95000
              2.75800   -2.75800
              1.95000   -3.37700
              1.00900   -3.76700
              0.0       -3.90000
             -1.00900   -3.76700
             -1.95000   -3.37700
             -2.75800   -2.75800
             -3.37700   -1.95000
             -3.76700   -1.00900
             -3.90000    0.0
             -1.00900
             -1.95000
             -2.75800
             -3.37700
             -1.95000
             -1.00900
```

**** Member property default values:

```
  Area                  =  100000.         sq. mm.
  Moment of Inertia     =  0.833000E+08   (mm)**4
  Young's Modulus       =  10000.0         MPa
  Coeff. of Thermal Exp. =  1.00000
```

**** Member data as input:

Member	I-node	J-node	Type	Area	Inertia	Young's Modulus	Tcoeff	(length)
1	1	2	0	100000.	0.833000E+08	10000.0	1.00000	0.509295
2	2	3	0	100000.	0.833000E+08	10000.0	1.00000	0.508847
3	3	4	0	100000.	0.833000E+08	10000.0	1.00000	0.509231
4	4	5	0	100000.	0.833000E+08	10000.0	1.00000	0.509231
5	5	6	0	100000.	0.833000E+08	10000.0	1.00000	0.509295
6	6	7	0	100000.	0.833000E+08	10000.0	1.00000	0.509295
7	7	8	0	100000.	0.833000E+08	10000.0	1.00000	0.508847
8	8	9	0	100000.	0.833000E+08	10000.0	1.00000	0.509231
9	9	10	0	100000.	0.833000E+08	10000.0	1.00000	0.508847
10	10	11	0	100000.	0.833000E+08	10000.0	1.00000	0.509295
11	11	12	0	100000.	0.833000E+08	10000.0	1.00000	0.509231
12	12	13	0	100000.	0.833000E+08	10000.0	1.00000	0.508847
13	13	14	0	100000.	0.833000E+08	10000.0	1.00000	0.509295
14	14	15	0	100000.	0.833000E+08	10000.0	1.00000	0.508847
15	15	16	0	100000.	0.833000E+08	10000.0	1.00000	0.509231
16	16	17	0	100000.	0.833000E+08	10000.0	1.00000	0.509231
17	17	18	0	100000.	0.833000E+08	10000.0	1.00000	0.508847
18	18	19	0	100000.	0.833000E+08	10000.0	1.00000	0.509295
19	19	20	0	100000.	0.833000E+08	10000.0	1.00000	0.509295
20	20	21	0	100000.	0.833000E+08	10000.0	1.00000	0.509295
21	21	22	0	100000.	0.833000E+08	10000.0	1.00000	0.508847
22	22	23	0	100000.	0.833000E+08	10000.0	1.00000	0.509231
```
```

```
117
118
119   23   23   24   0   100000.   0.833000E+08   10000.0   0.508847
120   24   24    1   0   100000.   0.833000E+08   10000.0   0.509295
121  **** Member property default values:
122       Area                   =  509050.    sq. mm.
123       Moment of Inertia      =  100.000    (mm)**4
124       Young's Modulus        =  11.7040    MPa
125       Coeff. of Thermal Exp. =  1.00000
126  **** Member data as input:
127
```

Member	I-node	J-node	Type	Area	Inertia	Young's Modulus	Tcoeff	(length)
25	1	25	1	509050.	100.000	11.7040	1.00000	1.95000
26	2	26	1	509050.	100.000	11.7040	1.00000	1.94928
27	3	27	1	509050.	100.000	11.7040	1.00000	1.94935
28	4	28	1	509050.	100.000	11.7040	1.00000	1.95020
46	22	46	1	509050.	100.000	11.7040	1.00000	1.95020
47	23	47	1	509050.	100.000	11.7040	1.00000	1.94935
48	24	48	1	509050.	100.000	11.7040	1.00000	1.94928

```
136
137  **** Member property default values:
138       Area                   =  509050.    sq. mm.
139       Moment of Inertia      =  100.000    (mm)**4
140       Young's Modulus        =  11.7040    MPa
141       Coeff. of Thermal Exp. =  1.00000
142  **** Member data as input:
143
```

Member	I-node	J-node	Type	Area	Inertia	Young's Modulus	Tcoeff	(length)
29	5	29	1	509050.	100.000	11.7040	1.00000	1.94935
30	6	30	1	509050.	100.000	11.7040	1.00000	1.94928
31	7	31	1	509050.	100.000	11.7040	1.00000	1.95000
32	8	32	1	509050.	100.000	11.7040	1.00000	1.94928
33	9	33	1	509050.	100.000	11.7040	1.00000	1.94935
34	10	34	1	509050.	100.000	11.7040	1.00000	1.95020
40	16	40	1	509050.	100.000	11.7040	1.00000	1.95020
41	17	41	1	509050.	100.000	11.7040	1.00000	1.94935
42	18	42	1	509050.	100.000	11.7040	1.00000	1.94928
43	19	43	1	509050.	100.000	11.7040	1.00000	1.95000
44	20	44	1	509050.	100.000	11.7040	1.00000	1.94928
45	21	45	1	509050.	100.000	11.7040	1.00000	1.94935

```
156
157  **** Member property default values:
158       Area                   =  509050.    sq. mm.
159       Moment of Inertia      =  100.000    (mm)**4
160       Young's Modulus        =  11.7040    MPa
161       Coeff. of Thermal Exp. =  1.00000
162  **** Member data as input:
163
```

Member	I-node	J-node	Type	Area	Inertia	Young's Modulus	Tcoeff	(length)
35	11	35	1	509050.	100.000	11.7040	1.00000	1.94935
36	12	36	1	509050.	100.000	11.7040	1.00000	1.94928
37	13	37	1	509050.	100.000	11.7040	1.00000	1.95000
38	14	38	1	509050.	100.000	11.7040	1.00000	1.94928
39	15	39	1	509050.	100.000	11.7040	1.00000	1.94935

```
170
171  **** External boundary conditions:
172       Joint   Rx  Ry  Rr
173       25       1   1   1
174       26       1   1   1
```

27
28
29
30
31
32
33
34
35
36
37
38
39
40
41
42
43
44
45
46
47
48

Load case no.

*** Joint loads as input (KN, mm, KN-m)

Node	U	V	R
1	0.0	-27.6210	0.0
2	-4.97800	-27.0630	0.0
3	-9.92500	-25.3250	0.0
4	-14.7260	-22.2440	0.0
5	-19.1360	-17.6470	0.0
6	-22.7740	-11.4640	0.0
7	-25.1660	-3.83600	0.0
8	-24.7900	4.82000	0.0
9	-24.1860	13.8110	0.0
10	-20.8640	22.2440	0.0
11	-15.2410	29.1610	0.0
12	-8.04800	33.7070	0.0
13	0.0	35.2930	0.0
14	8.04800	33.7070	0.0
15	15.2410	28.1610	0.0
16	20.8640	22.2440	0.0
17	24.1860	13.8110	0.0
18	24.7900	4.82000	0.0
19	25.1660	-3.83600	0.0
20	22.7740	-11.4640	0.0
21	19.1360	-17.6470	0.0
22	14.7260	-22.2440	0.0
23	9.92500	-25.3250	0.0
24	4.97800	-27.0630	0.0

**** Nodal displacements   Load case no.
                                 (mm & radians)

Node   X   Y   R

175
176
177
178
179
180
181
182
183
184
185
186
187
188
189
190
191
192
193
194
195
196
197
198
199
200
201
202
203
204
205
206
207
208
209
210
211
212
213
214
215
216
217
218
219
220
221
222
223
224
225
226
227
228
229
230
231
232

233	1	0.00	-1.54	-0.2537E-09
234	2	-0.03	-1.42	0.4377E-03
235	3	0.05	-1.11	0.7876E-03
236	4	0.29	-0.72	0.9854E-03
237	5	0.66	-0.37	0.9643E-03
238	6	1.04	-0.16	0.6897E-03
239	7	1.27	-0.07	0.1983E-03
240	8	1.22	-0.00	-0.4545E-03
241	9	0.88	0.20	-0.1038E-02
242	10	0.43	0.62	-0.1279E-02
243	11	0.09	1.15	-0.1135E-02
244	12	-0.03	1.61	-0.6683E-03
245	13	-0.00	1.79	0.2537E-09
246	14	-0.03	1.61	0.6683E-03
247	15	-0.09	1.15	0.1135E-02
248	16	-0.43	0.62	0.1279E-02
249	17	-0.88	0.20	0.1038E-02
250	18	-1.22	-0.00	0.4545E-03
251	19	-1.27	-0.07	-0.1983E-03
252	20	-1.04	-0.16	-0.6897E-03
253	21	-0.66	-0.37	-0.9643E-03
254	22	-0.29	-0.72	-0.9857E-03
255	23	-0.05	-1.11	-0.7876E-03
256	24	0.03	-1.42	-0.4377E-03
257	25	0.0	0.0	0.0
258	26	0.0000	0.0000	0.0000
259	27	0.0000	0.0000	0.0000
260	28	0.0000	0.0000	0.0000
261	29	0.0000	0.0000	0.0000
262	30	0.0000	0.0000	0.0000
263	31	0.0000	0.0000	0.0000
264	32	0.0000	0.0000	0.0000
265	33	0.0000	0.0000	0.0000
266	34	0.0000	0.0000	0.0000
267	35	0.0000	0.0000	0.0000
268	36	0.0000	0.0000	0.0000
269	37	0.0000	0.0000	0.0000
270	38	0.0000	0.0000	0.0000
271	39	0.0000	0.0000	0.0000
272	40	0.0000	0.0000	0.0000
273	41	0.0000	0.0000	0.0000
274	42	0.0000	0.0000	0.0000
275	43	0.0000	0.0000	0.0000
276	44	0.0000	0.0000	0.0000
277	45	0.0000	0.0000	0.0000
278	46	0.000	0.000	0.000
279	47	0.000	0.000	0.000
280	48	0.000	0.000	0.000

**** Member end forces (KN & KN-m)

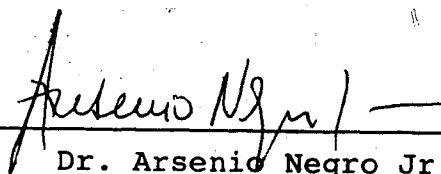| Member	I	J	Ni	Vi	Mi	Nj	Vj	Mj
1	1	2	86.751	-0.216	-0.771	-86.751	0.216	0.661
2	2	3	89.036	-0.347	-0.661	-89.036	0.347	0.485
3	3	4	93.274	-0.631	-0.485	-93.274	0.631	0.163
4	4	5	98.821	-0.779	-0.163	-98.821	0.779	0.233
5	5	6	104.791	-0.850	0.233	-104.791	0.850	-0.666
6	6	7	110.204	-0.542	0.666	-110.204	0.542	-0.942
7	7	8	114.208	-0.495	0.942	-114.208	0.495	-1.194
8	8	9	115.921	-0.942	1.194	-115.921	0.942	-0.715
9	9	10	115.774	1.255	0.715	-115.774	-1.255	-0.076
10	10	11	114.463	1.224	0.076	-114.463	-1.224	0.548
11	11	12	112.788	0.849	-0.548	-112.788	-0.849	0.980
12	12	13	111.665	0.445	-0.980	-111.665	-0.445	1.206
13	13	14	111.665	-0.445	-1.206	-111.665	0.445	0.980
14	14	15	112.788	-0.849	-0.980	-112.788	0.849	0.548
15	15	16	114.463	-1.224	-0.548	-114.463	1.224	-0.076
16	16	17	115.774	-1.255	0.076	-115.774	1.255	-0.715
17	17	18	115.921	-0.942	0.715	-115.921	0.942	-1.194
18	18	19	114.208	0.495	1.194	-114.208	-0.495	-0.942
19	19	20	110.204	0.542	0.942	-110.204	-0.542	-0.666
20	20	21	104.791	0.850	0.666	-104.791	-0.850	-0.233
21	21	22	98.821	0.779	0.233	-98.821	-0.779	0.163
22	22	23	93.274	0.631	-0.163	-93.274	-0.631	0.485
23	23	24	89.036	0.347	-0.485	-89.036	-0.347	0.661
24	24	1	86.751	0.216	-0.661	-86.751	-0.216	0.771
25	1	25	-4.709	0.0	0.0	4.709	0.0	0.0
26	2	26	-4.222	-0.000	0.0	4.222	0.000	-0.000
27	3	27	-2.868	-0.000	0.0	2.868	0.000	-0.000
28	4	28	-0.921	-0.000	0.0	0.921	0.000	-0.000
29	5	29	1.191	-0.000	0.0	-1.191	0.000	-0.000
30	6	30	2.955	0.0	0.0	-2.906	0.0	-0.000
31	7	31	3.870	0.000	0.0	-3.870	-0.000	0.000
32	8	32	3.594	0.000	0.0	-3.594	-0.000	0.000
33	9	33	2.014	0.000	0.0	-2.014	-0.000	0.000
34	10	34	-0.399	0.000	0.0	0.399	-0.000	0.000
35	11	35	-2.906	0.000	0.0	2.906	-0.000	0.000
36	12	36	-4.774	0.000	0.0	4.774	-0.000	0.000
37	13	37	-5.469	-0.000	0.0	5.469	0.000	0.000
38	14	38	-4.774	-0.000	0.0	4.774	0.000	0.000
39	15	39	-2.906	-0.000	0.0	2.906	0.000	-0.000
40	16	40	-0.399	-0.000	0.0	0.399	0.000	-0.000
41	17	41	2.014	-0.000	0.0	-2.014	0.000	-0.000
42	18	42	3.594	-0.000	0.0	-3.594	0.000	-0.000
43	19	43	3.870	0.000	0.0	-3.870	-0.000	-0.000
44	20	44	2.955	0.000	0.0	-2.955	-0.000	-0.000
45	21	45	1.191	0.000	0.0	-1.191	-0.000	-0.000
46	22	46	-0.921	0.000	0.0	0.921	-0.000	-0.000
47	23	47	-2.868	0.000	0.0	2.868	-0.000	-0.000
48	24	48	-4.222	0.000	0.0	4.222	-0.000	-0.000

Mrs S. Evison,
Dept. of Civil Engineering
The University of Alberta
Edmonton, Alberta
Canada T6G 2G7

Dear Mrs. Evison,

In reply to your request of 16/09/88, I am pleased to give you permission to reproduce in your MSc dissertation any figure or table of my PhD thesis you many need. Please, find enclosed copies of Figures 2.14, 2.15, 2.20, 4.2, 4.4, 7.1, 7.2, 7.3, 7.9, 7.11, 7.12, 7.13, 7.15, 7.16 and 7.17 of my thesis.

Looking forward to the results of your research work, I remain,

Your Faithfully

Dr. Arsenio Negro Jr.

Rua João Moura, 860 ap. 131
05412 São Paulo (SP)
Brazil